

**Investigation of the Temperature Impact of Hyporheic
Flow: Using Groundwater and Heat Flow Modeling and
GIS Analyses to Evaluate Temperature Mitigation
Strategies on the Willamette River, Oregon**

Final Report

Principle Investigators:

Stephen Lancaster (Asst. Prof., Geosciences, OSU)

Roy Haggerty (Assoc. Prof., Geosciences, OSU)

Collaborator:

Stan Gregory (Prof., Fisheries & Wildlife, OSU)

Research Assistants:

Kevin T. Farthing (Environmental Engineering, OSU)

Linda Ashkenas (Fisheries & Wildlife, OSU)

Project Manager:

Sonja Biorn-Hansen (Oregon Dept. Environmental Quality)



Abstract

Thermal energy is one of the most important pollutants to Oregon's waterways, driving total maximum daily loads (TMDLs) in the Willamette, Umatilla, and many other rivers during summer months. The goals of this project were to examine whether (1) injection of wastewater into the subsurface could mitigate excess thermal load due to a municipal wastewater plant and (2) restoration of floodplains could cool rivers during the critical summer/early fall months. We developed a model of a composite section of a southern Willamette Valley riparian zone using the computer program PetraSim/TOUGH2 to measure what subsurface and hydrologic parameters contributed to thermal energy entering the fluvial body. The results from the modeling suggest there are two components of heat transfer to rivers in the hyporheic zone: advection of groundwater, and conduction to the subsurface material. Advection is the largest driver of heat transfer, and it is most affected by variations in the hydraulic conductivity. Conduction plays a significantly lesser role in heat transfer, but the combination of subsurface specific heat and density do affect the temperature of a water body. Of the two afore-mentioned mitigation options, subsurface injection is the more viable option for temperature mitigation due to the large heat storage capacity of the ground. Specifically, peak temperature effects of warm effluent could probably be reduced 100-fold (e.g., increasing river temperature by 10^{-3} °C rather than 10^{-1} °C). The cooling capability due to restoring rarely (e.g., once per year) inundated side channels on the floodplain is probably small without great surface area and therefore infeasible purely for reasons of enhancing hyporheic flow.

Table of Contents

Abstract	2
Table of Contents	3
List of Figures	6
List of Tables	10
Introduction.....	12
Hyporheic Zone Background.....	12
This Study - Overview	19
Groundwater and Heat Flow Modeling	21
TOUGH2 Defining Equations	21
PetraSim.....	25
Hyporheic Zone Modeling Scenarios:	26
General Modeling Considerations:	26
Foundation Model:	27
Step I.....	27
Step II.....	29
Step III:	31
Step IV	31
SED Scenario	32
FPR Scenario:	33
Analysis of Simulation Results.....	33
Measurement of Heat and Temperature Effects in the River	33
Scaling of Simulation Results.....	35
Flood Plain Restoration Simulations	37
Results.....	38

Sensitivity Analysis	40
Floodplain Restoration: Distance.....	40
FPR: Hydraulic Conductivity	41
FPR: Porosity	44
FPR: Density.....	46
FPR: Specific Heat.....	48
FPR: Thermal conductivity.....	51
FPR: Variable Precipitation	53
FPR: Channel Volume	55
Subsurface Effluent Discharge Simulations	57
Results.....	58
Sensitivity Analysis	58
Surface Effluent Discharge (SED): Distance.....	58
SED: Hydraulic Conductivity.....	63
SED: Porosity.....	66
SED: Density	68
SED: Specific Heat	70
SED: Thermal conductivity	72
SED: Variable Precipitation.....	74
Maximum Injection Simulations.....	76
Direct Mixing Analysis.....	79
Discussion	81
FPR Scenario Feasibility.....	86
SED Scenario Feasibility	87
Further Study	88

Conclusions.....	88
Table of Variables.....	89
References.....	90
Appendix A: Annotated Bibliography of Heat Transport in the Hyporheic Zone of Big Rivers	93
Appendix B: Spatial Datalayers for Willamette Temperature Study.....	101
Spatial Containers	101
Base Datalayers.....	101
Results and Products	103

List of Figures

Figure 1. : Section One of the Clean Water Act passed by the U.S. Congress 1972 (http://www.epa.gov/region5/water/pdf/ecwa.pdf).....	13
Figure 2. Idealized stream channel, (Poole and Berman, 2000)	15
Figure 3. Conceptual rendering of the hyporheic zone for a typical stream (http://permanent.access.gpo.gov/waterusgsgov/water.usgs.gov/pubs/circ/circ1139/images/fig15.gif).....	16
Figure 4. The various components of equations (11) and,(12) and how they are spatially represented in TOUGH2 (Pruess, 1998).....	24
Figure 5. PetraSim’s visual rendering of model used in this project	28
Figure 6. Conceptual picture of the constant head boundary conditions.....	30
Figure 7. Constant-head boundary conditions as a percentage of water saturation. The red represents the 100% saturation of the porous subsurface; dark blue represents 0% saturation. In the case of the dark blue, the medium is the atmospheric boundary conditions above the water body.....	30
Figure 8. A conceptual rendering of the model’s precipitation recharge in the Z – Y Plane	31
Figure 9. Side view of the SED case in the X – Z plane The brown section is the vadose zone, the green section is the saturated zone, and the blue section is the river. For the default case, the injection cells were 30 meters away from the river along the x axis. The injection mass flow rate was 0.49 kg/s with an enthalpy of 9.66×10 J/ kg for 60 days. ..	33
Figure 10. Side view of the FPR case in the X – Z plane. The brown section represents the vadose zone, the green section is the saturated zone, and the blue section is the river. The side channel is 30 m from the river, spans the entire model along the y-axis, and is 2 m deep. The initial temperature of the side channel’s water was 8°C.	33
Figure 11. Heat balance for river channel.....	34
Figure 12. A conceptual drawing of the FPR modeling scenario; cool water travels out of the channel, into the subsurface, and then into the river where it lowers the river’s temperature	37
Figure 13. PetraSim’s graphical representation of the FPR scenario simulation results at 230 seconds. SW stands for percentage of water saturation for the model’s cells. In this figure the color red is the fully saturated zone with 100%, and blue is 0% saturation of the subsurface.	39

Figure 14. PetraSim’s graphical representation of the FPR scenario at 2250 seconds. All variables, symbols, and illustrative guides are the same as in Figure 13.....	40
Figure 15. The temperature v. time plot for the distance varying FPR case.....	41
Figure 16. The temperature v. time plot for the hydraulic conductivity varying FPR case	42
Figure 17. The heat flux (rate) v. time plot for the hydraulic conductivity varying FPR case. The scale is altered to show the negative heat rates that corresponds to the temperature drops in the fluvial body.	43
Figure 18. The temperature v. time plot for the porosity varying FPR case.....	44
Figure 19. The heat rate (ΔH) v. time plot for the porosity-varying FPR . The x- and y-axes have been altered to emphasize the negative heat rate that corresponded to the cooling of the river due to side channel.	45
Figure 20. The temperature v. time plot for the density-varying FPR case.....	46
Figure 21. The heat rate (ΔH) v. time plot for the density varying FPR case. The x- and y-axes have been altered to emphasize the negative heat rate that corresponded to the cooling of the fluvial body due to side channel.	47
Figure 22. Temperature versus time plot for the specific heat side channel restoration simulations.	49
Figure 23. Heat rate (ΔH) v. time plot for the specific heat-varying FPR case.	50
Figure 24. Temperature v. time plot for the thermal conductivity varying FPR case.	51
Figure 25. Heat rate (ΔH) v. time plot for the thermal conductivity varying FPR case. ..	52
Figure 26. Temperature versus time plot for the precipitation varying simulations:.....	53
Figure 27. Heat rate (ΔH) versus time plot for the variable precipitation case.....	54
Figure 28. Temperature versus time plots with varying side-channel volume.	55
Figure 29. Heat rate (ΔH) versus time plot for the variable precipitation FPR simulations	56
Figure 30. A conceptual drawing of the SED case.	57
Figure 31. Temperature versus time plot for SED simulations with varying distance.	59
Figure 32. Heat rate (ΔH) versus time plot with varying distance for SED case.....	60

Figure 33. Groundwater velocity along the x-axis leaving the model for the default case	61
Figure 34. Normalized heat rate versus time for the distance varying SED simulations .	62
Figure 35. Temperature versus time for the hydraulic conductivity varying SED simulations	64
Figure 36. Heat rate (ΔH) versus time for the hydraulic conductivity varying SED simulations.....	65
Figure 37. The temperature versus time plot for the varied porosity SED simulations....	66
Figure 38. The heat rate (ΔH) versus time plot for the varied porosity SED simulations.	67
Figure 39. The temperature versus time plot for the density varying SED simulations...	68
Figure 40. The heat rate (ΔH) versus time plot for the density varying SED simulations.	69
Figure 41. Temperature versus time plot for the specific heat injection simulations.....	70
Figure 42. Heat rate (ΔH) versus time plot for the density varying SED simulations.....	71
Figure 43. Temperature versus time plot for the thermal conductivity varying simulations.	72
Figure 44. Heat rate (ΔH) versus time plot for the thermal conductivity varying simulations.....	73
Figure 45. Temperature versus time plot for the precipitation varying SED simulations:	74
Figure 46. Heat rate (ΔH) versus time plot for the precipitation varying simulations.....	75
Figure 47. Temperature vs. time plot for the “best case” scenario.	77
Figure 48. Heat rate (ΔH) vs. time plot for the “best case” scenario.	78
Figure 49. Normalized heat rate (ΔH_N) vs. time plot for the “best case” scenario.	79
Figure 50. Idealized river-effluent interface as continuously stirred tank reactor (CSTR).	80
Figure 51. Groundwater velocity in the x-direction leaving the model. Greater velocity corresponds to greater discharge. At 60 days (2 months), subsurface injection ceased; for each of these simulations the drop off of groundwater velocity can be seen shortly thereafter.	84

Figure 52. A plan (x - y plane) view of an idealized portion of the Willamette Valley that has the model's groundwater movement and hypothetical realistic movement of groundwater in the valley..... 84

List of Tables

Table 1. Temperature criteria developed by the Willamette River TMDL Council.....	14
Table 2. Parameters and values for subsurface and atmospheric “materials.”	29
Table 3. Default parameters and values.....	32
Table 4. Normalized heat flux versus time integrated to yield the percentage of cooling entering the river.	43
Table 5. Minimum temperatures reached by river and scaled change in temperature due to cold banking for different values of hydraulic conductivity.....	44
Table 6. Percentage of total cooling “felt” by the river due to the FPR option with varying porosity.	45
Table 7. Minimum simulated river temperature and scaled change in temperature with varying porosity.	46
Table 8. Percentage of total cooling “felt” by the river due to the FPR option with varying density.....	47
Table 9. Minimum temperature values for the river, and the scaled changes in low temperatures for the density-varying simulations.....	48
Table 10. Percentage of cooling reaching the river with varying specific heat.....	50
Table 11. Low temperatures and scaled changes in temperature for varying specific heat.	50
Table 12. Percentage of cooling energy entering the river with varying thermal conductivity.....	52
Table 13. Low temperatures and scaled changes in temperature for varying thermal conductivity.....	53
Table 14. Percentage of cooling energy entering the river with varying precipitation.....	54
Table 15. Low temperatures and scaled changes in temperature for varying precipitation rate.....	54
Table 16. Integrated values for normalized heat rate with varying side-channel volume.	56
Table 17. Low temperatures and scaled changes in temperature for varying side-channel volume.....	56

Table 18. Total and “positive-only” percentages of heat entering the river with varying injection distance.	62
Table 19. Peak river temperatures and scaled maximum changes in temperature with varying injection distance.	63
Table 20. Percentage of injected heat entering river with varying hydraulic conductivity.	65
Table 21. Peak river temperatures and scaled maximum changes in temperature with varying hydraulic conductivity.	66
Table 22. Percentage of injected heat entering river with varying porosity.	67
Table 23. Peak river temperatures and scaled maximum changes in temperature with varying porosity.	68
Table 24. Percentage of injected heat entering river with varying density.	69
Table 25. Peak river temperatures and scaled maximum changes in temperature with varying density.	70
Table 26. Percentage of injected heat entering river with varying specific heat.	71
Table 27. Peak river temperatures and scaled maximum changes in temperature with varying specific heat.	72
Table 28. Percentage of injected heat entering river with varying thermal conductivity.	73
Table 29. Peak river temperatures and scaled maximum changes in temperature with varying thermal conductivity.	74
Table 30. Percentage of injected heat entering river with varying precipitation rate.	75
Table 31. Peak river temperatures and scaled maximum changes in temperature with varying precipitation rate.	76
Table 32. Parameters for and result of mixing analysis for combined temperature of river and effluent.	80
Table 33. Parameters for and result of mixing analysis for combined temperature of river and side channel.	81

Introduction

Hyporheic Zone Background

In recent years, increasing attention has been focused on improving water quality in Oregon's natural waterways such that they may meet the conditions necessary to realize their designated uses. Because the Willamette Valley houses roughly 70% of Oregon's population, water quality issues for the Willamette River (and its tributaries) have the potential to directly affect the majority of Oregon's citizens' general health and way of life (<http://www.deq.state.or.us/wq/willamette/WRBProblem.htm>).

Pollutants in the Willamette River motivating the establishment of water quality standards by the Oregon Department of Environmental Quality (DEQ) include bacteria, mercury, and temperature. Though it may seem counter-intuitive when compared with the afore-mentioned pollutants, thermal pollution places the greatest limitation on the state's waterways in terms of realization of designated uses because of the harm high water temperatures do to the aquatic organisms that inhabit Oregon's natural waterways (<http://www.deq.state.or.us/wq/willamette/WRBFactSheets.htm>).

The way that the Oregon DEQ quantifies the amount of pollution (of any sort) that can be put into a river are Total Maximum Daily Loads (TMDLs). TMDLs are the total amount of a given pollutant that is allowed by law to enter a water body for a 24-hour period. They have the potential to be different for every water body in both the pollutant regulated and the magnitude/concentration allowed into the water body. The motivation for the establishment of TMDLs came from the passage of the Clean Water Act in 1972.

The Clean Water Act is a law, enforced by the Environmental Protection Agency (EPA) that the federal government, working through the EPA, has for maintaining environmental standards to the Nation's natural water bodies. Figure 1 shows the first title of the Clean Water Act:

TITLE I—RESEARCH AND RELATED PROGRAMS

DECLARATION OF GOALS AND POLICY

SEC. 101. (a) The objective of this Act is to restore and maintain the chemical, physical, and biological integrity of the Nation's waters. In order to achieve this objective it is hereby declared that, consistent with the provisions of this Act—

(1) it is the national goal that the discharge of pollutants into the navigable waters be eliminated by 1985;

(2) it is the national goal that wherever attainable, an interim goal of water quality which provides for the protection and propagation of fish, shellfish, and wildlife and provides for recreation in and on the water be achieved by July 1, 1983;

(3) it is the national policy that the discharge of toxic pollutants in toxic amounts be prohibited;

(4) it is the national policy that Federal financial assistance be provided to construct publicly owned waste treatment works;

(5) it is the national policy that areawide treatment management planning processes be developed and implemented to assure adequate control of sources of pollutants in each State;

(6) it is the national policy that a major research and demonstration effort be made to develop technology necessary to eliminate the discharge of pollutants into the navigable waters, waters of the contiguous zone and the oceans; and

(7) it is the national policy that programs for the control of nonpoint sources of pollution be developed and implemented in an expeditious manner so as to enable the goals of this Act to be met through the control of both point and nonpoint sources of pollution.

Figure 1. : Section One of the Clean Water Act passed by the U.S. Congress 1972
(<http://www.epa.gov/region5/water/pdf/ecwa.pdf>)

Figure 1 shows the general goals of the Clean Water Act (CWA). These broad goals are seen in the above “Declaration of Goals and Policy” for the CWA. The Clean Water Act requires that individual states establish quality standards for water bodies within their borders. Water quality, according to the Clean Water Act, has three provisions associated with it: The first provision is that each water body will have a unique set of water quality standards. Second, water quality standards will have a combination of water criteria that quantitatively and qualitatively control the amount of a given pollutant that is allowed in a river. The third provision for water quality standards is the establishment of preventative measures for a given pollutant/s entering the river.

TMDL's for Oregon's water bodies address the second and third provisions set down by the Clean Water Act. TMDLs set numerical criteria that allow quantitative preventative measures for future development and regulate existing anthropogenic inputs to the river. This report will focus exclusively on , thermal pollution in natural waterways from municipal wastewater facilities. Working with TMDLs, Oregon's Department of Environmental Quality (DEQ) permits wastewater effluent into rivers and streams through NPDES permits (National Pollution Discharge Elimination System). These permits work with the TMDLs to set the limits on the effluent characteristics on point sources of pollution (temperature, BOD, Total Suspended Solids, etc), so that stream and river health are preserved.

A key component of TMDLs is the concept of a “pollutant offset”. For this report, the offset will be a “heat offset” and is defined as the difference between how much thermal

energy is currently in the river and how much can either be added and still meet the TMDL for temperature or how much needs to be removed to meet the TMDL. If the heat offset is positive, the TMDL acts as a guide for removal or mitigation of the excess thermal energy in the river. Important for the development of the TMDLs is determining the natural state of the river (That is, what would the water body's temperature be without anthropogenic inputs?).

For the establishment of temperature TMDLs for the Willamette River, the Willamette Valley was divided into a number of sub-catchments: Two regions were set aside for the main body of the Willamette River; nine other regions were developed for its major tributaries. A complex discussion of these regions, and their TMDLs, is beyond the scope of this report. However, it is important to note that temperature TMDLs were developed separately for each region (Willamette Basin TMDL: Main Stem Temperature).

Finally, the development of TMDLs for the Willamette River was made possible by a group of stakeholders (called the Willamette River TMDL Council). This group assisted in the following three tasks:

- Study existing information concerning excess thermal energy in the river.
- Select modeling and analytical tools for evaluation of mitigation techniques.
- Understand what additional data sources are necessary for completion of the Willamette River TMDLs.

The stakeholders for this group represented various interests, backgrounds, and points of view on how the Willamette River should be managed. These backgrounds included utility companies, lumber products companies, clean water organizations, universities, and individual watershed councils. The result of this collaboration can be seen in Table 1.

Table 1. Temperature criteria developed by the Willamette River TMDL Council¹.

Water Use	Temperature Criterion	Time Period
Migration Corridor	20 °C	Year Round
Salmon/Trout Rearing	18.0 °C	late spring/early fall
Core Cold Water Habitat	16°C	late spring/early fall
Steelhead Spawning	13°C	late spring/early fall
Bull Trout Rearing /Spawning	12°C	Year Round

¹ http://www.deq.state.or.us/wq/wqfact/WR_tempFS.pdf

These temperature criteria give the state of Oregon clear guidelines for when and how warm the river can be for the given section where aquatic organisms (mainly fish sought after by fishermen) reproduce and migrate for reproduction.

One point source of thermal energy is municipal wastewater treatment facilities. While wastewater treatment facilities contribute less than 0.5 °C each to thermal load in Oregon streams, they are one of the sources regulated by DEQ and therefore are a focus of our work. Standard practices for the treatment of wastewater in the Willamette Valley include direct injection of treated water into water bodies. As the water temperature increases, the amount of dissolved oxygen in the river decreases. Many aquatic organisms (e.g., salmon and trout) rely on dissolved oxygen for respiration, and as river temperatures rise, these organisms' health can be compromised. In particular, during the months of August through October, the combination of high ambient temperatures and low flows produce the highest water temperatures.

High stream temperatures are not only a function of warm water entering streams from waste water treatment facilities. Reduction of local floral and fauna near streams can reduce shading, increase amounts and magnitudes of solar radiation to which streams are exposed, and thus increase stream temperatures. Dams, and other obstructions in the river that slow down and collect flow also warm rivers. Slower flows and larger exposed surface areas warm rivers because of increased exposure to solar radiation. Note that the majority of heat entering the river comes from solar radiation (http://www.deq.state.or.us/wq/wqfact/WR_tempFS.pdf), not from wastewater effluent.

River temperatures are important because they affect the life spans and metabolic rates of the organisms, as well as nutrient cycling (which will also affect the quality of life of river-dwelling creatures). Rivers can be divided into three separate zones: the main body of the river, the riparian zone, and an alluvial aquifer (Poole and Berman, 2000). Thus the temperature of the river is also a function of these three parts of the river (Figure 2).

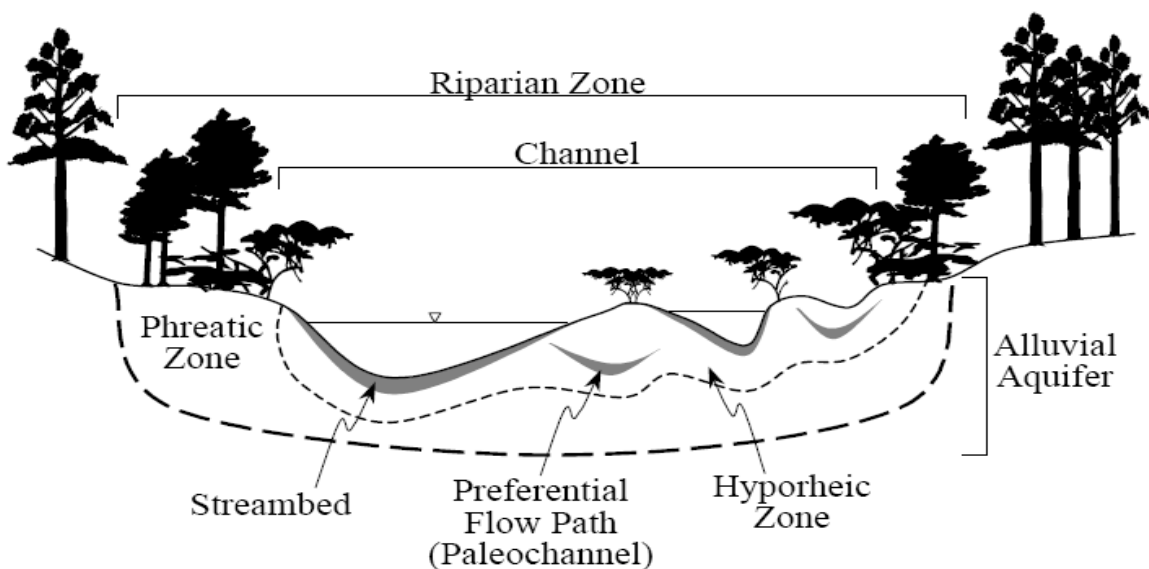


Figure 2. Idealized stream channel, (Poole and Berman, 2000)

Water temperature is proportional to its thermal energy divided by its volume. All water has thermal energy, and water's temperature is a measure of its thermal energy concentration. If only mixing is accounted for, (no evaporation or radiative heat transfer), the addition of colder water to a stream/river does not "eliminate" the heat, rather it dilutes the heat. The same total heat exists; however, it now exists in a greater volume of water. As a result, the temperature of that body of water will fall, but the total amount of heat in the system is the same (Poole and Berman, 2000).

This zone is typically composed of permeable gravels, sands, and silts, and allows significant mixing of river water with groundwater at various sections of the river. For certain river sections, the distinction between groundwater and surface water becomes essentially meaningless as river water and groundwater mix and flow freely through the hyporheic zone to emerge downstream in the river based on the hydraulic properties of the river.

The hyporheic zone is a complicated region whose boundaries are not always easy to define. The complexity is illustrated by the very general definition given by DS White. (1993): "Hydrologically, the hyporheic zone is established by channel water advection and may be defined as a "middle zone" between the channel waters above and the groundwaters below" (pg. 61; Figure 3).

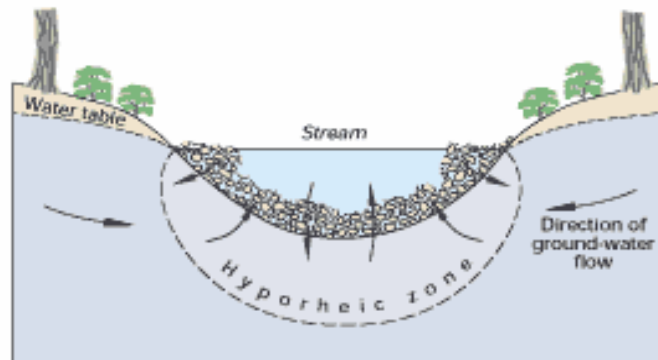


Figure 3. Conceptual rendering of the hyporheic zone for a typical stream (<http://permanent.access.gpo.gov/waterusgsgov/water.usgs.gov/pubs/circ/circ1139/images/fig15.gif>).

The study of the hyporheic zone is complicated by small local heterogeneities intrinsic to the zone. These micro-heterogeneities in the subsurface medium are further complicated by the time dependent aspect of the hyporheic zone. Large regions can have complicated hydrologic interactions (precipitation patterns that affects whether a stream is gaining or losing for a given time), that will affect the water saturation percentage of the zone. Seasonal variations in particular can affect the location and size of the hyporheic zone. These variations, in turn, can affect the creatures living in interstitial spaces in the river bed gravel (Fraser and Williams, 1997).

The animals that live within the interstitial spaces range from microbes capable of to various sizes of insect larvae (Wroblicky, 1994). Within the hyporheic zone, there are micro-fluctuations in the aquatic chemistry that stratified local micro-organism

populations. There is a marked, year-round difference the water chemistry of the hyporheic zone versus the groundwater.

The cooling (or heating) that the river experiences from hyporheic zone water flow is a part of transient storage of water in river bodies. Transient storage is a measure of the exchange of water between a river, the hyporheic zone, and the surface water dead zones (Fernald et al., 2001). This exchange of thermal energy within the hyporheic zone is important to the Pacific Northwest because of its reliance on Salmon for both sport and commercial fishing. The hyporheic zone is the spawning ground for these fish, and its physical and chemical properties can affect local species of salmon (and possibly other aquatic life) in the same river (Giest et al, 2002).

It should be noted that discussion of the hyporheic zone rarely occurs in a vacuum; it is usual accompanied by the fact that the hyporheic zone is a complex, ecologically diverse region that could potentially have vast capabilities for being both a thermal and biochemical “filter” for rivers in Oregon. “Filter” in this case means that the hyporheic zone, under certain circumstances, could remove/mitigate the pejorative effects of anthropogenic inputs to a stream. Chemical inputs include biologically active phosphorous (PO_4^{-3}), nitrate (NO_3^-) and BOD.

Aerobic and anaerobic zones can coexist side-by-side with each other in a small area, along with “dead zones” that allow little/zero water flow with the surrounding areas (Fernald et al, 2001). These variable zones are caused by material distribution irregularity. Large variations in porosity within the hyporheic zone cause variations with the flow regime: Given that the hyporheic zone is composed of loose gravel and varying sediment particle diameters, turbulent flow is prevalent. As the scale of the examination (for whatever physical/chemical parameter) decreases, the hyporheic zone becomes increasingly difficult to make generalities (Boulton et al, 1998). Fortunately, for this report, the model was sufficient large enough to ignore micro-variations in the zone and assume that the large scale size averaged out any heterogeneities in the subsurface.

DEQ is interested in exploring alternatives to direct surface water discharge, alternatives that would involve additional water flow in the hyporheic zone. DEQ perceives that suitable alternatives might have ancillary benefits that would not be achieved via a strict emphasis on temperature reduction at point source outfalls. The hyporheic zone is an intermediate zone between the subsurface alluvial aquifer and a river body through which some of the river’s water flows; hyporheic is derived from the Greek for “under river”².

One possible alternative is the injection of the treated waste water into the hyporheic zone and, thereby, to store excess heat load in the alluvium in that hyporheic zone. The warm treated wastewater, which would have been directly injected into the river/stream, is injected up-gradient into the hyporheic zone where some of the heat might be absorbed.

²<http://willametteexplorer.info/issues/floodplain/hydrophericzone.php>

The indirect discharge of wastewater to surface water via groundwater through the hyporheic zone is gaining attention. For example, a recent concept paper [Bowman, 2003] states:

Recent studies of the Willamette River have revealed that a significant amount of the river's flow passes through gravels below and at the margins of the river – an area referred to as the hyporheic zone. When passing through hyporheic gravels, the water cools considerably and other favorable chemical changes take place. By one estimate, the river's historical access to hyporheic gravels may have been five times as great as under current conditions, due to factors such as the absence of bank/hardening structures and the presence of more islands, side channels, and alcoves.

The potential exists to take advantage of the cooling function of the river's hyporheic gravels to "treat" the river's elevated water temperature problems. Additional gravels could be accessed by the river if it were allowed to flow more freely over adjacent lands that historically were subject to at least periodic inundation by the river. In other words, if the river were allowed to regain some of its channel width and complexity, its natural functions could have a greater mediating effect on water temperature.

This passage from Bowman succinctly and qualitatively voices the impetus for this study, namely, the importance of quantifying the feasibility and design parameters for floodplain restoration using the hyporheic zone as the mechanism for temperature mitigation. The modeling in this project is the first step in understanding how thermal energy is transported through the hyporheic zone, and its importance is derived from the need to lower river temperatures in the Willamette Valley so that aquatic life can thrive.

DEQ is interested in evaluating options that take advantage of the cooling capabilities of hyporheic zones. Two such options are as follows:

1. Side-Channel/Floodplain-Channel Restoration. This consists of re-connecting floodplains and associated side channels that have been cut off from the river's mainstem. As a result, high flow events during the fall, winter, and spring would serve to recharge historic hyporheic zones and their associated aerated (i.e., soil) and non-aerated (i.e., regolith) zones and allow for the seepage of cooled waters to the mainstem throughout the summer months. We will refer to this delay of cold water to the river due to floodplain-channel restoration as "cold banking".
2. Discharge to Hyporheic Zone. A source would discharge to surface water indirectly via the hyporheic zone rather than discharging directly to the river. The goal of this injection is the use of the hyporheic zone as a heat sink for the excess thermal energy from the waste water. The gravel/sand/silt of the hyporheic zone acts as a heat exchanger between the warm waste water and the river. In addition to mitigating the thermal effects on the river, the hyporheic zone may delay a pulse of warm waste water from entering the river until after the critical summer months have passed. The effluent pulse would also be attenuated by mixing

(dispersion) with cooler subsurface water before entering the river. We will refer to this temporary storage of warm water in the hyporheic zone as “warm banking”.

To date, discussion of options involving hyporheic flow has focused on policy issues such as meeting Underground Injection Control (UIC) and Groundwater Quality Protection rules. In general, for discharge to the groundwater/hyporheic zone to be an option, a source will have to demonstrate to DEQ’s satisfaction that all the effluent discharged to the groundwater would discharge to the river via the hyporheic zone.

In short, streams throughout Oregon are water-quality–limited for temperature. This has focused DEQ’s attention on the temperature impact of permitted point sources that discharge to these streams, and on how to reduce or offset this impact. Both point and non-point sources of thermal pollution exist within Oregon, but for this study we examined only point sources. Among point sources, waste water treatment facilities account for 15-20% of total thermal pollution present in Oregon’s rivers and streams. Because of the pernicious effects of the pollution, municipalities across the state would like to find a way to mitigate the excess heat load that they are placing within the river/stream, or find a way to cool rivers/streams during the river’s most susceptible months (August – October).

Still, a basic technical question remains: What is the cooling capability of the underlying porous medium and to what extent might increased hyporheic flow result in lower river temperatures? If the degree of cooling likely to take place turns out to be insignificant, then groundwater discharge options will not be feasible and sources can choose to focus their resources on other options such as riparian shading, land application, and different treatment technologies. An annotated bibliography of relevant literature is provided in **Appendix A**, but the above questions are not adequately addressed in existing literature.

This Study - Overview

The impact of groundwater flow on stream temperature will of course to a large extent be site-specific, and yet some generalizations should be possible. The goal of this study is to provide a rough idea as to what site conditions and how many acres might be necessary to decrease or offset temperatures of a range of sources discharging to rivers in Oregon. An understanding of the magnitude of cooling that may be achieved via such actions will in turn inform related policy questions and assist sources in directing their own investigations of groundwater discharge. The intended audience is not only DEQ but also sources who may be interested in pursuing these options.

Toward the above goal, this study uses groundwater and heat flow modeling to analyze the cooling impacts associated with the following two hypothetical examples of hyporheic flow.

1. Floodplain-Channel Restoration (FPR): Determine the effect that floodplain-channel restoration has upon the temperature of the main body of the fluvial system. A side channel above the water table will be inundated with flood waters

and is here termed a floodplain channel. Upon inundation, flood waters will then seep through the subsurface as hyporheic flow into the main body of the fluvial system.

2. Subsurface effluent discharge (SED) to hyporheic zone: Determine the degree of cooling likely to take place for a particular discharge.

Sensitivity analyses are performed on each of the above scenarios to determine which parameters have the most impact on the degree of cooling achieved.

This study also utilizes a geographic information system (GIS) analysis to identify historic floodplains and opportunities for restoration. In addition to being useful to sources interested in pursuing floodplain restoration, it is hoped that this information will be useful to organizations that may choose to serve as “brokers” for such sources. Description of the GIS analysis and resulting data layers is provided in **Appendix B**.

To examine feasibility of the two possible stream-temperature-lowering techniques (warm-water injection and floodplain-channel restoration), a program named PetraSim was used. PetraSim is the graphical user interface for the TOUGH2 code. TOUGH2 was originally developed to model subsurface interactions of geothermal vents, buried nuclear waste containers, and VOC (volatile organic contaminants) interaction with a saturated/unsaturated subsurface (Preuss, 1998)

Using PetraSim/TOUGH2, a model was constructed that simulated a composite section of a riparian zone along the southern portion of the Willamette River. Composite in this case means that no specific site on the river was modeled, rather the model’s dimensions and values are average or representative values taken from a DEQ report on the southern Willamette Valley (Oregon DEQ, 2003). This model includes a main river channel, a slanted water table that empties into the river, an unsaturated zone, recharge due to precipitation, and representative values for subsurface parameters.

The subsurface parameters of interest were hydraulic conductivity, porosity, thermal conductivity, specific heat, and density. A sensitivity analysis varied these parameters to determine the effects of those variations on the transfer of thermal energy into the river, and ultimately river temperatures.

The sensitivity analysis also varied the injection and channel placement points. The maximum distance from the river that was analyzed by the model was 305 m. Over this 305 meter distance, different injection and channel points (30, 150, and 300 meter) were used to see the effect that distance had had upon heat mitigation using the hyporheic zone.

Simulated temperature changes were converted into heat fluxes (J/s), and the total heat flux (for each given case in the sensitivity analysis) into the river was computed. These computed fluxes were then scaled based on Willamette River to find the ultimate changes in temperature that would occur from the injection of wastewater into the subsurface for the months of August – October. Scaling parameters were based on the Metropolitan Wastewater Management Commission (MWMC) for a representative city in the southern

Willamette Valley. The MWMC was chosen as a representative example because it is the largest point source of heat influencing the TMDL along the upper main stem Willamette (ODEQ, 2004).

These temperature mitigation values were also compared with the current situation of direct injection of wastewater into the Willamette River. These temperature effects were found based on weighted average calculation that assumed that the river was instantaneously thermally mixed.

Finally, the hydraulic conductivity and the mass flow rate were increased to the model's computational limit. These conditions represented the "best case" scenario for wastewater injection. This hydraulic conductivity and flow rate were combined with the subsurface "default" injection case to formulate a "real world" scenario to help understand what the dimensions of the wastewater diffuser would need to be in order to handle an effluent load of 1.95 m³/s (68.8 cfs).

Groundwater and Heat Flow Modeling

Few software packages can account for both groundwater flow and heat flow in the subsurface in three dimensional; the modeling program PetraSim/TOUGH2 was utilized for this project. TOUGH2 is a numerical simulator that was developed by researchers at the Lawrence Berkley Laboratory to track heat, water, radionuclides, and Volatile Organic Contaminants (VOCs) interactions in the subsurface (Pruess, 1998).

TOUGH2 is also able to model multi-phase subsurface interactions between the liquid, gaseous, and solid phases for the afore-mentioned subsurface variables (heat, water, radionuclides, VOC's). In addition to multiphase interactions, TOUGH2 can model the unsaturated (vadose) zone. This aspect of TOUGH2 is of particular importance for this modeling application where a channel above the fully saturated zone is filled with water that travels through the subsurface into the river.

TOUGH2 Defining Equations

TOUGH2 uses an integral finite difference numerical solving strategy, which means that it leaves the defining mass and energy balance equations in their integral form, rather than as partial differential equations. The solving strategy allows variable and irregular grid discretization for models in all three dimensions (Pruess, 1998). As a result, the mass and energy equations are functions of time and are coupled and solved via a Newton-Raphson iteration method

(http://web.mit.edu/10.001/Web/Course_Notes/NLAE/node6.html)

The Newton-Raphson iteration is used to find the root of complex equations whose analytical solution is either prohibitively difficult or impossible to solve. Equation (1) depicts the simplest form of this numerical method:

$$(1) \quad x_{n+1} = x_n - \frac{f(x_n)}{f'(x_n)}$$

where x_{n+1} is the desired value, x_n a known value, $f(x_n)$ is the value of the function at x_n , and $f'(x_n)$ is the derivative of the function at x_n . For complex functions, the derivative often cannot be found analytically, so the $f'(x_n)$ becomes:

$$(2) \quad f'(x_n) = \frac{f(x_{n+1}) - f(x_n)}{\Delta x}$$

where all variables are the same as in equation (1) and Δx represents the differential change of the function (dx).

The defining mass and energy balance that TOUGH2 uses in its most general form is shown in equation (3):

$$(3) \quad \frac{d}{dt} \int_{V_n} M^K dV_n = \int_{\Gamma_n} \vec{F} \cdot \vec{n} d\Gamma_n + \int_{V_n} q^K dV_n$$

where M^K is the mass or energy per unit volume, V_n is the chosen volume that is being integrated over, the superscript K above M is an integer that indexes substances (air, water, VOC, etc). For the right hand side of the equation, the vector \mathbf{F} is the mass/energy flux through the surface Γ , and the vector \mathbf{n} is the normal vector that is orthogonal to Γ . The flux term is then integrated over entire surface area Γ . For the source/sink term, q^K is the mass/energy in per unit volume into the model integrated over the total volume V_n . The accumulation term then must equal the energy and mass flux through an arbitrary surface plus a source/sink for mass and energy as a function of time

The accumulation term of equation (3) can be further dissected to yield a more complete view of the mass and energy balance. Equation (4) shows M^K as only a mass accumulation term:

$$(4) \quad M^K = n \sum_B S_B \rho_B X_B^K$$

Here n is porosity of the material, S_B is the fraction of the pore volume that phase B occupies, ρ_B is density of phase B , and X_B^K is the fraction of mass for component K in phase B . For the energy accumulation term,

$$(5) \quad M^K = (1-n)\rho_R C_R T + \sum_B S_B \rho_B u_B$$

Here all the variables are the same except ρ_R is the grain density of the subsurface medium, C_R is specific heat of the subsurface, T is the temperature of the subsurface, and u_B is the specific internal energy of phase B .

From the right-hand side of equation (3), the advective flux \mathbf{F} can be further broken down:

$$(6) \quad \bar{F}_{Adv} = \sum_B X_B^K \bar{F}_B$$

All variables are the same as above. TOUGH2 is a groundwater model, and so the individual fluxes, \mathbf{F}_B , are defined by is a multi-phase version of Darcy's Law that accounts for absolute and relative permeability, viscosity, and pressure:

$$(7) \quad \bar{F}_B = -k \frac{k_{rB}}{\mu_B} (\nabla \bar{P}_B - \rho_B \bar{\mathbf{g}})$$

Here k is the permeability, k_{rB} is the relative permeability of phase B , μ_B is the viscosity of the fluid in phase B , the vector \mathbf{P}_B is the pressure of phase B , and the vector \mathbf{g} is gravitational acceleration. \mathbf{P}_B is the combined reference pressure in the gas phase and the capillary pressure. The "del" operator evaluates the changes in pressure in the three spatial dimensions. All other variables are the same as previously defined.

The heat flux component of \mathbf{F} accounts for conductive and advective fluxes:

$$(8) \quad \bar{F}_{B,Heat} = -\lambda \nabla T + \sum_B h_B \bar{F}_B$$

where λ is the thermal conductivity and h_B is the specific enthalpy of phase B . Again, the 'del' operator evaluates the temperature in three dimensions.

TOUGH2 includes equations that define diffusive fluxes:

$$(9) \quad \bar{F}_{B,Dif} = -\sum_B \rho_B \bar{D}_B^K \nabla X_B^K$$

where \mathbf{D} is the vector of diffusion coefficients in three dimensions. Of particular interest for this project is the diffusion equation that defines how water moves through the vadose zone to the water table. If temperature-driven changes in liquid viscosity and density are neglected, the TOUGH2 equation that defines vadose zone water movement is shown by:

$$(10) \quad \frac{\partial}{\partial t} n = \nabla \cdot [K \nabla h_H]$$

Here n is the porosity multiplied by the fraction of the pore volume taken up by water, the vector \mathbf{K} is the three dimensional hydraulic conductivity (for this project \mathbf{K} equals K for all directions), and h_H is the hydraulic head (which is the addition of pressure and elevation heads).

Finally, a brief section on the discretization scheme that TOUGH2 uses is necessary for a fuller understanding of how the model arrived at its results. Again, TOUGH2 uses an integral finite difference discretization method to solve the couple energy and mass balance equations. Taking TOUGH2's basic energy and mass balance equation,

discretizing with respect to space, and volume averaging the values, the accumulation term of equation (3) becomes:

$$(11) \quad \int_{V_n} M^K dV = V_n M_n$$

Here M_n is the volume averaged value of either heat or mass. The heat and mass flux values on the right side of equation (3) are similarly discretized over an average surface area A_{nm} and the corresponding mass/heat flux \mathbf{F}_{nm} passing through that area (Figure 4):

$$(12) \quad \int_{\Gamma_n} \bar{\mathbf{F}}^K \cdot \bar{\mathbf{n}} d\Gamma = \sum_m A_{nm} \bar{\mathbf{F}}_{nm}$$

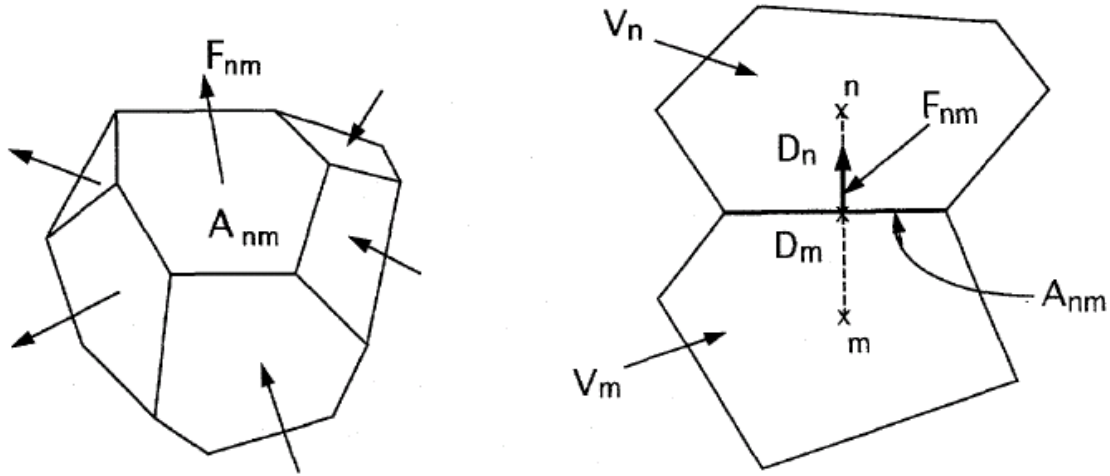


Figure 4. The various components of equations (11) and (12) and how they are spatially represented in TOUGH2 (Pruess, 1998)

\mathbf{F}_{nm} for the mass flux is the multi-phase version of Darcy's Law (equation (7)) but in its discretized form, which illustrates how TOUGH2 spatially solves the groundwater flux component of the mass/energy equation:

$$(13) \quad \bar{\mathbf{F}}_{nm} = k_{nm} \left[\frac{k_{rB} \rho_B}{\mu_B} \right]_{nm} \left[\frac{P_{B,n} - P_{B,m}}{D_{nm}} - \rho_{B,nm} g_{nm} \right]$$

From equation (13) and Figure 4, TOUGH2's method for evaluating groundwater movement between cells can be seen. D_{nm} is the distance between the center of the two cells, $P_{B,n}$ and $P_{B,m}$ are the total pressures for points m and n . The $P_{B,n}$ and $P_{B,m}$ divided by D_{nm} averages the pressure between the two cell nodes (as seen in Figure 4). All other variables are the same as the previous Darcy's Law equation, except now they represent the averaged values between the two cells m and n .

Substituting equations (11) and (12) into equation (3), the discretized basic energy and mass balance equation with the source/sink term added becomes:

$$(14) \quad \frac{dM_n^K}{dt} = \frac{1}{V_n} \sum_m A_{mn} \bar{F}_{nm}^K + q_{nm}^K$$

which is an ordinary coupled differential equation. The last step is to discretize equation (14) with respect to time. The result is an equation that varies in four dimensions (x, y, z, and time):

$$(15) \quad 0 = R_n^{K,k+1} = M_n^{K,k+1} - M_n^{K,k} - \frac{\Delta t}{V_n} \left[\sum_m A_{mn} \bar{F}_{nm}^K + V_n q_{nm}^K \right]$$

This final equation has k as the time index, Δt is time step (therefore, $k + 1$ is simply $k + \Delta t$), and R_n is the residual. This final equation is combined with the Newton-Raphson iteration method and evaluated based upon model parameters and convergence requirements set by the user.

PetraSim

TOUGH2 is a complex (and robust) program. As a result, using TOUGH2 in its full form is both difficult and time consuming. To remove the difficulty of using TOUGH2 in its code form a Graphical User Interface (GUI) called PetraSim was created by Thunderhead Engineering. PetraSim enables users to manipulate both the inputs and outputs of TOUGH2 in a way that avoids some of the cumbersome aspects TOUGH2. The trade off of using PetraSim is that some of the more detailed data outputs from TOUGH2 are obscured, and for very complex applications/projects, analysis of the complete TOUGH2 output file would be necessary.

For this project, however; PetraSim's outputs were sufficient to model a representative section of the southern Willamette Valley. The variables/dimensions of interest, separated into fluvial, waste water effluent, and hyporheic zone classifications for the PetraSim/TOUGH2 model were:

River Characteristics:

- Temperature
- Dimensions

Effluent Characteristics:

- Flow
- Temperature
- Magnitude of excess heat load

Hyporheic Zone and Floodplain Characteristics:

- Depth through which subsurface flow make take place
- Hydraulic conductivity of subsurface materials
- Groundwater gradient/flow velocity
- Thermal conductivity

- Density
- Specific Heat
- Ambient subsurface temperature before addition of effluent
- Source/magnitude of groundwater recharge, such as that from upland flow or winter/spring flooding events

With these variables and model dimensions agreed upon as the prime factors that affect hyporheic cooling, a basic model was created using PetraSim that incorporated nearly all of the above characteristics. This basic model then served as a foundation for both the Flood Plain Restoration (FPR) and the Subsurface Effluent Discharge (SED) scenarios.

Hyporheic Zone Modeling Scenarios:

Modeling for this project took two distinct, but inter-connected steps. The first step was to create a foundation model that would serve as the starting point for both the Floodplain Restoration (FPR) and the Subsurface Discharge SED scenarios. The second step was to create two distinct models for the FPR and SED scenarios using the foundation model.

General Modeling Considerations:

Necessary modeling parameters include:

Model Parameters:

- Equation of State
- Temperature
 - Ground/Subsurface
 - Atmospheric
 - River
 - Groundwater
- Dimensions
 - Total model
 - Fluvial body
 - Flood plain restoration channel

Warm Water Injection Initial Conditions:

- Flow rate
- Injection time
- Temperature

Hyporheic Zone and Floodplain Parameters and Boundary Conditions:

- Vadose zone depth
- Hydraulic conductivity of subsurface parameters
- Groundwater flow into a river
- Thermal conductivity
- Specific Heat
- Density
- Precipitation recharge

Special note should be made of the Equation of State modeling parameter. Because TOUGH2 has the ability to model a wide range of subsurface phenomenon, to reduce computation time, an initial Equation of State (EOS) is selected at the beginning of the modeling that defines what subsurface parameters are available for manipulation.

Foundation Model:

A default model incorporated the above-mentioned boundary/initial conditions, with default subsurface parameters values that were representative of values found in the southern Willamette Valley. The foundation model was created in four separate steps. The first step was selection of the basic characteristics of the model e.g., the entire domain's dimensions, dimensions of individual cells, the appropriate Equation of State (EOS) module within TOUGH2, and specification of the various "materials," both subsurface and atmospheric, employed by the model.

The second step involved the creating the models boundary conditions, and creating constant head initial conditions. The third step used the constant head initial conditions to set up a steady state with a slanted water table that was fed by constant precipitation recharge. The final step involved the addition of a static water body used to simulate the Willamette River.

Step I

The overall dimensions of the model were decided upon based on both project requirements and restrictions on the number of cells feasibly modeled by PetraSim/TOUGH2.

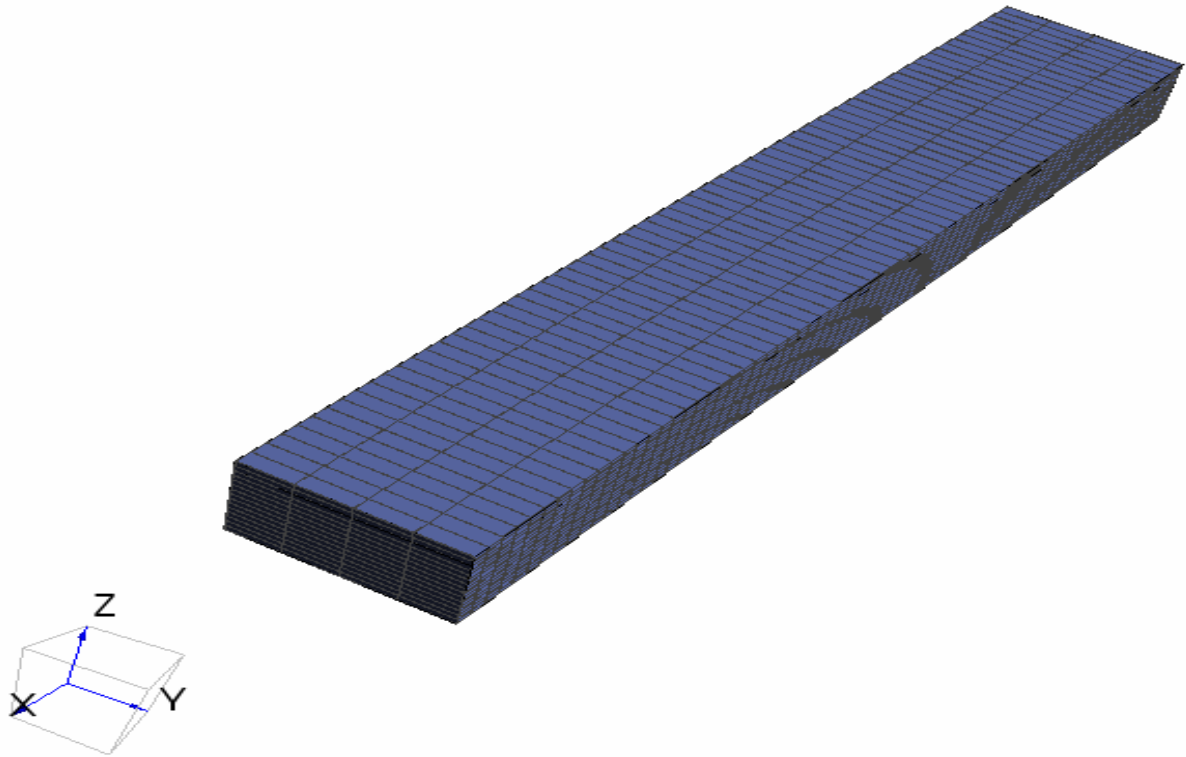


Figure 5. PetraSim's visual rendering of model used in this project

The x-axis distance was the driving dimension because it had to have the main channel of the water body, accommodate for flood restoration channel, and 305 m (1000 ft) for maximum distance for hyporheic flow.

The model dimensions and cell divisions for the foundation model:

- Model Dimensions:
 - X-axis: 355 m
 - Y-axis: 60 m
 - Z-axis: 30 m
- Cells Divisions:
 - X-axis: 71 @ 5 m
 - Y-axis: 4 @ 15 m
 - Z-axis: 15 @ 2 m
 - Volume: 150 m³
- Total Cells (including boundary cells):
 - 2460

For this project, an EOS called T2VOC was selected. While primarily designed to model VOCs, T2VOC also allows simple specification of a slanted groundwater table and was chosen for that reason, though VOCs are not part of this project's scope.

The final portion of step one involved establishing the materials for the subsurface, atmospheric, and open water boundary conditions. This was especially important

because, though the subsurface variables can be varied in PetraSim, a “base” setting for material variables would need to be created for the sensitivity analysis. To this end, two initial materials were created (Table 2).

Table 2. Parameters and values for subsurface and atmospheric “materials.”

Subsurface Properties		Air/Standing Water Properties	
Density (kg/m ³)	2650	Density (kg/m ³)	2650
Porosity (-)	0.3	Porosity (-)	0.999
X Permeability (m ²)	4×10 ⁻¹²	X Permeability (m ²)	4×10 ⁻⁹
Y Permeability (m ²)	4×10 ⁻¹²	Y Permeability (m ²)	4×10 ⁻⁹
Z Permeability (m ²)	4×10 ⁻¹²	Z Permeability (m ²)	4×10 ⁻⁹
Thermal Conductivity (W/m-K)	0.52	Thermal Conductivity (W/m-K)	3.1
Specific Heat (J/kg-K)	1840	Specific Heat (J/kg-K)	1000

It should be noted that the atmospheric material is 99.9% porous. This means that the material is air for all intents and purposes (density, thermal conductivity, etc.) Atmospheric conditions and standing water have very similar material parameters. The only difference between the two is the water saturation for atmospheric conditions is set at 0% while the water saturation for the open water has a water saturation of 100%. Because the material is basically 100% porous (void space filled with air), when this material is completely saturated, the material is standing water. Also, all of the densities in this report are grain densities.

Step II

With the basic model dimensions, cell divisions, equations of state in place and material specifications created, constant head boundary conditions for the model had to be established. Also, the atmospheric material was applied to the top of the model, and temperature and pressure initial conditions were programmed and fixed for the atmosphere.

The first boundary condition was a thin atmosphere at the top of the model. At 29.9 m on the z-axis another cell division that created a 0.1 meter thick plane of cells (in the x-y plane). The temperature was set to 20°C (this value is arbitrary, and was changed to fit the specific modeling scenario), the pressure was 1.01×10⁵ Pa, which is standard atmospheric pressure, and the water saturation was set to zero. These conditions were then fixed for the boundary condition cells at the top (x – y plane) of the model.

The second boundary condition was setting constant groundwater pressure head boundaries on the z – y planes at the ends of the model (Figure 6, Figure 7).

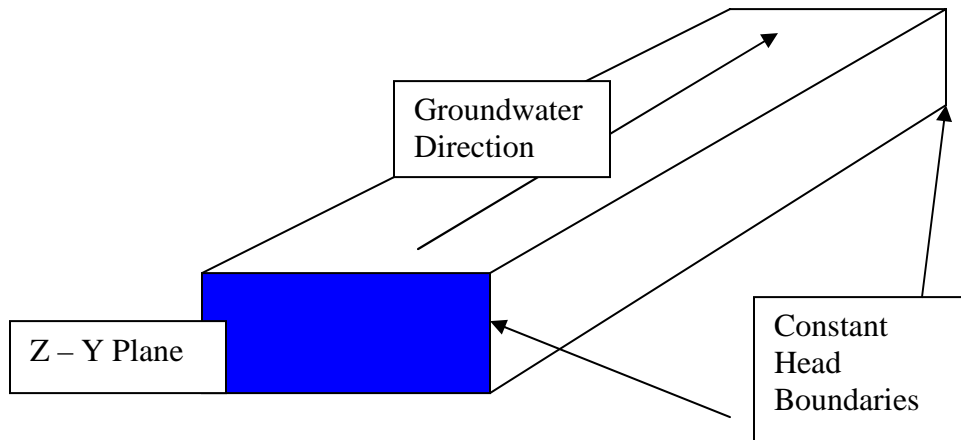


Figure 6. Conceptual picture of the constant head boundary conditions.

The constant head conditions implemented were based upon an Oregon DEQ groundwater report for the Southern Willamette Valley (REF). This report stated that the hydraulic gradient of the Willamette Valley ranges 2-60ft per mile, with an average value of 0.0057 m/m. The models dimensions are 355 m on the x-axis with a two meter difference in the water table depth along the z-axis for a hydraulic gradient of 0.0056 m/m.

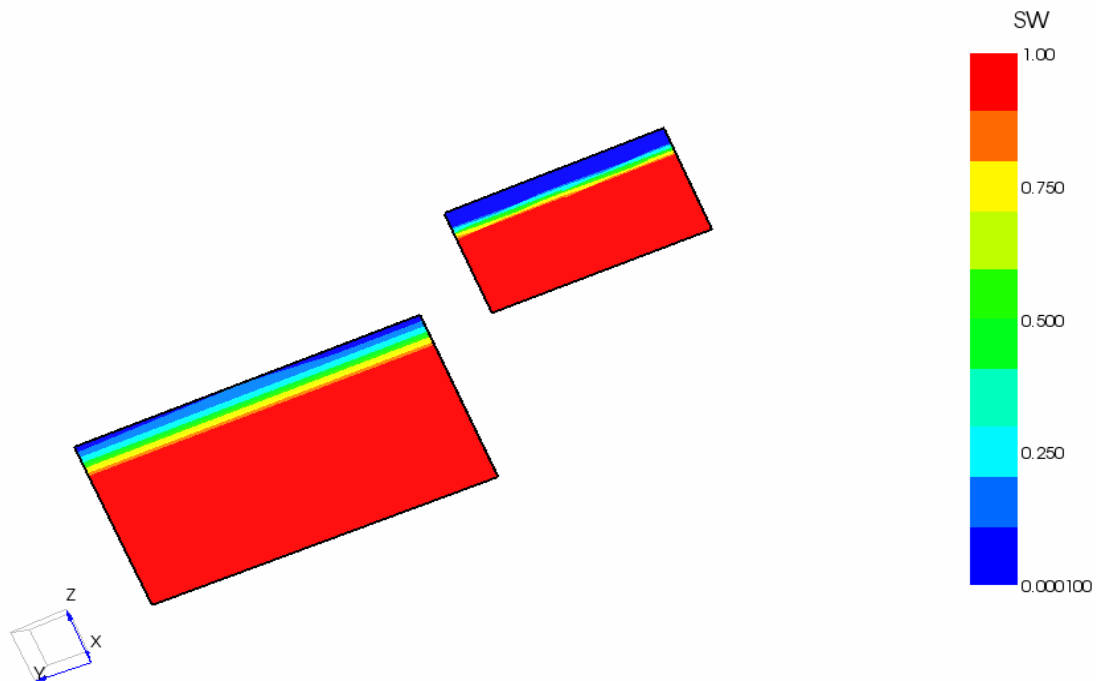


Figure 7. Constant-head boundary conditions as a percentage of water saturation. The red represents the 100% saturation of the porous subsurface; dark blue represents 0% saturation. In the case of the dark blue, the medium is the atmospheric boundary conditions above the water body.

One of the sides (the rectangles in the figure) has a larger zero water saturation zone at the top of model. This is both the atmospheric boundary conditions above the model, and

the slanted water table. By offsetting the saturation conditions in the z – y planes of the model, it forced groundwater to flow from the higher saturation to the lower saturation condition.

The vadose zone depth for the model is two m (6.6 feet). This is a reasonable value for the Willamette Valley, though it is somewhat thicker than one would expect in close proximity to a water body. The constant head conditions themselves were set up in PetraSim through fixing the subsurface water saturation at the ends of the model (Figure 7), not fixing different pressure head values for the model’s ends.

Step III:

For the third step of the model, a groundwater recharge source was added to the cells just below the atmosphere cells. The precipitation rate was one foot per year, or 1 inch per month distributed over the entire area of the model. The final recharge value changed to a mass rate based on the density of water, and was further scaled down one thousand times to 7.34×10^{-7} kg/s per cell to reflect the effluent injection rate (Figure 8).

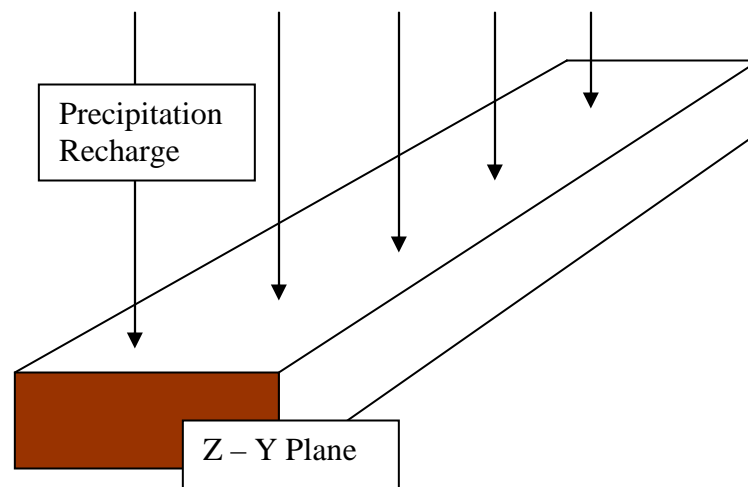


Figure 8. A conceptual rendering of the model’s precipitation recharge in the Z – Y Plane

After the precipitation recharge was established, the constant head boundary conditions were imported from the previous simulation and fixed at both ends of the model. The model was then run for one hundred years. The one hundred year run time was used in order to establish a steady-state slanted water table that was fed by the precipitation.

Step IV

After establishing the water table, a “river channel” was constructed by converting some of the cells down gradient into atmospheric materials. These converted cells were then fully saturated with water, and the model ran for another one hundred years. Again, the purpose of the hundred year model run time was to establish a water body within the model to which there was groundwater discharge.

The water body's dimensions were 50 m on the x-axis, 60 m on the y-axis, and 2 m in the z-axis for a total volume of 6000 m³. These dimensions conform to a general rule of thumb that the width of a river is roughly twenty times depth.

For the final foundation model run, "default" subsurface parameter values were established. These parameters were used as the "base case" for the sensitivity analysis. Unless otherwise stated, these values served as the default values for the sensitivity analysis, and were only varied one at a time:

Table 3. Default parameters and values

Parameter	Value
Density (kg/m ³)	2650
Porosity	0.3
Hydraulic Conductivity (m/s)	5×10 ⁻⁴
Thermal conductivity (W/m×°K)	0.52
Specific Heat (J/kg×K)	1840

With these parameters in place along with a river body that collected the groundwater recharge, the SED and FPR scenarios could be individually modeled. It should be noted that the worst case scenario for health of natural water bodies in Oregon the month of August. Thus, if the temperature impacts to rivers could be mitigated using the hyporheic zone during that month, the fluvial temperature effects for the other late summer/early fall months could presumably also be treated by the hyporheic zone.

SED Scenario

After the foundation model was created, the SED scenario was created. First, all of the atmospheric and subsurface temperatures were changed to 8°C. Then the precipitation recharge enthalpies were changed to 3.37×10⁴ J/ kg (8°C), and the river's temperature was also adjusted to 8°C. With these conditions in place, the injection cells were placed 6 m down from the ground-atmosphere interface perpendicular with the river on the x - z plane (Figure 9).

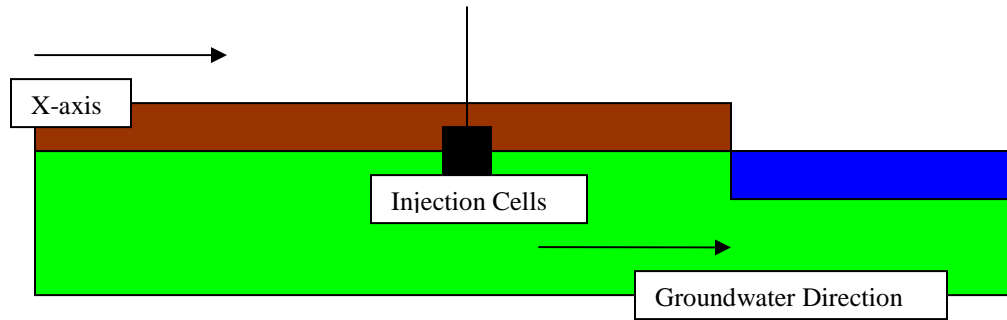


Figure 9. Side view of the SED case in the X – Z plane The brown section is the vadose zone, the green section is the saturated zone, and the blue section is the river. For the default case, the injection cells were 30 meters away from the river along the x axis. The injection mass flow rate was 0.49 kg/s with an enthalpy of 9.66×10^4 J/ kg for 60 days.

FPR Scenario:

After the foundation model was created, the FPR scenario was created (simultaneously with the SED scenario). First, the subsurface and atmospheric temperatures were changed to 20°C. Then the precipitation recharge was adjusted to 9.40×10^4 J/ kg (20°C). Finally, the river's temperature was adjusted to 20°C as well. This ensured that the only thermal perturbation to the model would come from the side channel's cool water traveling through the subsurface into the river (Figure 10).

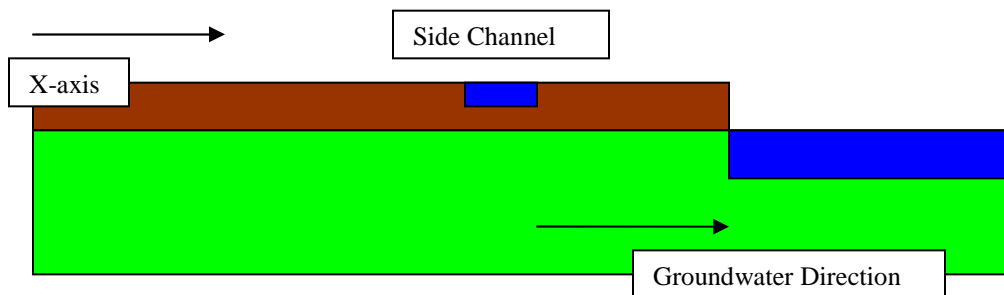


Figure 10. Side view of the FPR case in the X – Z plane. The brown section represents the vadose zone, the green section is the saturated zone, and the blue section is the river. The side channel is 30 m from the river, spans the entire model along the y-axis, and is 2 m deep. The initial temperature of the side channel's water was 8°C.

Analysis of Simulation Results

Measurement of Heat and Temperature Effects in the River

Metrics were developed to explain how much heat was entering the river in the SED case and how much of a decrease in temperature was occurring for the FPR case. The first obvious metric answers the question: How much heat (in Watts) is entering the river due to the wastewater injection case? This metric is called the heat offset:

$$(16) \quad \Delta H = H_R - H_0$$

where H_R is the heat rate (J/s) entering the river for the injection case, H_0 is the heat rate (J/s) entering the river for the non-injection, “natural” case, and ΔH is the heat offset due solely to the injection of warm wastewater.

ΔH was found by placing a control volume around the river and then performing a heat balance based upon thermal inputs, outputs, and storage within the river (Figure 11).



Figure 11. Heat balance for river channel.

This heat balance states that the heat flux entering the river body must equal the heat flux leaving plus the the rate of change of thermal energy stored in that body:

$$(17) \quad H_R = H_{out} + \frac{dE_T}{dt}$$

where E_T is the thermal energy stored in the river, H_R is the heat flux into the river, and H_{out} is the heat flux leaving the river. H_{out} was found from

$$(18) \quad H_{out} = nV_x AC_{water} \Delta T \rho_{water}$$

and the necessary model outputs, where all variables are the same except V_x is the velocity of water in the x-direction (m/s) and A is the cross-sectional area orthogonal to V_x (m^2). For the river body, the porosity to find H_{out} was 1 (water being completely mobile). The H_{out} term neglects heat leaving through the atmosphere. The heat leaving through the atmosphere was several orders of magnitude lower than the heat leaving through the river cells, and was thus negligible. Equation (18) can be applied to the subsurface; however, an adjustment to n has to be made. The rate of change in heat storage for the entire river is

$$(19) \quad \frac{dE_T}{dt} = \frac{C_{water} V \rho_{water} \Delta T_{Step}}{\Delta t}$$

where all variables are the same except ΔT_{Step} is the present time step’s temperature minus the previous time steps temperature, and Δt is the accompanying time step for the temperature change. Substituting equations (18) and (19) into equation (17), H_R was solved for each time step.

The second metric developed to understand how and when heat was moving into the fluvial body is the normalized heat offset. This metric seeks to quantify the amount of heat entering the river as a percentage of total heat injected into the system:

$$(20) \quad \Delta H_N = \frac{H_{River} - H_0}{\int H_{Injection} dt}$$

Here all variables are the same as above except $H_{Injection}$ is the heat rate being injected into the model in J/s. The integrated value of $H_{Injection}$ is simply the total amount of heat injected in Joules.

If the ΔH_N is graphed with respect to time and then integrated with respect to time, the area under the curve will equal 1 if all of heat injected into the model has left the model via the fluvial body as time goes to infinity:

$$(21) \quad \int_{t=0}^{t=\infty} \Delta H_N(t) dt = 1$$

If time does not go to infinity, equation (21) simply represents the amount of heat that has passed through the river for the model's given run time normalized by the total heat injected into the model. For this modeling application, ΔH_N as a function of time was not known, so a numerical integration technique needed to be applied to equation (21) to find the normalized amount of heat passing through the river.

The normalized heat rate was found by dividing the heat rate values by the total heat injected. To find the percentage of heat that had entered the fluvial body, a simple numerical integration technique was used. The integration technique used was the trapezoid method:

$$(22) \quad \int_{t=0}^t \Delta H_N(t) dt \cong \sum_{t=n+1} (t_{n+1} - t_n) \frac{1}{2} (\Delta H_{N,n} + \Delta H_{N,n+1})$$

The numerical integration for the SED case was presented two ways: The first way was the total integration of the normalized heat rate versus time curve. This integration scheme summed both the positive and negative values of the curve. The positive portion of the curve represented the warm water entering the river while the negative values represented the re-conduction of heat back into the subsurface.

The second way the SED integration was presented was by neglecting the negative normalized heat rate values. By excluding the negative heat rate, the total heat entering the river was represented. Re-conduction of heat to the river bed may happen in the real world; however, for the purposes of this report the total amount of injected heat entering the river is important. For the FPR simulations, the amount of "negative" energy was only presented; that is, the negative area under the normalized heat rate curve.

The final metric was simply temperature versus time for each of the modeling scenarios.

Scaling of Simulation Results

Because the river body in the model is static, the temperature differences from the model had to be scaled to the real world. Four factors contribute to the scaling factor: the

volume of the model's channel, the flow rate of the river, the flow rate out of the model, and a characteristic time:

$$(23) \quad f_s = \frac{V_{Channel} + Q_{River}t}{V_{Channel} + Q_{model}t}$$

where $V_{Channel}$ is the volume of static river body in the model in meters, Q_{River} is the flow rate of the river at low flow conditions in m^3/sec , Q_{model} is the flow rate leaving the model in m^3/sec , t is the characteristic time, and f_s is the scaling factor that the temperature outputs from the model are divided by to get the real river temperature. The characteristic time is the to peak temperature for the SED case or time to low temperature for the FPR case,

Equation (23) can be further simplified to yield a simpler result based on separating the numerator's terms under a common denominator:

$$(24) \quad f_s = \frac{V_{Channel}}{V_{Channel} + Q_{model}t} + \frac{Q_{River}t}{V_{Channel} + Q_{model}t}$$

Q_{model} is the velocity of water leaving the model in the x-direction multiplied by the cross-sectional area normal to the flow direction. Typical values of water velocity leaving the model are between 10^{-6} to 10^{-7} meters per second, and the cross-sectional area is 30 meters², for an average flow rate of 1.5×10^{-4} m^3/s . The low flow condition of the Willamette is approximately 141 m^3/s . Compared to flow rate for the river, the amount of water leaving the model is seven orders of magnitude lower than August low flow condition for the river.

$$(25) \quad f_s = 1 + \frac{Q_{River}t}{V_{Channel} + Q_{model}t}$$

This equation can be further simplified because Q_{River} multiplied by the injection time is much larger than Q_{model} multiplied for that same injection time. Also the flow rate of the river multiplied by the injection time, and then divided by the channel volume will be much greater than one. Thus, equation (25) further reduces to:

$$(26) \quad f_s \cong \frac{Q_{River}t}{V_{Channel}}$$

For both the FPR and the SED simulations, the characteristic time, t , was different because for each the time to peak (or low) temperature was different based on the subsurface parameter/initial condition that was being varied. Each of these characteristic times was included, along with the resulting scaling factor, in the results section of the FPR and SED sensitivity analysis.

Flood Plain Restoration Simulations

The Flood Plain Restoration case seeks to answer the question: Could rehabilitation of land that historically was connected to the main channel of the Willamette River during flood events serve as cooling mechanism via the hyporheic zone? Assumed for this scenario is that hyporheic flow is going to be cooler than the flow in the main channel of the Willamette River (Figure 12).

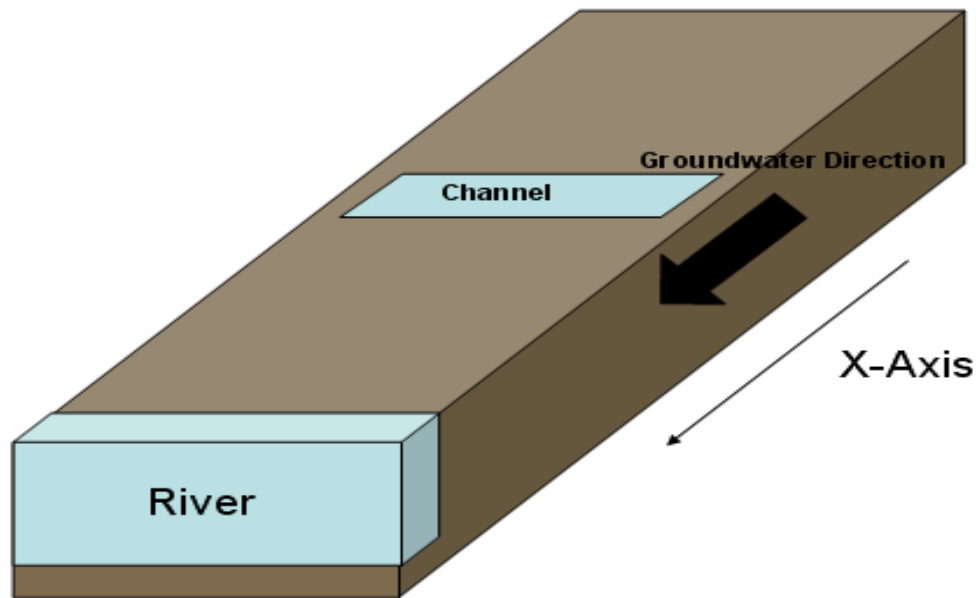


Figure 12. A conceptual drawing of the FPR modeling scenario; cool water travels out of the channel, into the subsurface, and then into the river where it lowers the river's temperature

The months of August – October are when Oregon's rivers are the warmest. High ambient temperatures combined with low flow rates in river bodies combine to create the worst-case situation where aquatic organisms are left vulnerable to low dissolved oxygen levels. Below summarizes the temperature and flow conditions for the months of August –October:

Stream Flow Characteristics:

- Flow: The main channel of the river will be considered to be static.
- Stream temperature = 8.0 °C (48 F) for floodwaters from November through April.
- Scaling Flow: 141m³/s (5000 cfs) in August.

Flood Plain Restoration Channel:

- 15 m x 60 m x 2 m, volume 600 m³
- Distance from the fluvial body is parameter to be explored in the sensitivity analysis
- Temperature of floodplain restoration channel is 8 °C

Though the river in the model was a static water body, the model's output will be scaled using the Willamette River's flow rates for August and the flow rate of water out of the model.

Results

In the subsequent plots of temperature versus time, the initial river temperature was slightly higher (0.008 degrees Celsius) than the preset 20°C. This slight temperature variation played a significant role because of the small change in temperature that the addition of a restored side channel caused to the river.

As a result, the data were analyzed in a slightly different fashion than the SED case. The difference lay in numerical integration scheme that was used to find the percentage of “cool” that entered the river as a result of the floodplain restoration. Instead of integrating the total area under the normalized heat rate versus time, positive heat rate values were eliminated so that the cooling effect due to the channel would not be lost due to minor positive temperature variations.

TOUGH2 was originally designed to model extreme subsurface phenomenon (i.e. nuclear waste seepage, VOC injection, etc). This means that TOUGH2 takes variables into account that other programs might not include. Because the changes in temperature for all of the FPR cases were very small, pressure effects from the side channel may have slightly raised the temperature of the river. The SED case experienced a similar effect, except that that the temperature of the river dropped slightly (0.005 °C) initially.

Finally, the normalized heat rate versus time plots were produced by first eliminating the positive heat rate values and then dividing the remaining data points by the total amount of “negative” energy that was contained within the channel. Using the following equation:

$$(27) \quad Energy = C \Delta T \rho_{water} V_c$$

where C is the specific heat of water (4186 J/°K-kg), ΔT is side channel’s change in temperature (20°C to 8°C), ρ_{water} is the density of water (998.29 kg/m³), and V_c is the volume of the channel (600 m³). Applying the values to equation (27), the total cooling effect due to the side channel is 7.52×10^9 J.

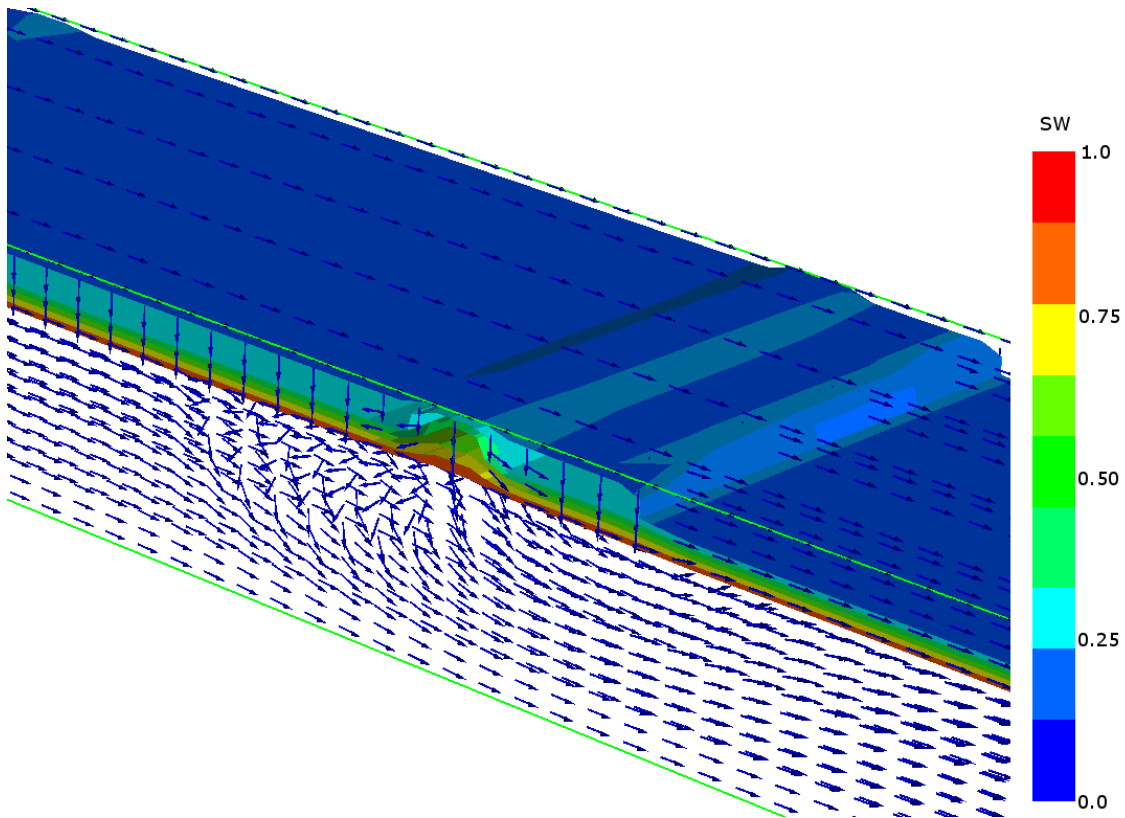


Figure 13. PetraSim’s graphical representation of the FPR scenario simulation results at 230 seconds. SW stands for percentage of water saturation for the model’s cells. In this figure the color red is the fully saturated zone with 100%, and blue is 0% saturation of the subsurface.

In the graphical representation of the simulation results (Figure 13), the multi-colored layer near the top of the model is the capillary fringe, i.e., the transition between the vadose zone and the fully saturated zone. Also, the abrupt “step” near the right end of Figure 13 is the transition from the ground to the river. The capillary fringe present above the river is only an artifact of the interface that PetraSim uses to graphically represent TOUGH2’s output. The river cells do not have variable saturation; they are all fully saturated.

The arrows in Figure 13 are the groundwater velocity vectors. At roughly half way in Figure 13 a ridge (or groundwater mound) can be seen in the water saturation iso-surfaces. This is the side channel while it still has water within it. Downward vectors can be seen emitting outward in all directions in the x-z plane. This is a groundwater mound due to “pooling” of water on top of the vadose zone.

As the simulation continued the mound’s size decreased until all of the water had seeped out of the side channel, through the vadose zone, into the water table, and ultimately into the river (Figure 14).

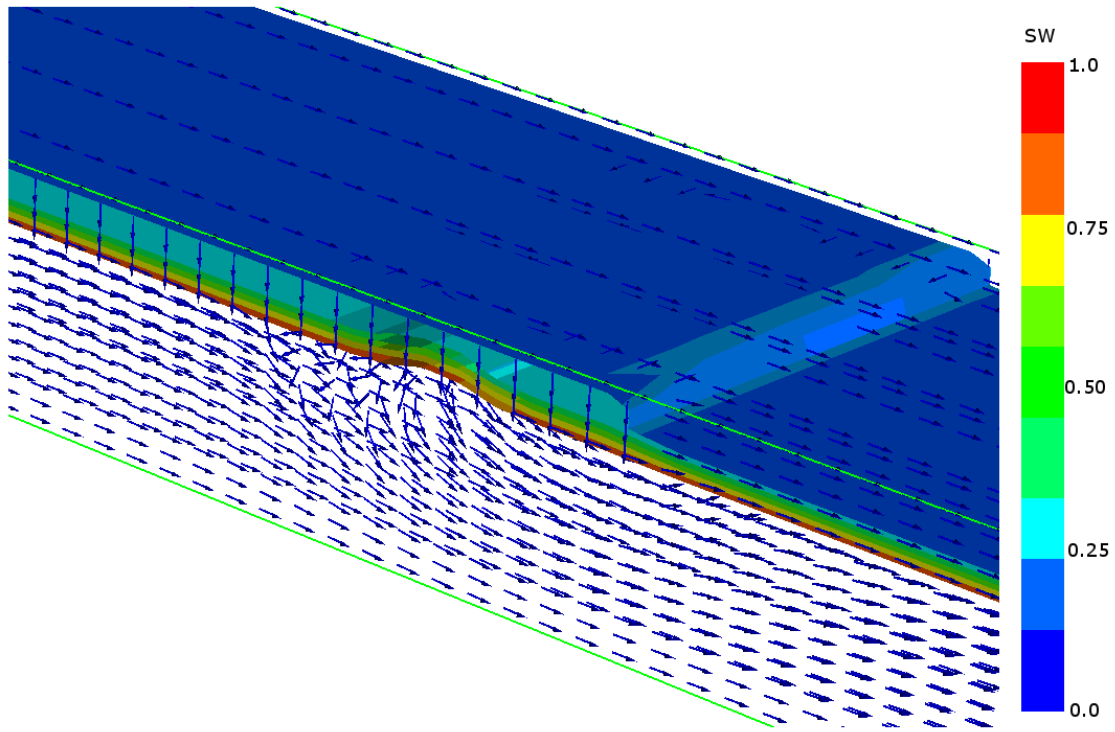


Figure 14. PetraSim’s graphical representation of the FPR scenario at 2250 seconds. All variables, symbols, and illustrative guides are the same as in Figure 13.

In Figure 14, the groundwater mound evident in Figure 13 is significantly smaller, and the model perturbation to groundwater velocity due to the mounding is less.

Sensitivity Analysis

Floodplain Restoration: Distance

For this series of simulations, the distance between the river and side channel was varied between 30 and 300 m (approximately 100 to 1000 ft). All other subsurface parameters were set to the default parameters (Table 3).

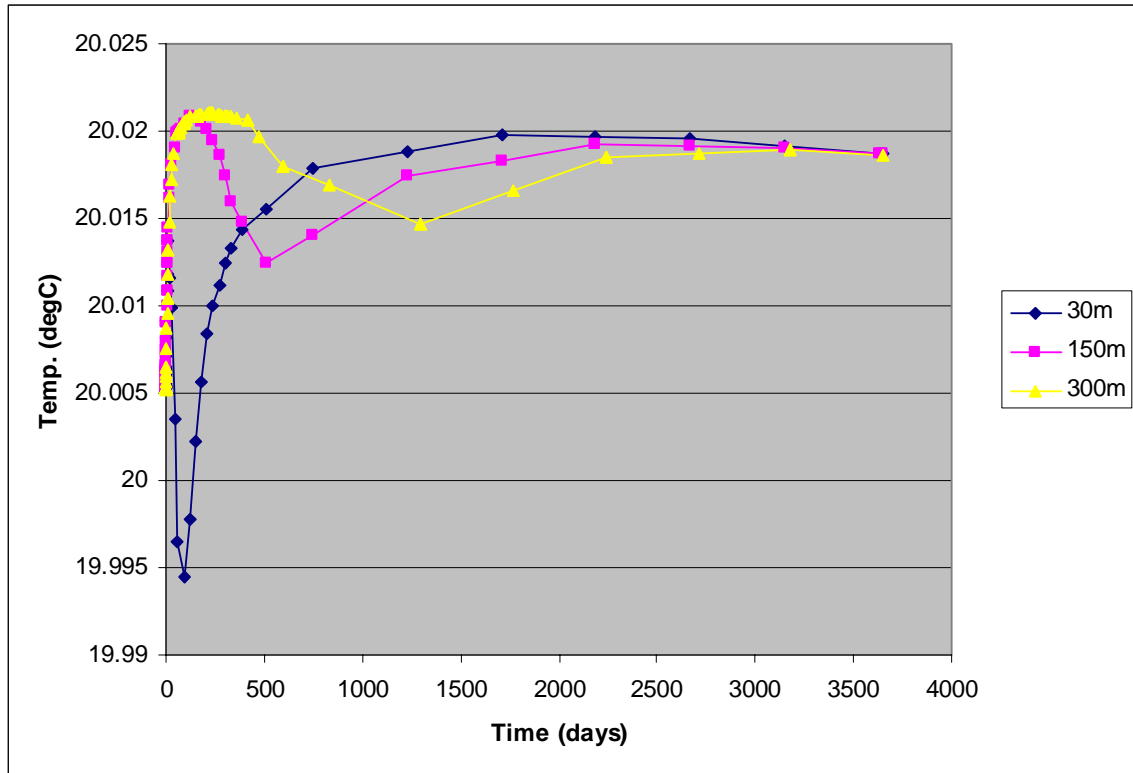


Figure 15. The temperature v. time plot for the distance varying FPR case

In Figure 15, the slight raising of temperature can be seen along with the fall in temperature for all three distances. The most pronounced dip in temperature occurs for the 30-m simulation at approximately 100 days. The next two distances have smaller temperature reductions, and at longer times.

FPR: Hydraulic Conductivity

The hydraulic conductivity is a proportionality constant in Darcy's Law (see equation (10)) that measures to what degree the subsurface transmits water. Subsurface mediums can have highly variable hydraulic conductivities (10^{-2} meters per second for loose gravel, 10^{-11} meters per second for impervious clay layers) and in many cases can be non-isotropic. For the simulations presented herein, hydraulic conductivity was isotropic, i.e., the same in all directions ($K_x = K_y = K_z = K$).

In the sensitivity analysis, the hydraulic conductivity was varied from 5×10^{-5} to 5×10^{-3} , the side-channel cells were 30 m from the river, and all other parameters conformed to the default case (Figure 16).

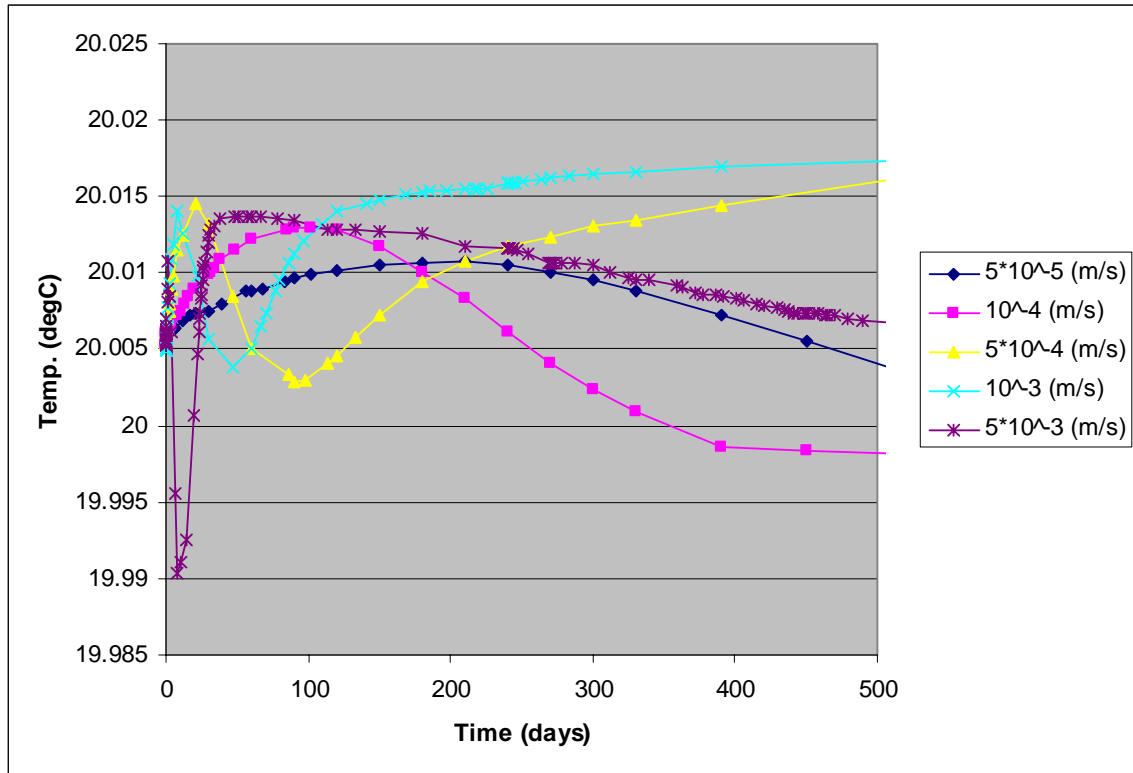


Figure 16. The temperature v. time plot for the hydraulic conductivity varying FPR case

From Figure 16, the lowest temperature drop due to side-channel cooling occurred at the highest hydraulic conductivity of 5×10^{-3} meters per second. The next highest value (10^{-3} m/s) did not have the next lowest temperature. The higher value of 10^{-4} m/s was next lowest value. This particular order of cooling effects is likely due to conduction of heat from the bed and banks, as the heat fluxes have a logical progression from highest to lowest conductivities, and the highest hydraulic conductivity has the largest negative heat flux (Figure 17, Table 4).

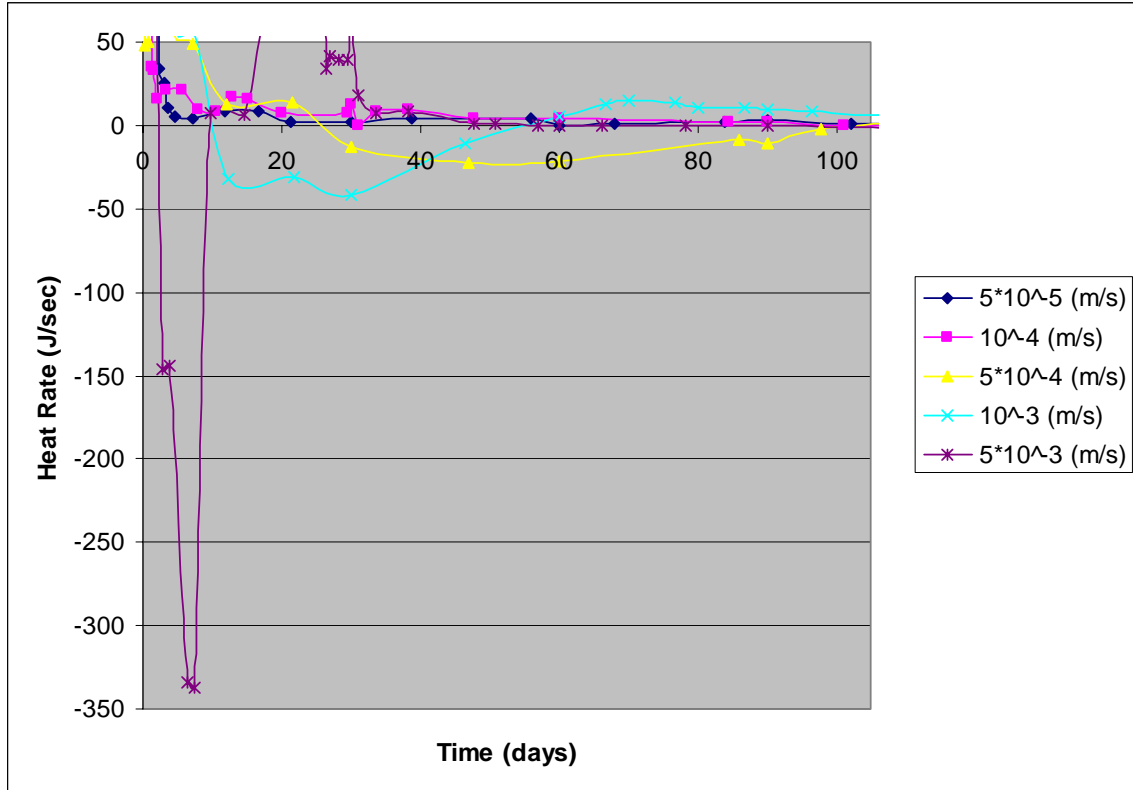


Figure 17. The heat flux (rate) v. time plot for the hydraulic conductivity varying FPR case. The scale is altered to show the negative heat rates that corresponds to the temperature drops in the fluvial body.

Table 4. Normalized heat flux versus time integrated to yield the percentage of cooling entering the river.

Hydraulic Conductivity (m/s)	Percentage of Heat Entering the River
5×10^{-5}	-0.78%
1×10^{-4}	0.00%
5×10^{-4}	-1.24%
1×10^{-3}	-1.33%
5×10^{-3}	-12.32%

Using the scaling factor from Table 5, the scaled temperature change for each case was calculated:

$$(28) \quad T_{Scaled} = \frac{T_{peak} - T_{Low}}{f_s}$$

where T_{Peak} is the peak temperature of the river body, T_{Low} is the lowest temperature experienced by the river body, f_s is the scaling factor, and T_{Scaled} is the scaled temperature.

Table 5. Minimum temperatures reached by river and scaled change in temperature due to cold banking for different values of hydraulic conductivity.

Hydraulic Conductivity (m/s)	Maximum Temperature (°C)	Peak Times (sec)	Scaling Factor	Scaled Delta Temperature (°C)
5×10^{-5}	19.998	1.11E+08	26176650	6.00E-10
1×10^{-4}	20.00	4.92E+07	11569050	-1.73E-06
5×10^{-4}	20.0029	7.78E+06	1827360	-1.09E-05
1×10^{-3}	20.00389	4.02E+06	944641.25	-2.12E-05
5×10^{-3}	19.9903	5.44E+05	127872.43	-1.56E-04

FPR: Porosity

For this simulation all other variables were the same as the default case (Table 3), except that the porosity was varied among the values, 0.15, 0.3, and 0.45. The porosity is the percentage of the subsurface that is empty space divided by the unit subsurface volume.

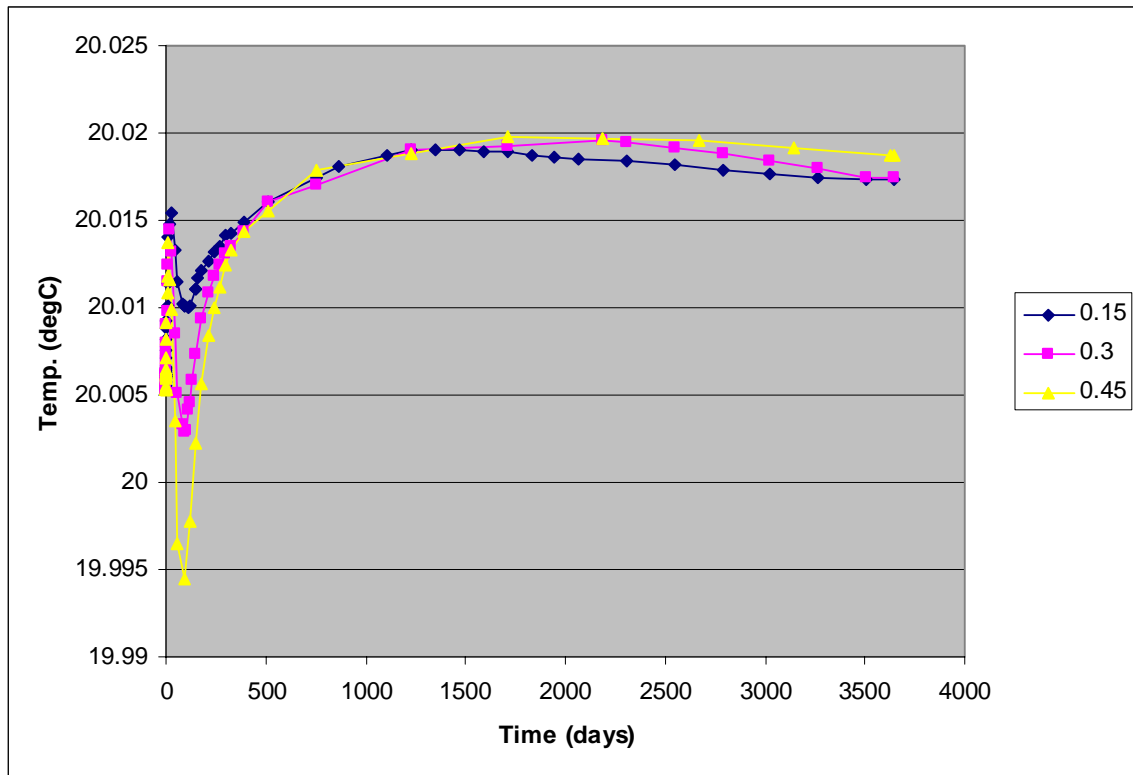


Figure 18. The temperature v. time plot for the porosity varying FPR case

Of note for the varying porosity case is that the highest porosity value of 0.45 had the largest decline in temperature due to the side channel (Figure 18). As porosity declined maximum temperature declined with the smallest temperature decrease accompanying

the smallest porosity. (This is especially worthy of comment given that the results of the injection case, presented below, did not follow this same trend.)

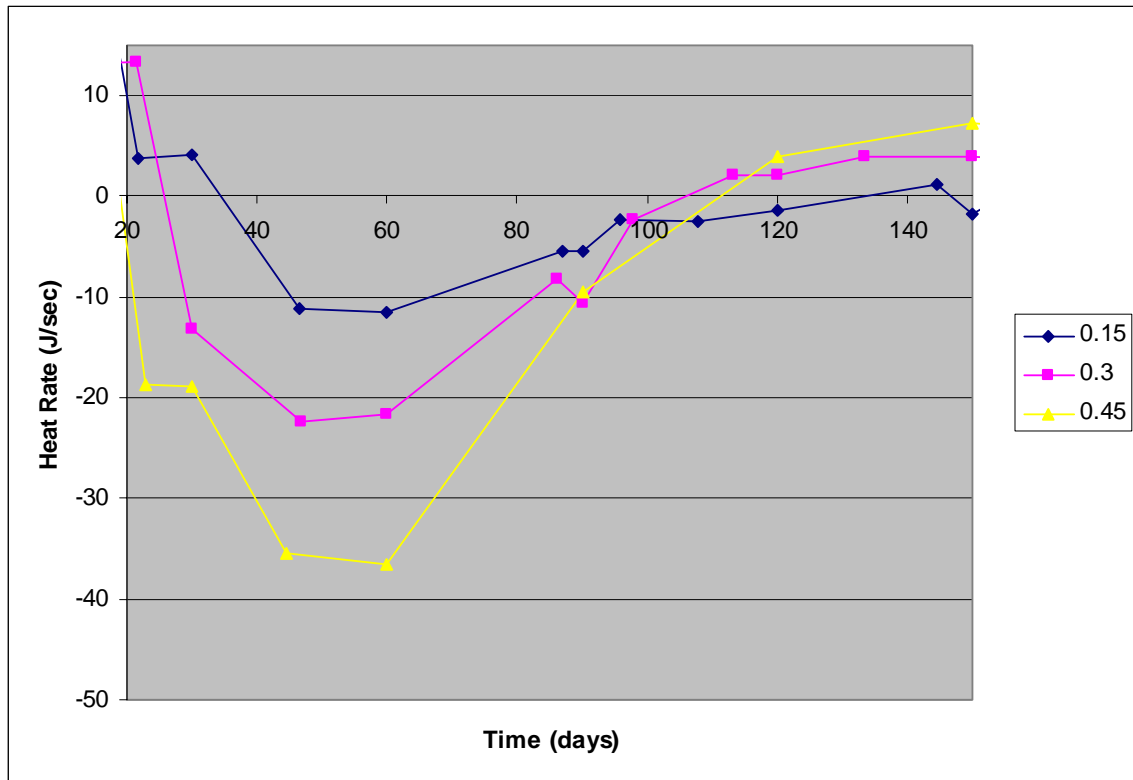


Figure 19. The heat rate (ΔH) v. time plot for the porosity-varying FPR . The x- and y-axes have been altered to emphasize the negative heat rate that corresponded to the cooling of the river due to side channel.

The cooling effect mirrors the temperature versus time plot: The highest porosity (0.45) accompanied the largest negative heat rate (Figure 19), but the integrated heat fluxes are counter-intuitive, as the largest percentage of cool water entering the river is due to the smallest porosity value (Table 6).

Table 6. Percentage of total cooling “felt” by the river due to the FPR option with varying porosity.

Porosity	Percentage of Heat Entering the River
0.15	-0.681%
0.3	-1.24%
0.45	0.000%

It should be recognized that the zero percentage value for porosity of 0.45 was not zero; however, it was so small that at three percentage-adjusted decimal points it was still zero.

Table 7. Minimum simulated river temperature and scaled change in temperature with varying porosity.

Porosity	Minimum Temperature (°C)	Peak Times (sec)	Scaling Factor	Scaled Delta Temperature (°C)
0.15	20.01	9313950	2188778	-3.16E-05
0.3	20.0029	7776000	1827360	-6.89E-05
0.45	19.9945	5180000	1218240	-1.13E-04

From these simulations, the porosity played a relatively small role in the transfer of cold water to the fluvial body. This was similar to the results from the injection case for varied porosity. Despite the relatively small scaling factor, the scaled change in temperature was small because of slight change in temperature due to the side channel (Table 7).

FPR: Density

Density of the subsurface medium was varied from 1515 kg/m³ (a representative grain density for soil) to 2650 kg/m³ (a representative grain density for stone). Density is a measure of mass per unit volume for a given material. All other parameters were set for the default case.

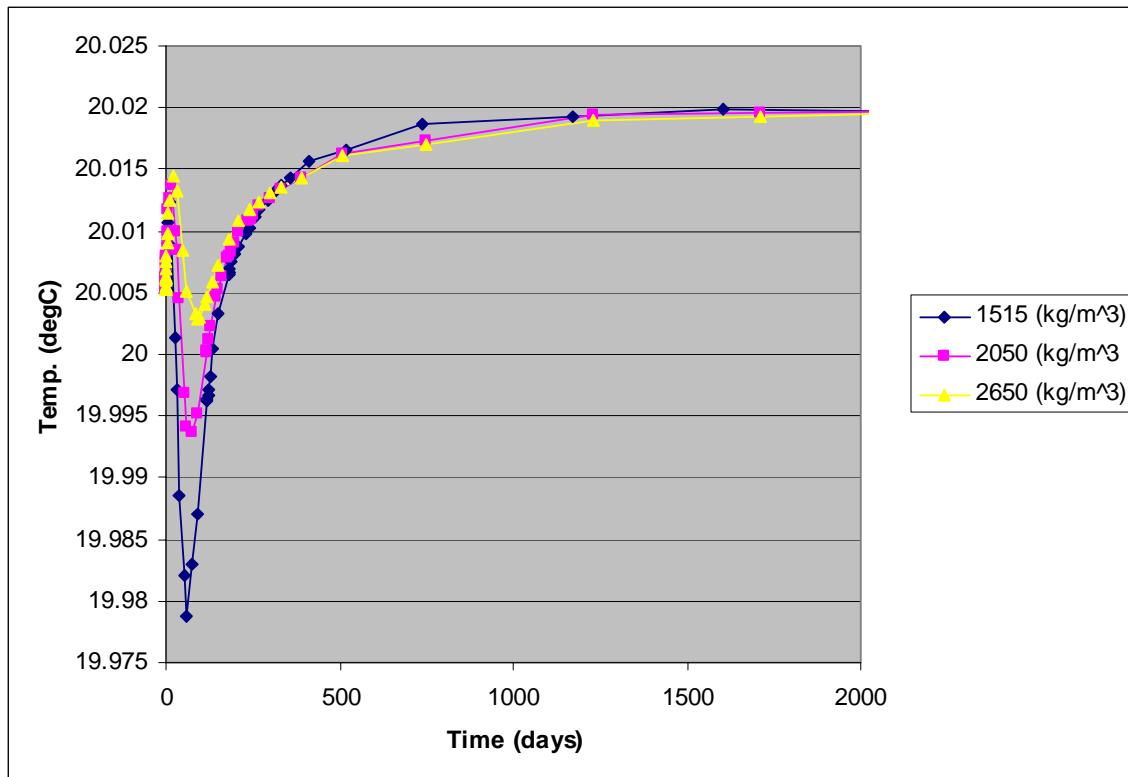


Figure 20. The temperature v. time plot for the density-varying FPR case

The minimum temperature becomes larger as the density increases (Figure 20). This is an interesting phenomenon because Darcy’s Law does not have a density term included. This means that there are other significant heat transfer factors at work in the subsurface in addition to groundwater movement. From equation (9), which defines diffusive fluxes, it can be seen that density is explicitly in the diffusion equation. This again shows that groundwater movement defined by Darcy’s Law is not the only significant contributor to thermal energy movement in the subsurface. Diffusion and conduction play a noticeable role in how river bodies are heated and/or cooled by subsurface groundwater flow.

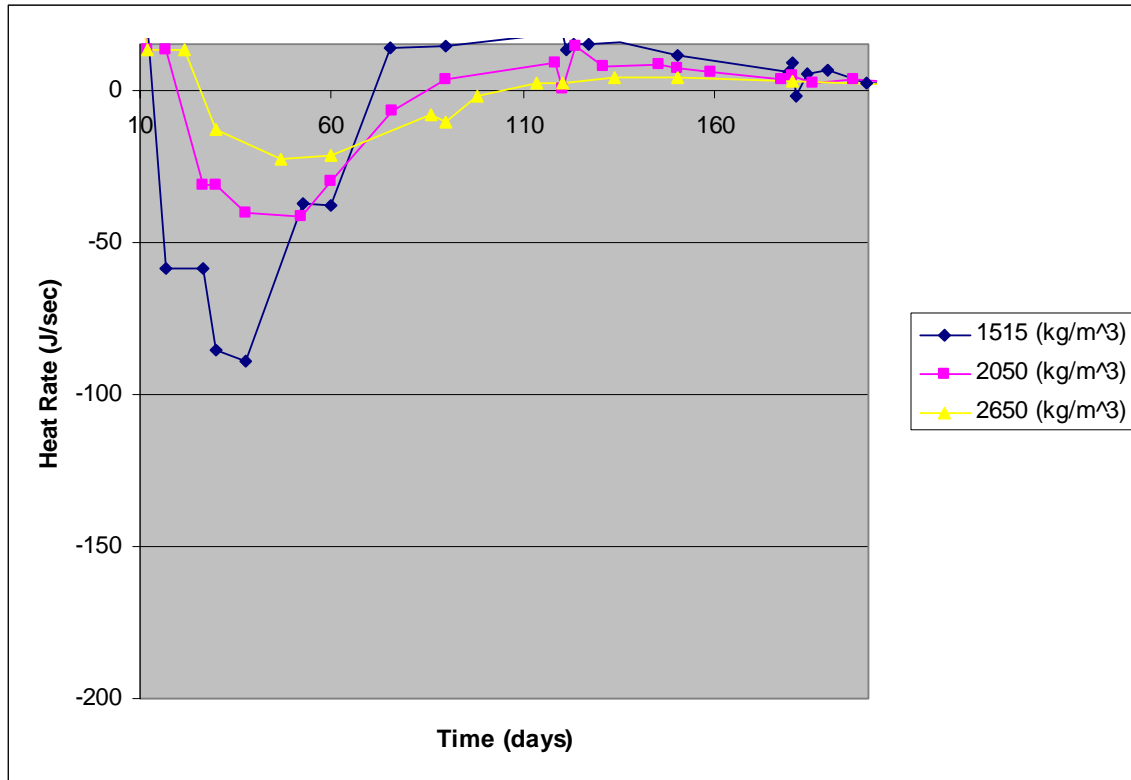


Figure 21. The heat rate (ΔH) v. time plot for the density varying FPR case. The x- and y-axes have been altered to emphasize the negative heat rate that corresponded to the cooling of the fluvial body due to side channel.

The “cooling flux” mirrors the temperature versus time plot: The lowest density (1515 kilograms per meters³) accompanied the largest negative heat rate (Figure 21).

Table 8. Percentage of total cooling “felt” by the river due to the FPR option with varying density.

Density (kg/m ³)	Percentage of Cool Energy Entering the River
1515	-2.99%
2050	-1.81%
2650	-1.24%

The percentage of negative thermal energy entering the river and the scaled temperature change are highest for the lowest-density subsurface material (Table 8, Table 9). This makes sense given that at lower material densities, thermal energy has less mass to travel through at lower densities (assuming that the specific heats are held constant). (The results for the injection case are similar except that the highest temperatures are associated with the lowest density.)

Table 9. Minimum temperature values for the river, and the scaled changes in low temperatures for the density-varying simulations

Density (kg/m ³)	Minimum Temperature (°C)	Peak Times (sec)	Scaling Factor	Scaled Delta Temperature (°C)
1515	19.9787	5.18E+06	1218240	-0.0002
2050	19.9936	6.56E+06	1541003	-0.00012
2650	20.0029	7.78E+06	1827360	-6.9E-05

FPR: Specific Heat

The specific heat is the measure of how much heat is needed to raise the temperature of one gram of a substance by 1° C. The units of specific heat are energy per unit mass multiplied by the temperature (in Kelvin). The specific heat represents the amount of thermal energy that a substance can absorb per unit mass. For this group of simulations, the specific heat was varied between 800 and 1840 J/ kg-°K (this range represented specific heat values between soil, stone, and sand).

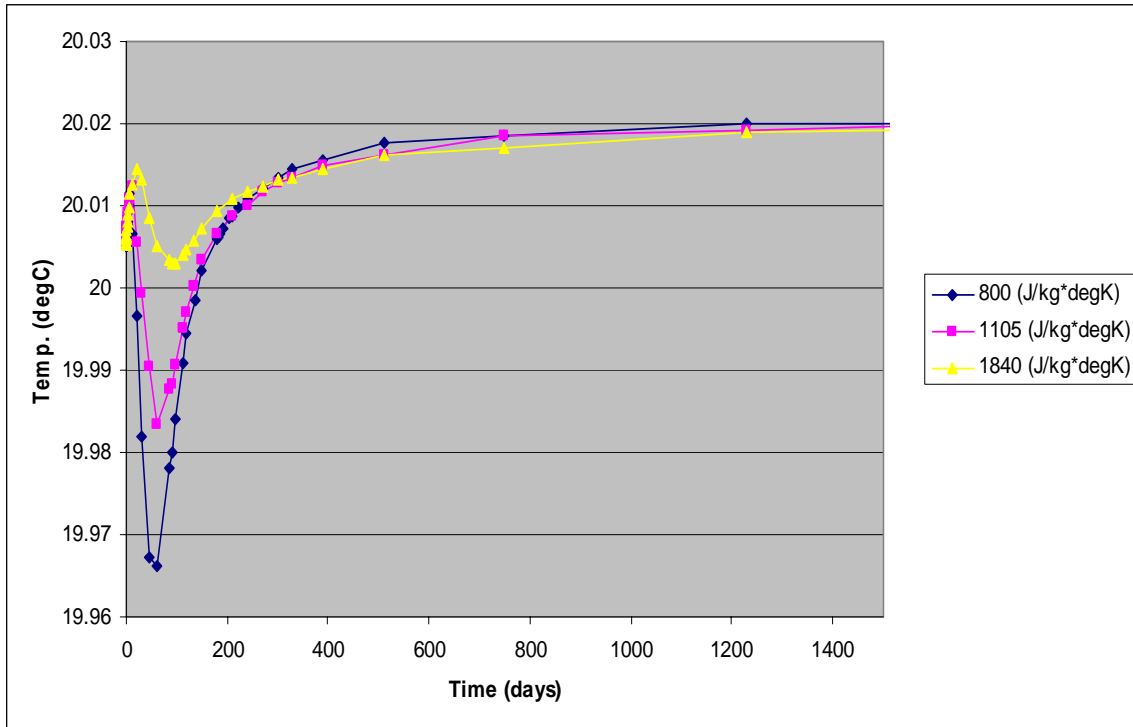


Figure 22. Temperature versus time plot for the specific heat side channel restoration simulations.

Figure 22 shows that lower values of specific heat cause both the temperature of the river to be lower and the time it takes for the low temperature to reach the river to be longer. For the specific heat values of 800 J/°K-kg and 1105 J/°K-kg, the differences are slight; however, for 1840 J/°K-kg (that corresponds to a specific heat for soil), the differences for both the low river temperatures were more pronounced.

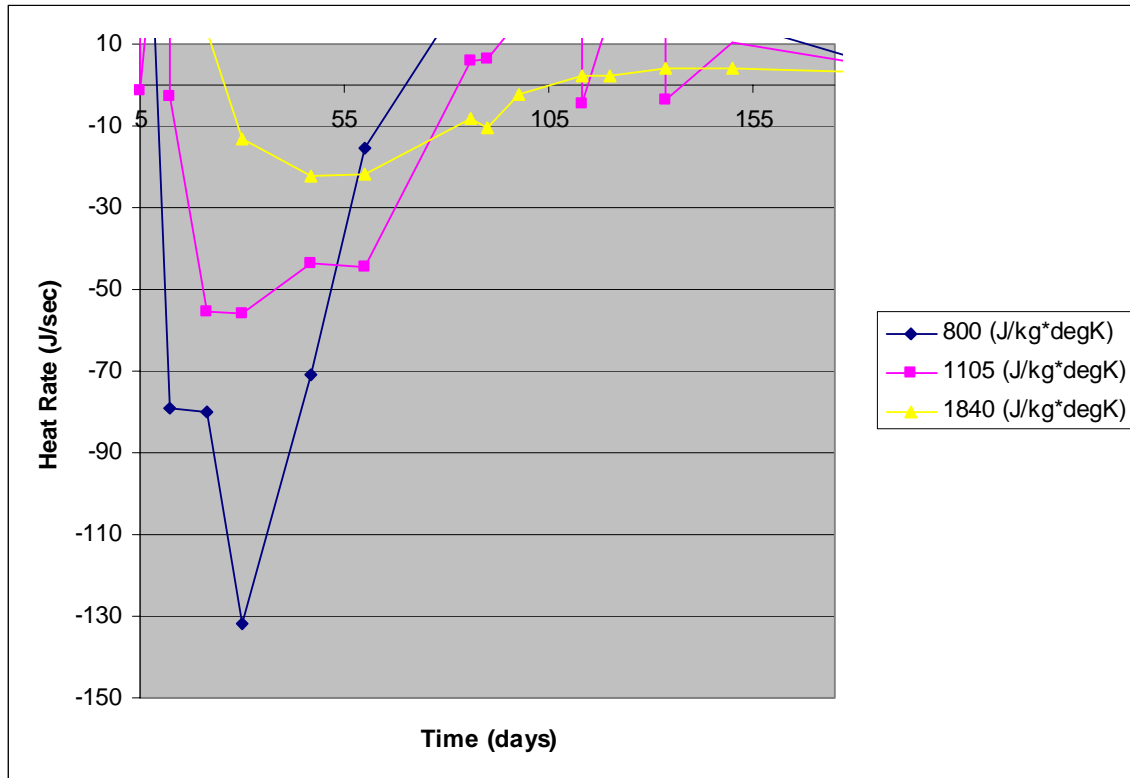


Figure 23. Heat rate (ΔH) v. time plot for the specific heat-varying FPR case.

Figure 23 shows that the most negative heat rate for this group of simulations is the 800 J/ $^{\circ}$ K-kg simulation. This low-temperature–specific-heat relationship points to specific heat being an important design consideration for the FPR scenario.

Table 10. Percentage of cooling reaching the river with varying specific heat.

Specific Heat (J/ $^{\circ}$ K-kg)	Percentage of Cooling Energy Entering the River
800	-0.00004105%
1105	-0.00002759%
1840	-1.24%

The percentages of cooling reaching the river (Table 10) are found by eliminating the positive heat rate values and dividing the remaining negative data points by the total amount of cooling energy. This curve was then integrated numerically (see the **Metrics** section). The scaled temperature changes (Table 11) are consistent with the temperature changes shown in Figure 22.

Table 11. Low temperatures and scaled changes in temperature for varying specific heat.

Specific Heat (J/ $^{\circ}$ K \times kg)	Minimum Temperature ($^{\circ}$ C)	Peak Times (sec)	Scaling Factor	Scaled Delta Temperature ($^{\circ}$ C)

800	19.9661	1.22E+06	286286.4	-8.31667E-05
1105	19.9835	5.18E+06	1218240	-5.41667E-05
1840	20.0029	7.78E+06	1827360	-2.18333E-05

FPR: Thermal conductivity

The thermal conductivity of a material is the ability of a material to transmit heat as a function of time. The units for thermal conductivity are Watts (energy per unit time) over °K multiplied by meters. For this group of simulations, the thermal conductivity was varied between the values of 0.52 – 2.6 W/m-°K. These values are representative values for different subsurface substances (soil, sand, and stone).

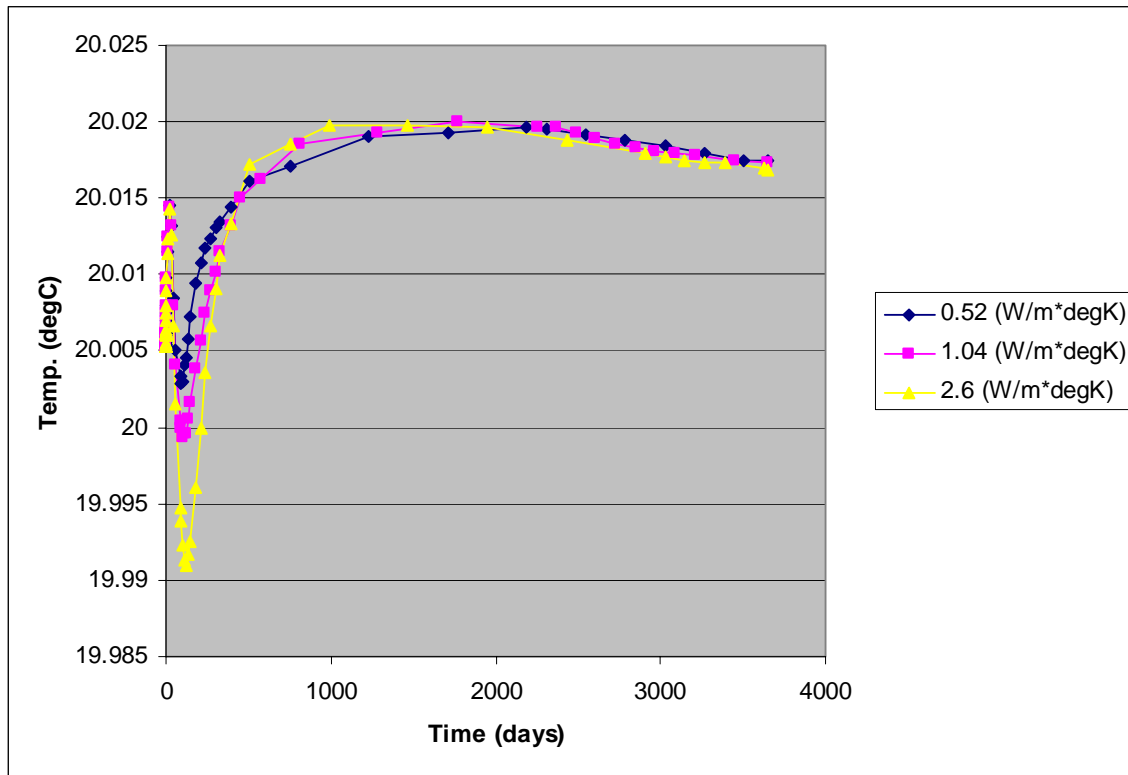


Figure 24. Temperature v. time plot for the thermal conductivity varying FPR case.

The largest temperature decline corresponds to the highest thermal conductivity, and the lowest temperature change corresponds to the lowest value of the thermal conductivity (Figure 24). As a material’s ability to conduct heat increases, the amount of heat (and therefore temperature) that enters the river will also increase.

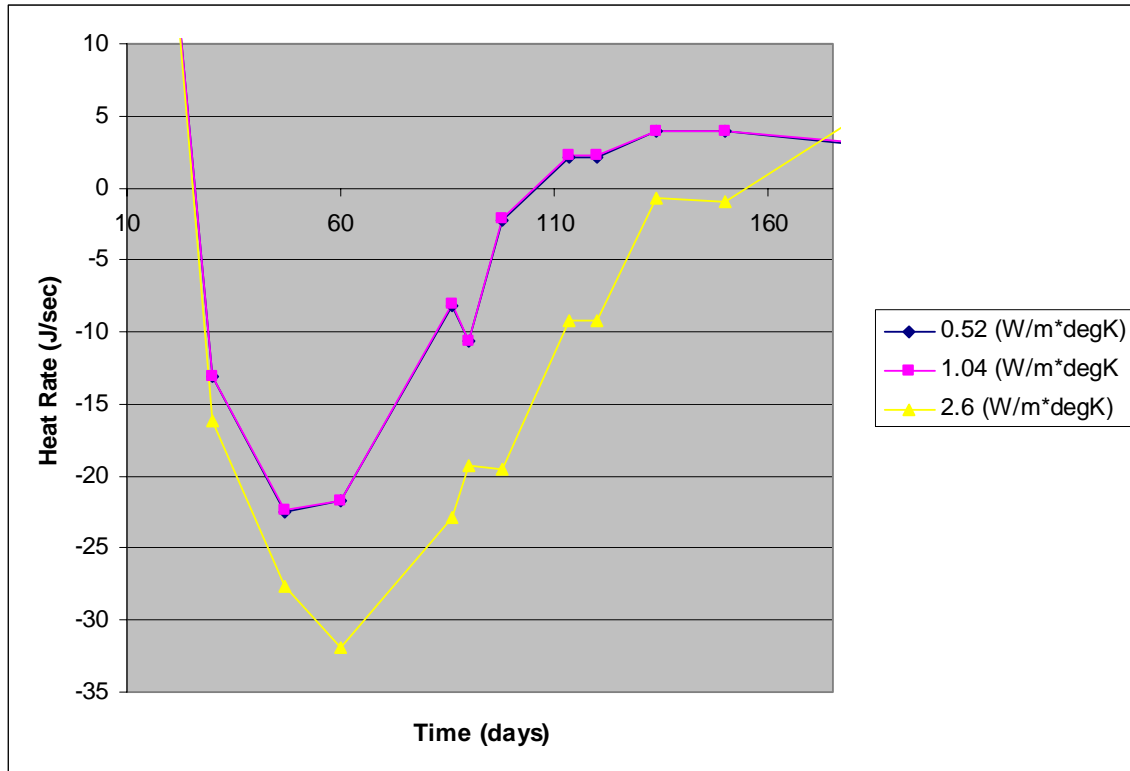


Figure 25. Heat rate (ΔH) v. time plot for the thermal conductivity varying FPR case.

The heat fluxes mirror the results from the temperature versus time plots (Figure 25). The 2.60 W/m-°K simulation has the lowest negative values for the heat rate, and the simulations with 0.52 and the 1.04 W/m-°K are virtually the same, though all three simulations are similar in both magnitude and shape.

Table 12. Percentage of cooling energy entering the river with varying thermal conductivity.

Thermal conductivity (W/m-°K)	Percentage of Cooling Energy Entering the River
0.52	-1.24%
1.04	0.00%
2.6	0.00%

Table 12 shows that only the 0.52 W/m-°K case has an appreciable amount of cooling that the fluvial body experienced. This result does not make sense given that the largest temperature drop corresponded with the largest value for the thermal conductivity. It should be understood that the percentage cooling values for the 1.04 and 2.6 W/m-°K cases are not zero but are small when compared to the 0.52 W/m-°K simulation. The scaled temperature changes are consistent with the temperature results in Figure 24 (Table 13).

Table 13. Low temperatures and scaled changes in temperature for varying thermal conductivity.

Thermal conductivity (W/m×°K)	Minimum Temperature (°C)	Peak Times (sec)	Scaling Factor	Scaled Delta Temperature (°C)
0.52	20.0029	7.78E+06	1827360	-2.18333E-05
1.04	19.9994	8.45E+06	1984810	-2.76667E-05
2.6	19.9909	1.04E+07	2436950	-4.18333E-05

FPR: Variable Precipitation

Another parameter that was varied for both the SED and the FPR case was the precipitation rate that fed the water table (and increased the groundwater velocity into the river). For this set of simulations, the precipitation/groundwater recharge ranged from 10^{-7} to 10^{-5} kg/sec.

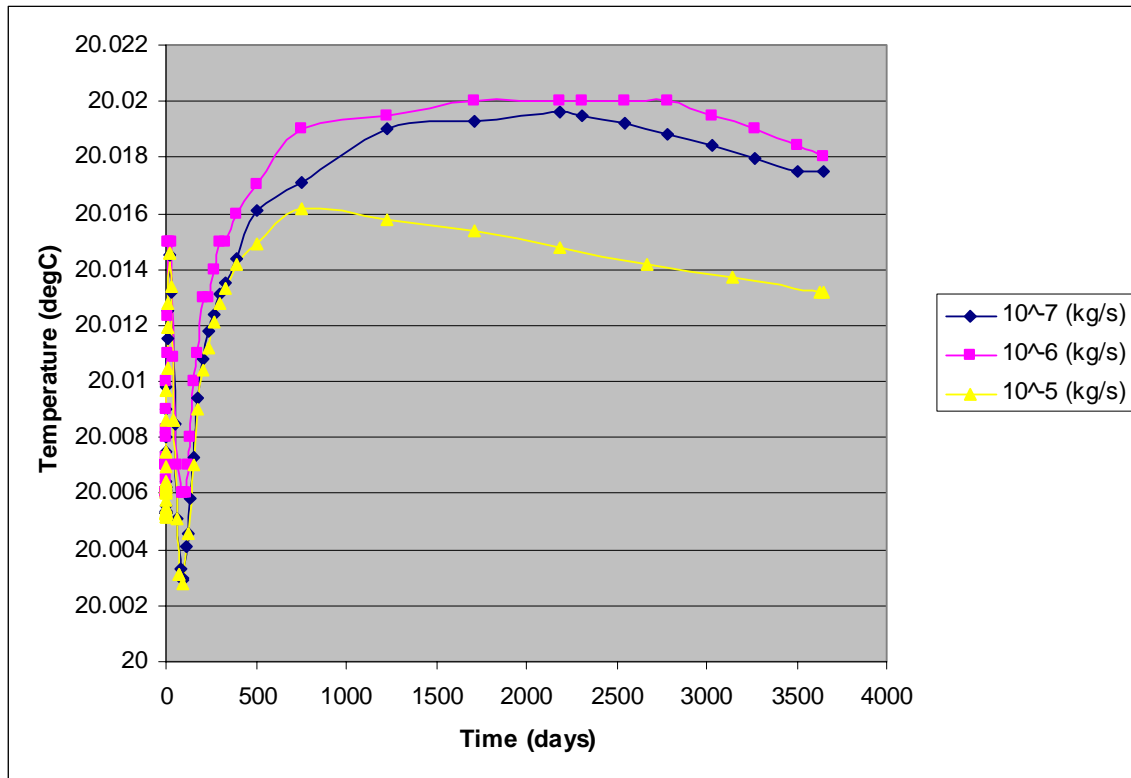


Figure 26. Temperature versus time plot for the precipitation varying simulations:

Figure 26 shows that there is little difference in temperature drops due to different precipitation rates.

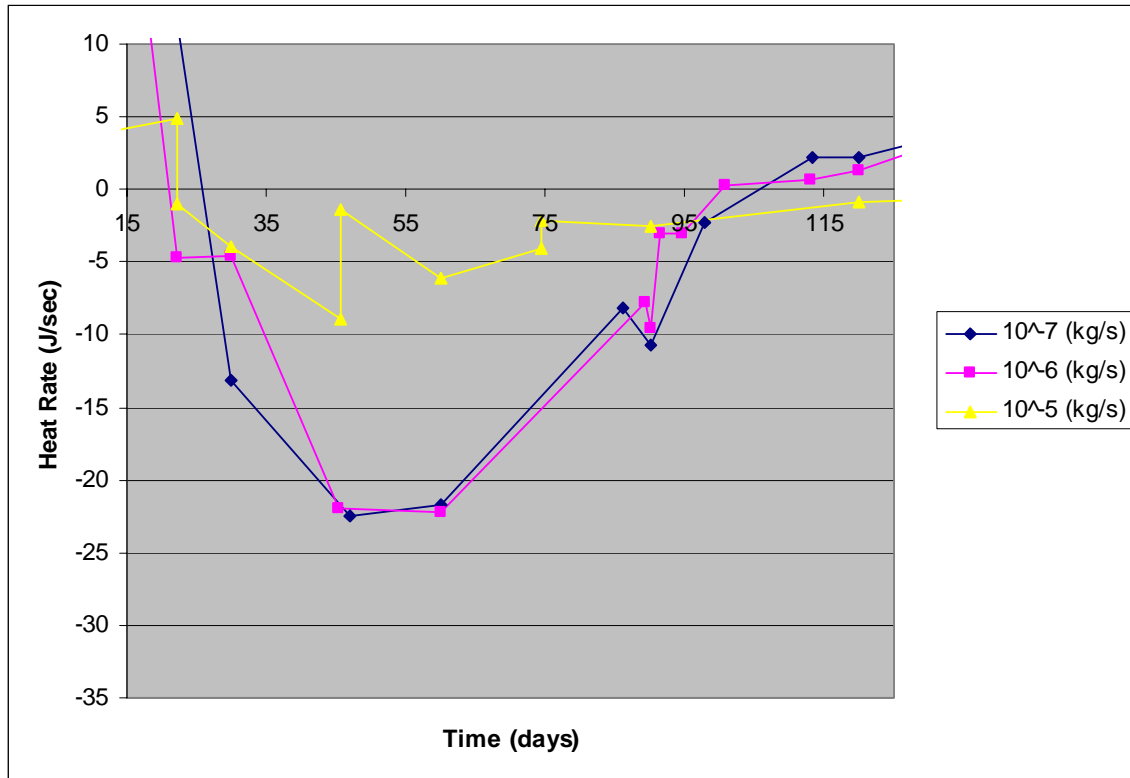


Figure 27. Heat rate (ΔH) versus time plot for the variable precipitation case

Heat fluxes to the river and temperature changes are not particularly sensitive to precipitation rate (Figure 27, Table 14) but do not appear to be consistent with the simulated and scaled changes in temperature (Figure 26, Table 15).

Table 14. Percentage of cooling energy entering the river with varying precipitation.

Precipitation Rate (kg/sec)	Percentage of Cool Energy Entering the River
10^{-5}	-1.24%
10^{-6}	-1.24%
10^{-7}	-0.39%

The percentages of cooling thermal energy reaching the river are virtually the same for the cases with greater precipitation.

Table 15. Low temperatures and scaled changes in temperature for varying precipitation rate.

Precipitation Rate (kg/sec)	Minimum Temperature (°C)	Peak Times (sec)	Scaling Factor	Scaled Delta Temperature (°C)
10^{-5}	20.0029	7.78E+06	1827360	-7.16881E-09

10^{-6}	20.006	7.78E+06	1827360	-5.47238E-09
10^{-7}	20.0028	7.78E+06	1827360	-7.22354E-09

Here a very slight temperature drop due to the influence of the side channel can be seen. The greatest temperature drop for all of the precipitation-varying cases has a lower magnitude than the ambient increase that the river experiences. This points to the FPR option not being an efficient method for fluvial cooling.

FPR: Channel Volume

For the final FPR sensitivity analysis, and unique to the FPR design scenario, a group of simulations kept the default subsurface parameters, and the temperature of the subsurface and river remained 20°C, but the side channel volume was varied among 600 (the default), 1200, and 1800 m³.

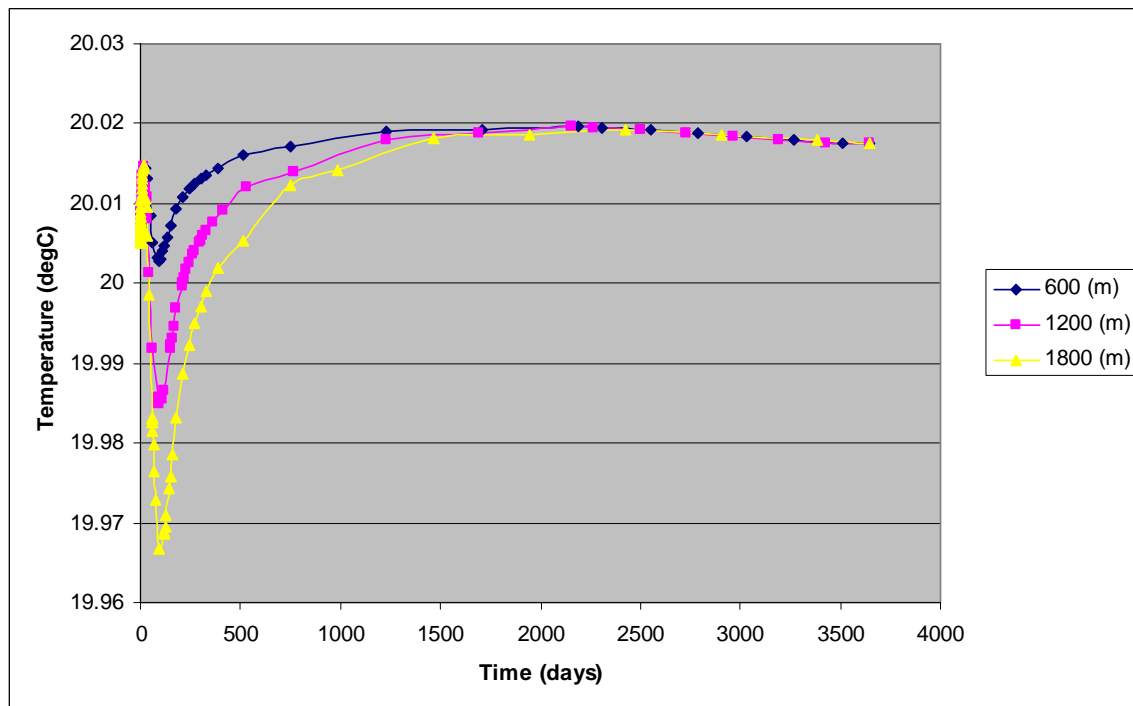


Figure 28. Temperature versus time plots with varying side-channel volume.

The results for temperature are predictable: Increasing the size of the channel increases the amount of cooling benefit (Figure 28).

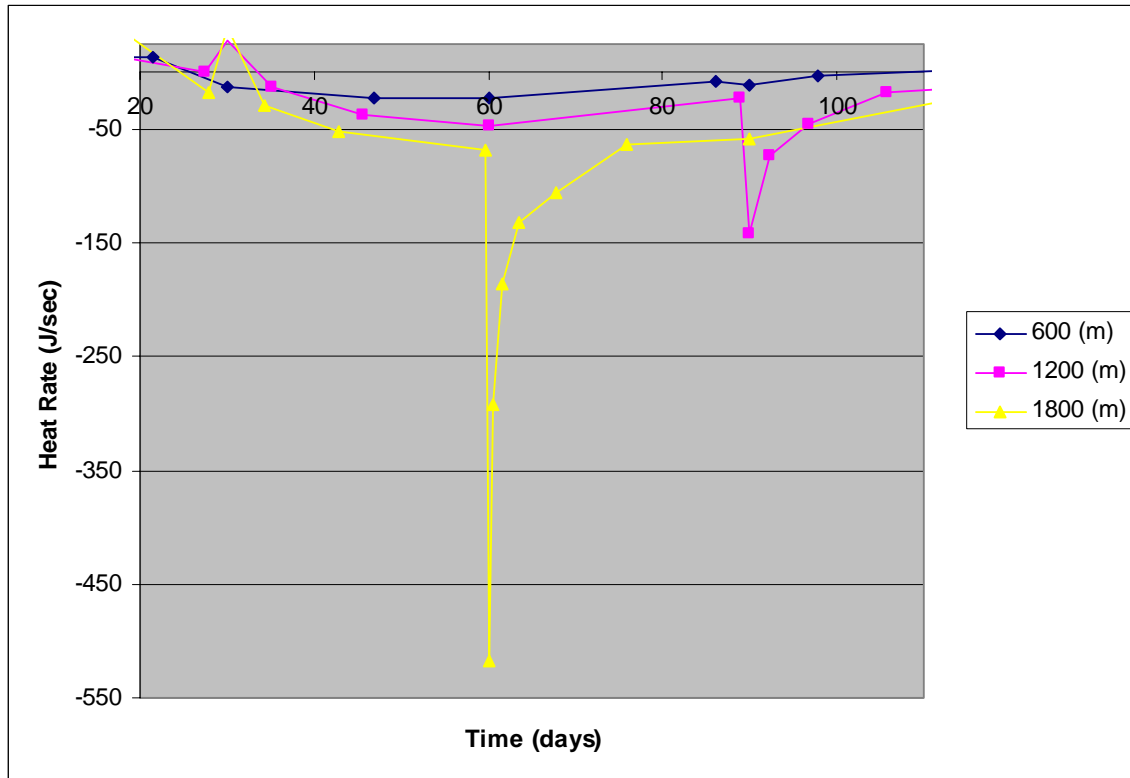


Figure 29. Heat rate (ΔH) versus time plot for the variable precipitation FPR simulations

Heat fluxes have the same trend as temperatures: The largest channel volumes correspond to the largest negative heat rate (Figure 29). The curves for the 1800- m^3 and 1200- m^3 heat fluxes are dominated by large negative spike at approximately 60 days and 90 days, respectively. Table xxx is the. These values were found by eliminating the positive heat rate values, and then numerically integrating the remaining curve:

Table 16. Integrated values for normalized heat rate with varying side-channel volume.

Volume (m^3)	Percentage of “Cool” Energy Entering the River
600	-0.01%
1200	0.00%
1800	0.00%

Only the smallest side-channel volume, corresponding to the smallest change in river temperature (Table 17), had an appreciable percentage of cooling (“negative”) energy reaching the river.

Table 17. Low temperatures and scaled changes in temperature for varying side-channel volume.

Volume(m^3)	Minimum Temperature	Peak Times	Scaling Factor	Scaled Delta Temperature
-----------------	---------------------	------------	----------------	--------------------------

	(°C)	(sec)		(°C)
600	20.0029	7.78E+06	1827360	-7.16E-09
1200	19.9849	7.78E+06	1827360	-1.70E-08
1800	19.9667	7.78E+06	1827360	-2.69E-08

Subsurface Effluent Discharge Simulations

The Subsurface Effluent Discharge scenario seeks to answer the question: Can the subsurface be used as heat sink/bank for warm wastewater during the months of August – October to assist in lowering river temperatures? This scenario assumes that the hyporheic zone is always (initially) cooler than the wastewater effluent.

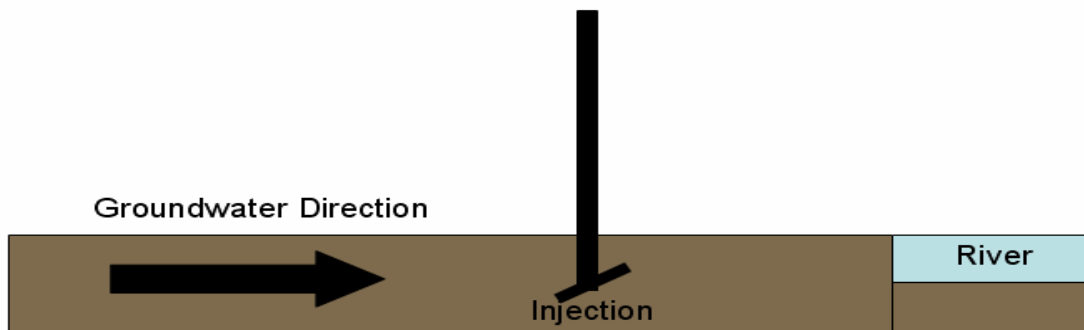


Figure 30. A conceptual drawing of the SED case.

As previously stated, August – October is the time when Oregon’s rivers are the warmest. High ambient temperatures combined with low flow rates in streams combine to create the worst-case situation where aquatic organisms are left vulnerable to low dissolved oxygen levels. Below summarizes the temperature and flow conditions for the months of August –October:

Stream Flow Characteristics:

- Flow: The main channel of the river will be considered to be static. This assumption can be made because of the relatively small effect that convective heat transfer will play in the transfer of thermal energy from the hyporheic zone to a fluvial body.
- Stream temperature = 68 F (20 C) for August, 55 F (12.8 C) for October, and 48 F (8.9 C) for floodwaters from November through April.
- Scaling Flow: 5000 cfs in August, 6500 cfs in October

Wastewater Effluent Characteristics:

- Effluent temperature = 73 F (22.8 °C) for August and 71 F (21.7 °C) for October.
- The effluent temperature and flow rate will be parameters that will be examined in the sensitivity analysis.
- For August – October, wastewater effluent flow rate is 1.95 m³/s (68.8 cfs)

It should again be noted that there is currently no modeling software that combines surface water (fluvial) flow, subsurface flow, and the temperature interactions between the two. As a result, the river in the model is a static body of water.

Results

For the SED case temperature versus time plots, ΔH versus time plots, percentage of heat that entered the river, and maximum scaled river temperatures for each case were produced and evaluated. The sensitivity analysis varied hydraulic conductivity, porosity, density, thermal conductivity, specific heat, and distance of the injection point from the river. For all cases, the default subsurface and injection parameters were used except for the parameter of interest that was being varied.

Normalized heat rate versus time plots were generated for all of the following SED simulations. The normalized heat rate versus time plot differ from the heat rate versus time plot only by a scaling factor that normalizes the data points. Because the plots are otherwise identical they have been omitted except for the simulations with varying distance. The integrated results of the normalized plots are presented for every case. These results take two forms: the total integration (includes negative values due to re-conduction of heat into the river bed), and only the positive rate values.

Sensitivity Analysis

Surface Effluent Discharge (SED): Distance

For this case, the distance between the injection point and the river was varied between 30 and 300 meters (approximately 100 – 1000 feet). Again, the default subsurface conditions were used for all simulations; only the distance from the river was varied for these simulations.

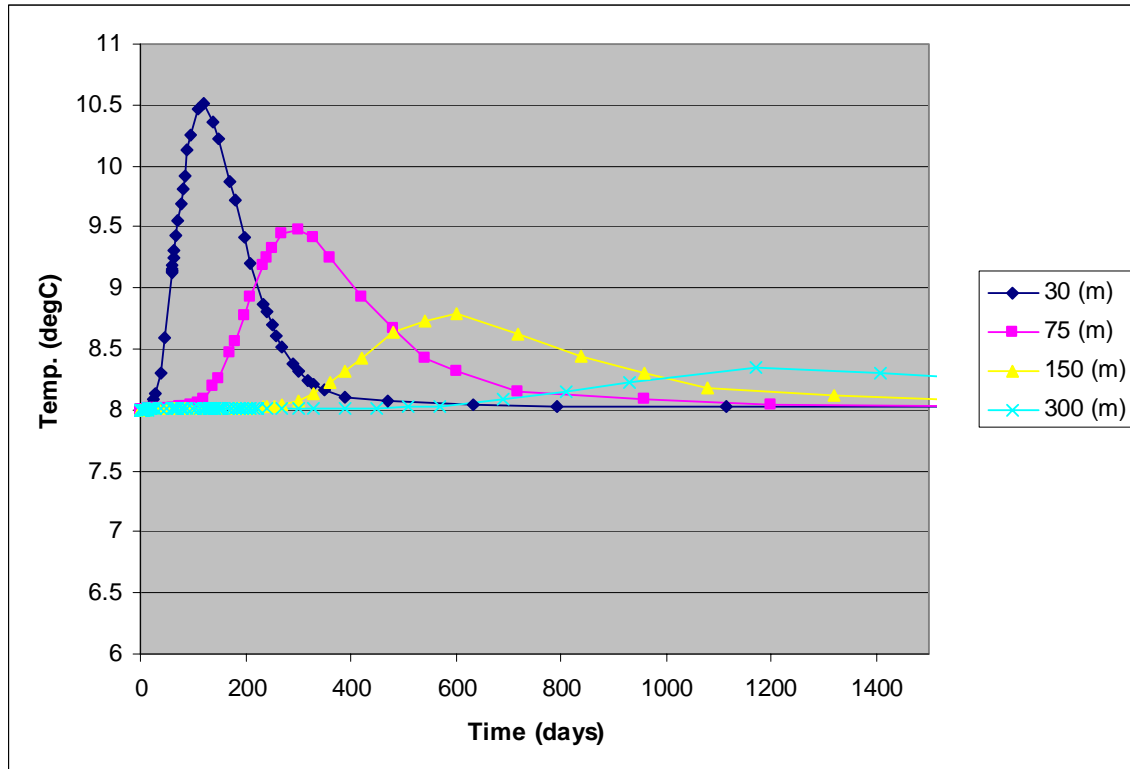


Figure 31. Temperature versus time plot for SED simulations with varying distance.

Predictably, in the 30-m (100 ft) injection simulation, warm water entered the river first and caused the highest peak temperature (Figure 31). As distances between the river and the injection points increased, the warm water took longer to reach the fluvial body, the peak temperature was lower, and the “bell curve” shape of the temperature versus time graphs became more spread out. This spreading was due to conduction/diffusion of heat and warm water to the subsurface as the groundwater made its way to the fluvial body.

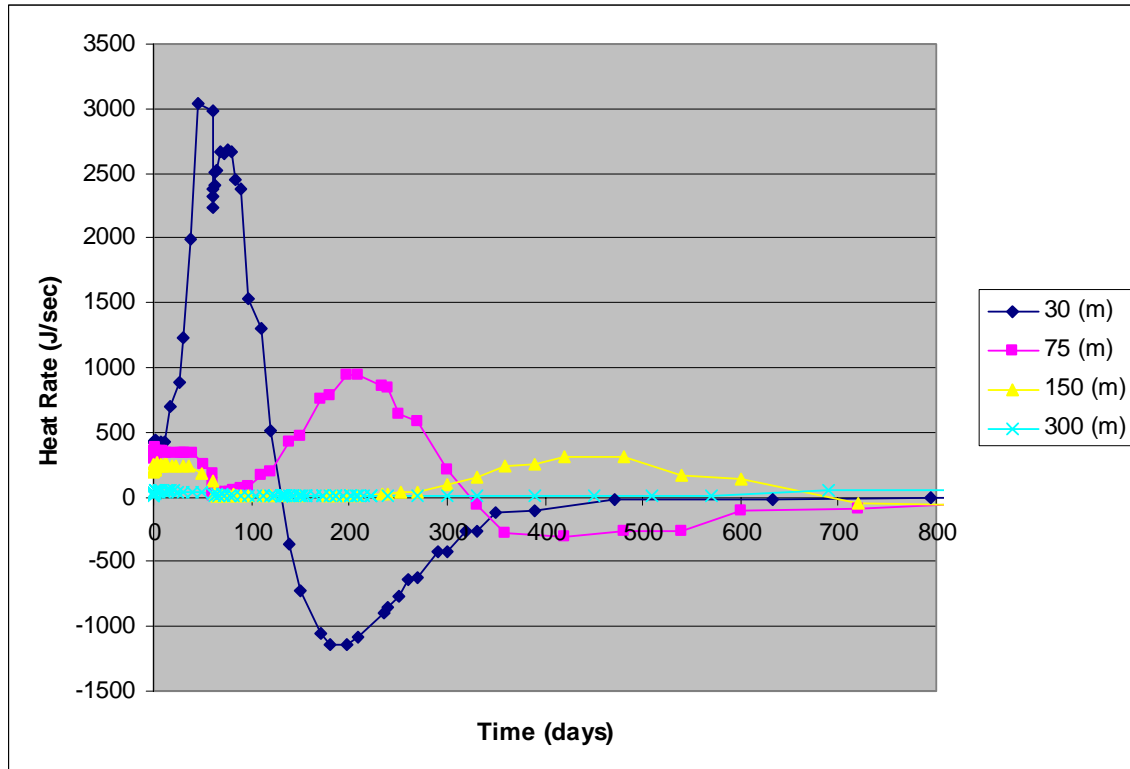


Figure 32. Heat rate (ΔH) versus time plot with varying distance for SED case.

In the plot of heat flux vs. time, the effect of an injection-induced “pressure wave” on the heat flux is evident (Figure 32). On the heat rate curve for the 30-m case, an initial spike occurs almost instantaneously. This immediate spike in energy per unit time (Watts) into the river, without an accompanying increase in temperature (Figure 31), is due to the increased groundwater velocity along the x-axis due to injection.

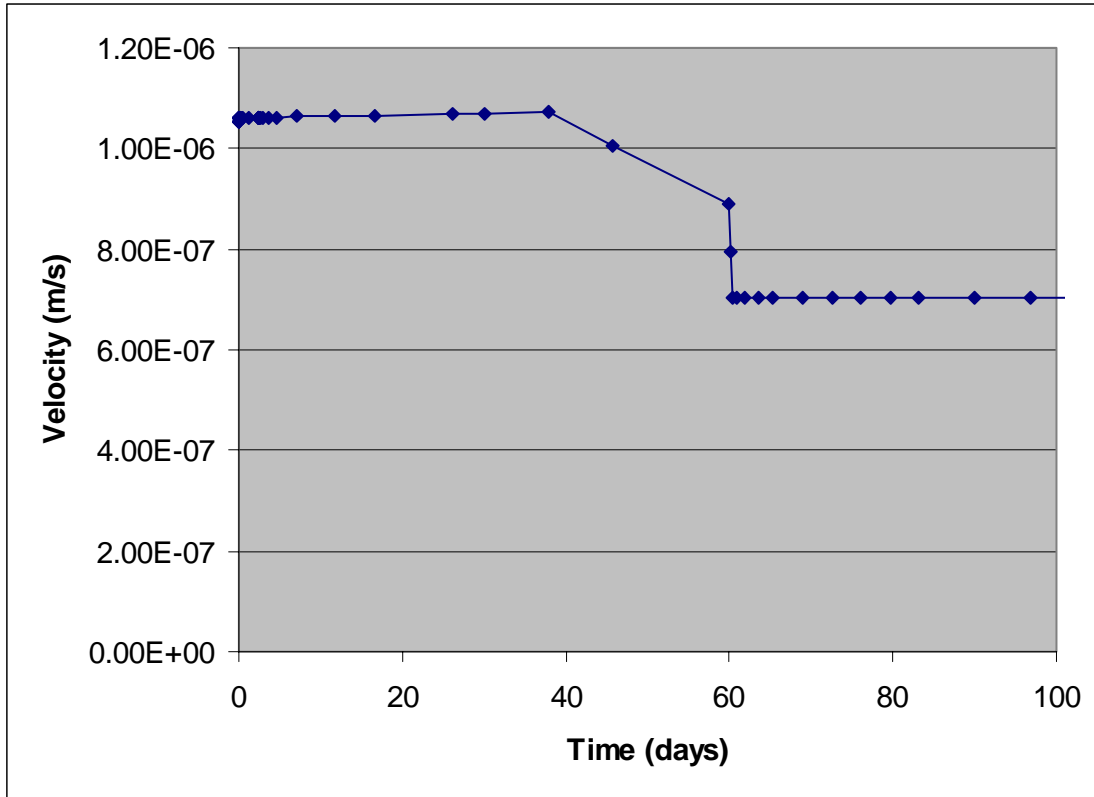


Figure 33. Groundwater velocity along the x-axis leaving the model for the default case

Figure 33 shows that groundwater velocity in the x -direction out of the model increases immediately due to the injection 30 meters away. At 60 days there is an immediate drop in groundwater velocity due to cessation of wastewater injection. Thus, the immediate rise in heat rate in Figure 32 is because more groundwater per unit time is moving out of the model due to injection. The groundwater has a finite amount of energy per unit mass (enthalpy). If the water velocity increases, the amount of water, and therefore energy, per unit time also increases. The temperature of the river doesn't rise because the groundwater, at least until the injected warm water reaches the river, is the temperature of the subsurface (which is the same temperature as the initial temperature of the river).

Finally, if the initial increase in heat rate is due to the “pressure effect” from injection (and the accompanying increase in groundwater velocity), for longer distances between the injection points and the river, there should be another spike in the heat rate when the waste water enters the fluvial body. Examining the ΔH versus time curve for 75 m, an initial “pressure” spike is seen from 0 days to approximately 80 days. The heat rate then falls only to increase again at 100 days, which is when the warm water reaches the river. This secondary increase in heat rate confirms that there is a “pressure wave” due to injection, and that the model is physically meaningful (Figure 32).

The normalized ΔH versus time plot for varying distance differs from ΔH only by a scaling factor of one over the total thermal energy injected into the system (Figure 34).

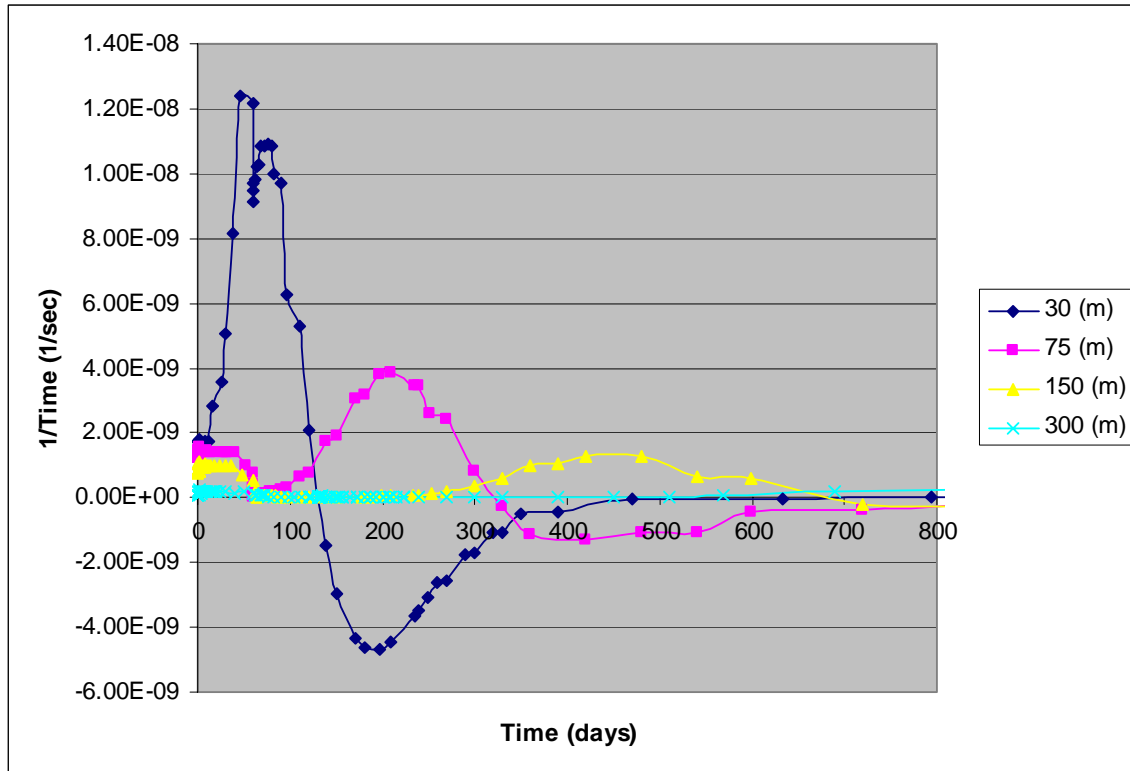


Figure 34. Normalized heat rate versus time for the distance varying SED simulations

Table 18 shows that the percentages of injected heat entering the river during the simulations are low (between 2.03% and 1.14%).

Table 18. Total and “positive-only” percentages of heat entering the river with varying injection distance.

Distance from the River (m)	Percentage of Heat Entering the River	Positive Integration Values
30	1.63%	7.54%
75	2.03%	4.67%
150	1.78%	3.19%
300	1.14%	1.39%

Somewhat interesting is the fact that at 30 m from the river, the total amount of heat entering the system is less than that of the 75-m injection distance. This counter intuitive result comes from the integration of the normalized heat curve. Both the positive and negative heat rate values were summed. Because more heat from 30-m simulation entered the river due to the shorter travel distance, a larger temperature gradient between the river water and the bed and banks was created such that more heat was conducted back out of the river. Thus the total percentage of heat entering the river is lower for the 30-m case, while peak temperature (and the integrated positive heat flux) was highest (Table 18).

The “positive integration values” section neglects the negative heat rates, and percentage of total heat entering the river increases as the distance between the river and the injection point decreases.

The scaled temperature changes are the peak temperatures minus the initial subsurface/river/atmospheric temperature divided by the scaling factor (equation (26)).

Table 19. Peak river temperatures and scaled maximum changes in temperature with varying injection distance.

Distance from the River (m)	Maximum Temperature (°C)	Peak Time (sec)	Scaling Factor	Scaled Delta Temperature (°C)
30	10.511	1.04E+07	2436950	1.03E-06
75	9.4831	2.59E+07	6091200	2.43E-07
150	8.8383	4.15E+07	9743100	8.60E-08
300	8.0171	1.01E+08	23742050	7.20E-10

Maximum peak temperature occurs for the 30-m case, and the scaled temperature changes are small (Table 19).

SED: Hydraulic Conductivity

Figure 35 shows the temperature versus time for injection cells 30 m from the river, hydraulic conductivity varying from 5×10^{-5} to 5×10^{-3} , and all other parameters conforming to the default case.

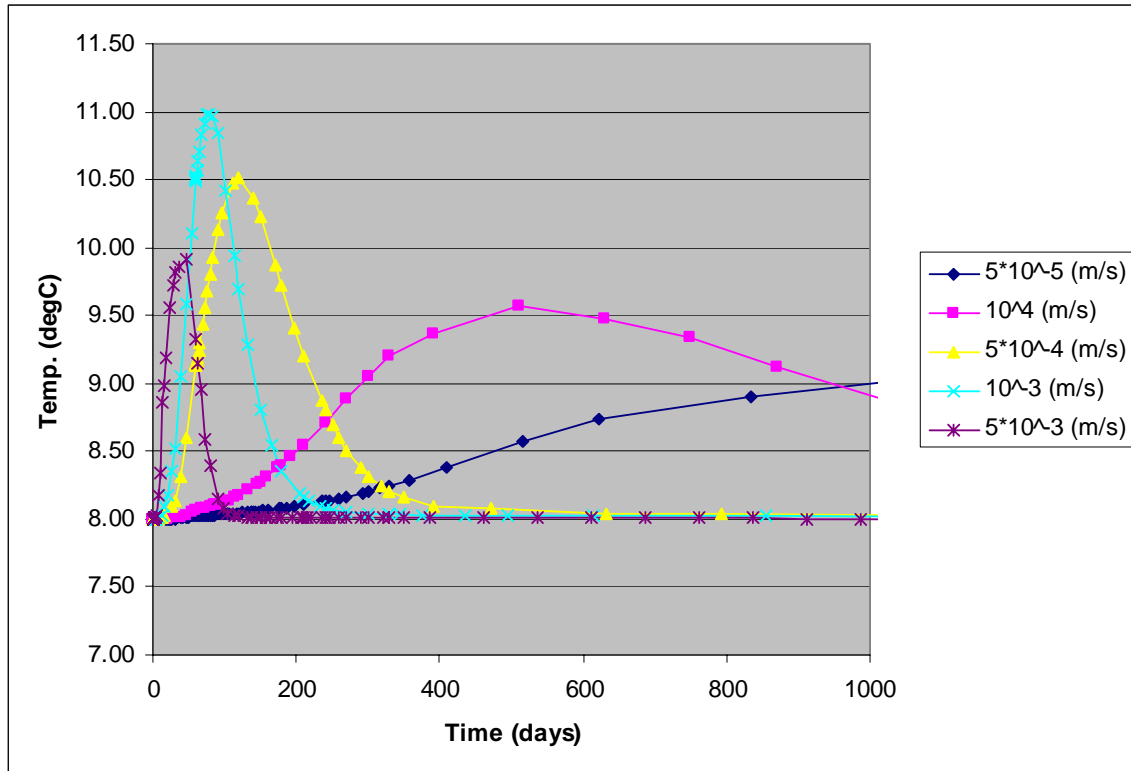


Figure 35. Temperature versus time for the hydraulic conductivity varying SED simulations

Of interest on Figure 35 is the fact that, at the highest hydraulic conductivity (5×10^{-3} m/s), the peak temperature of the river is less than the peak temperatures at hydraulic conductivities of 10^{-3} and 5×10^{-4} m/s. The temperature of the river increases most quickly for the highest hydraulic conductivity because of greater groundwater velocities, but this quick evacuation of warm water from the ground to the river also creates a large temperature gradient between the two and thereby promotes the greatest conduction of heat back into the bed and banks (Figure 36): At the lowest hydraulic conductivity (5×10^{-5} m/s), the heat rate as a function of time plot has the greatest extremes of positive and negative heat flux.

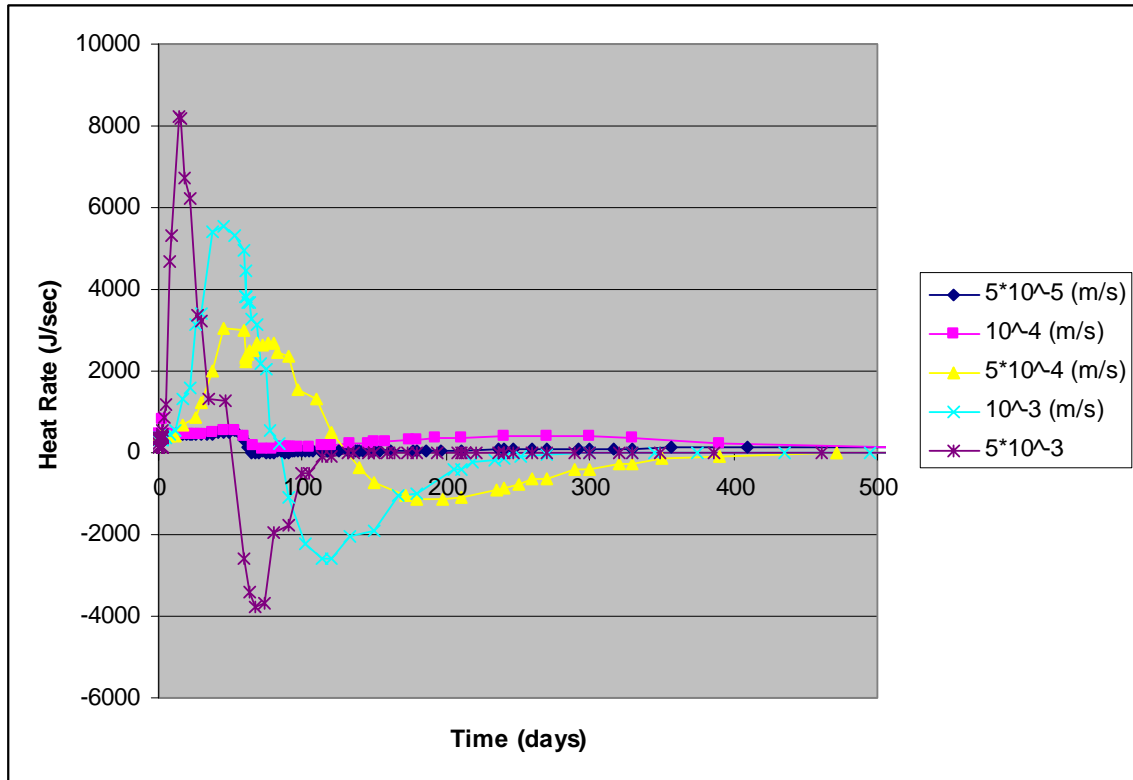


Figure 36. Heat rate (ΔH) versus time for the hydraulic conductivity varying SED simulations.

Table 20. Percentage of injected heat entering river with varying hydraulic conductivity.

Hydraulic Conductivity (m/s)	Percentage of Heat Entering the River	Positive Integration Values
5×10^{-5}	1.29%	3.21%
1×10^{-4}	1.61%	4.52%
5×10^{-4}	1.63%	7.15%
1×10^{-3}	2.31%	8.81%
5×10^{-3}	0.850%	5.20%

According to the integrated heat fluxes (Table 20), as the hydraulic conductivity increases, the percentage of heat entering the river also increases until the highest value of hydraulic conductivity (5×10^{-3} meters per second) is reached. At this value of hydraulic conductivity, the percentage of heat that entered the river falls to less than 1%, and even the integral of only positive heat flux values drops. The drop at high hydraulic conductivity is due to the conduction of heat back out of the river.

The scaled temperature changes are consistent with the above results (Table 21).

Table 21. Peak river temperatures and scaled maximum changes in temperature with varying hydraulic conductivity.

Hydraulic Conductivity (m/s)	Maximum Temperature (°C)	Peak Times (sec)	Scaling Factor	Scaled Delta Temperature (°C)
5×10^{-5}	9.0188	9.04E+07	21242590	4.80E-08
1×10^{-4}	9.5776	4.41E+07	10351750	1.52E-07
5×10^{-4}	10.511	1.04E+07	2436950	1.03E-06
1×10^{-3}	10.98575	6.71E+06	1577296.5	1.89E-06
5×10^{-3}	9.919	4.01E+06	943290	2.03E-06

SED: Porosity

For this simulation all other variables were the same as the default case, except that the porosity was varied from 0.15, 0.3., and 0.45. The porosity is the fraction of the subsurface that is void space.

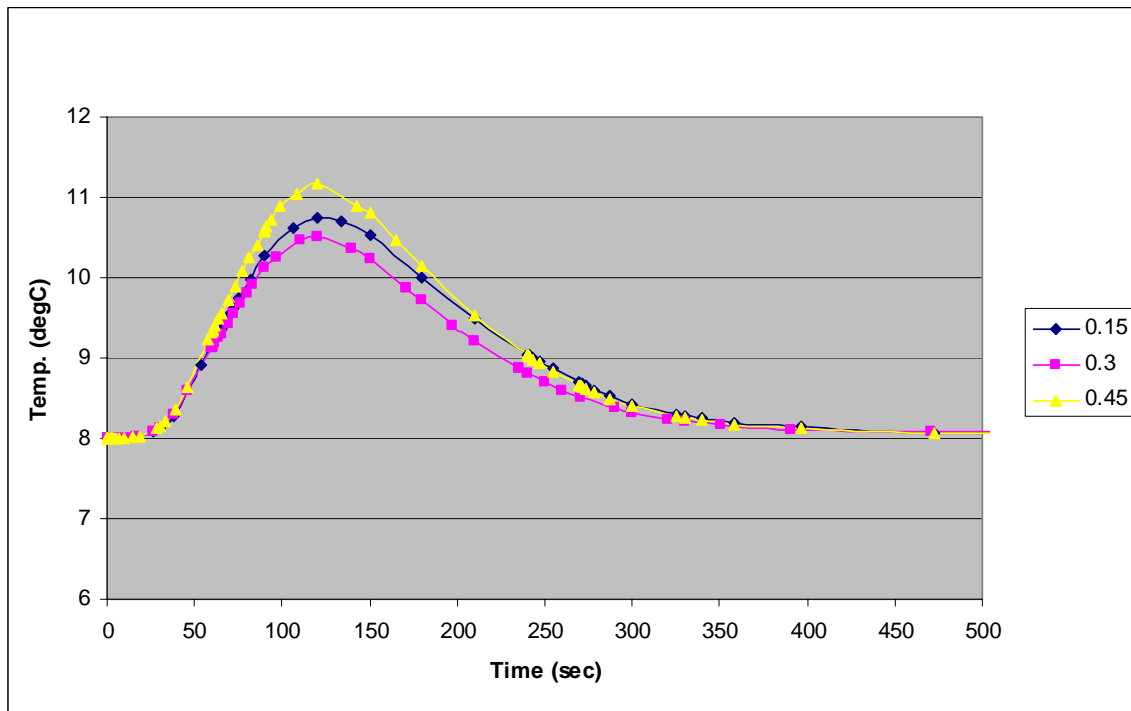


Figure 37. The temperature versus time plot for the varied porosity SED simulations

Of interest in Figure 37 is that the highest river temperature corresponds to a porosity of 0.45, but the next highest peak temperature occurred for the porosity of 0.15. Higher peak temperature at lower porosity makes sense given that groundwater velocity is inversely proportional to porosity. The effects of a greater volume fraction of water on thermal conductivity and heat capacity likely explain why the highest peak temperature

corresponded to a porosity of 0.45. Relative magnitudes of heat fluxes correspond to the temperature results (Figure 38).

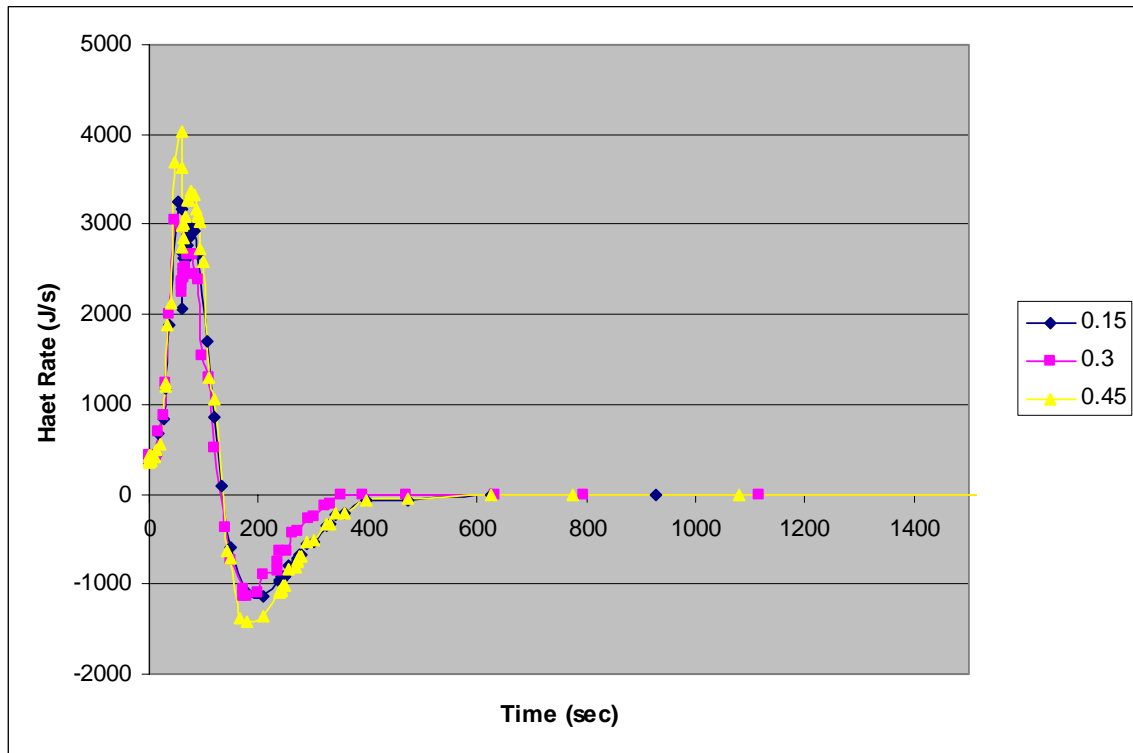


Figure 38. The heat rate (ΔH) versus time plot for the varied porosity SED simulations.

Sensitivity, in both temperature and heat flux, is apparently low (Figure 37, Figure 38). This result points to conduction and diffusion playing a large part in the movement of heat in the subsurface, and that porosity as a design consideration for subsurface injection of waste water is negligible.

Table 22. Percentage of injected heat entering river with varying porosity.

Porosity	Percentage of Heat Entering the River	Positive Integration
0.15	1.61%	7.69%
0.3	1.63%	7.15%
0.45	2.19%	9.05%

Percentages of injected heat entering the river decreased with decreasing porosity but not in proportion to the porosity changes (Table 22). These total integrals were not consistent with the temperature results, but the integrals of only positive heat-flux values mirrored the temperature results (Table 23).

Table 23. Peak river temperatures and scaled maximum changes in temperature with varying porosity.

Porosity	Maximum Temperature	Peak Time (sec)	Scaling Factor	Scaled Temperature
0.15	10.7358	1.04E+07	2436950	1.12E-06
0.3	10.511	1.04E+07	2436950	1.03E-06
0.45	11.1669	1.04E+07	2436950	1.3E-06

Similar to the other injection simulations, the scaled changes in temperature are small.

SED: Density

For these simulations the (grain) density of the subsurface medium was varied from 1515 kg/m³ (a representative density for soil) to 2650 kg/m³ (a representative density for stone). Density is a measure mass per unit volume for a given material. All other parameters were set for the default case.

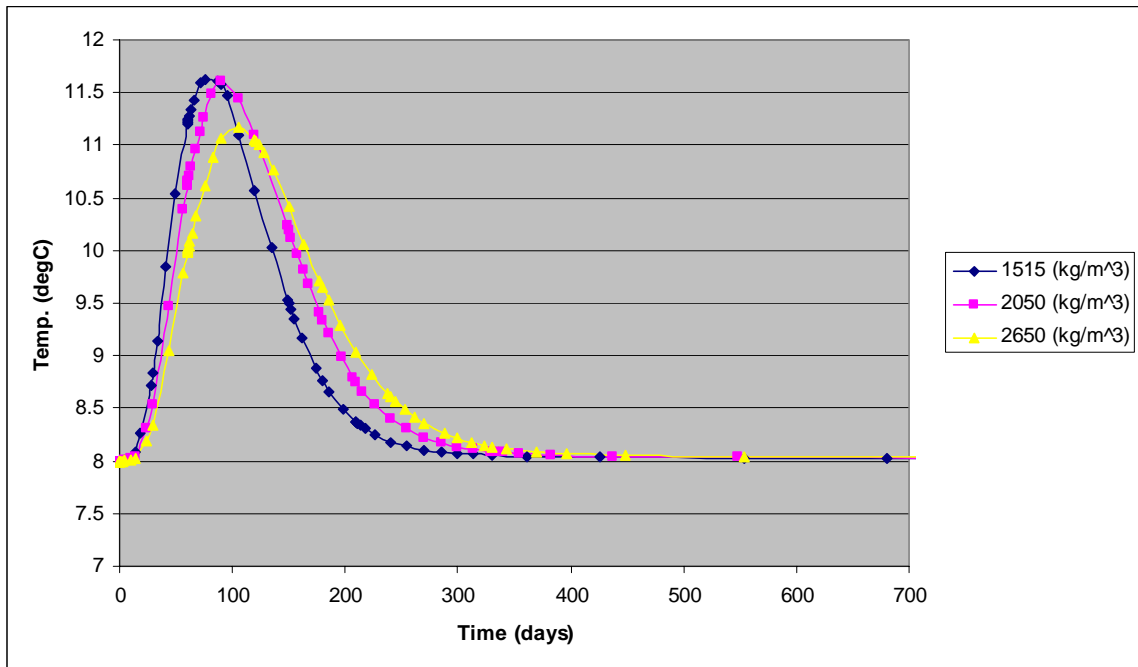


Figure 39. The temperature versus time plot for the density varying SED simulations.

From Figure 39 it can be seen that the lowest densities have the heat from the waste water enter the fluvial body at slightly faster times (95 days to the temperature peak for the lowest density case compared to approximately 110 days for the highest density case). Also, the peak temperature for the lowest density case was slightly higher than the high density simulation. The middle density case (2050 kg/m³) for both the peak temperature and the time to peak temperature was between the high and low density values.

Given that Darcy's Law does not contain a density term (either explicitly or implicitly), the changes in peak temperature and time to peak temperature with density are due to changes in heat transfer due to conduction and diffusion. Density is explicitly in the diffusion equation (9). This again shows that groundwater movement defined by Darcy's Law is not the only significant contributor to thermal energy movement in the subsurface. Diffusion and conduction play a noticeable role in how river bodies are heated and/or cooled by subsurface groundwater flow. Figure xxx is the accompanying versus time plot for this group of simulations:

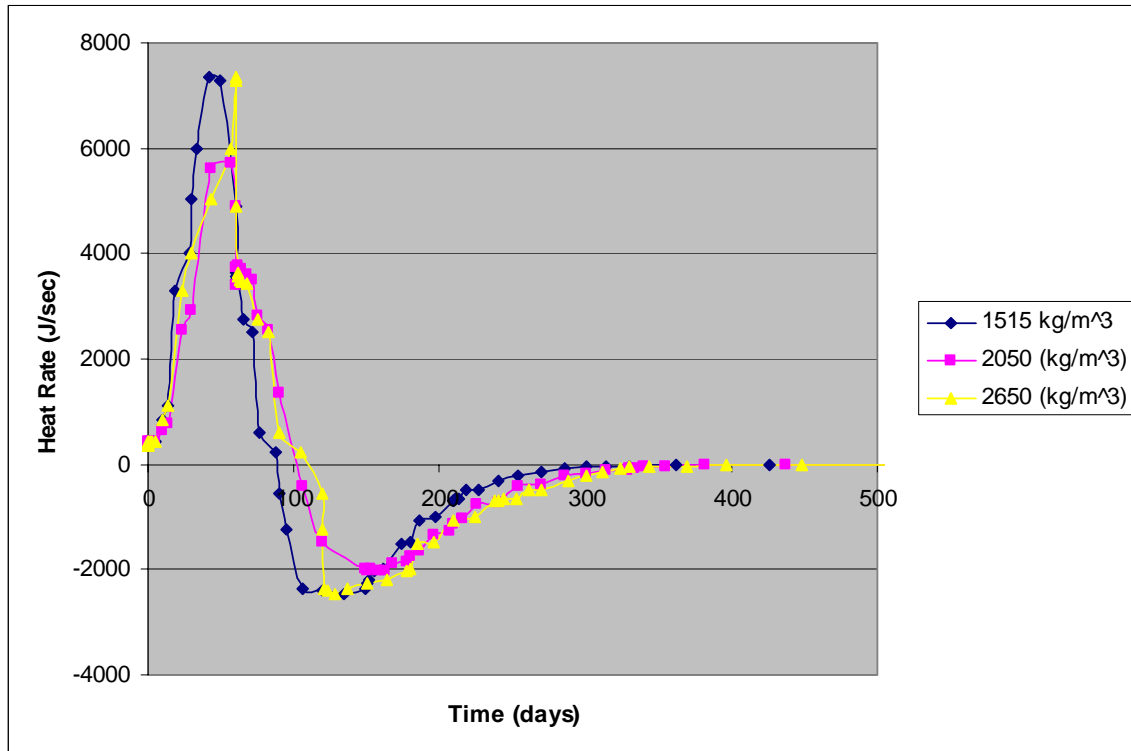


Figure 40. The heat rate (ΔH) versus time plot for the density varying SED simulations.

The results from Figure 40 mirror the results from the temperature versus time plot above. Though interesting, the fact that density plays a role in fluvial heat transfer is offset by the relatively minor contribution that density will have to the overall transfer. As a design consideration for wastewater injection to the subsurface, density of the subsurface medium would fall as a secondary or tertiary concern.

Table 24. Percentage of injected heat entering river with varying density.

Density (kg/m ³)	Percentage of Heat Entering the River	Positive Integration
1515	1.84%	10.19%
2060	1.97%	10.32%
2650	1.63%	11.61%

From Table 24 it can be seen that the percentage of total injected heat entering the river is in the same range as the previous injection examples, and that the percentage from only the positive heat flux values increases as density increases.

Table 25. Peak river temperatures and scaled maximum changes in temperature with varying density.

Density (kg/m ³)	Maximum Temperature (°C)	Peak Time	Scaling Factor	Scaled Delta Temperature (°C)
1515	11.62107	6611720	1553754	2.33E-06
2060	11.6031	7.78E+06	1827360	1.97E-06
2650	11.1768	1.04E+07	2436950	1.30E-06

The values for the maximum river temperature and scaled change in temperature were similar to values for the previous injection cases (Table 25).

SED: Specific Heat

The specific heat is the measure of how much heat needed to raise the temperature of one gram of a substance 1 °C. The units of specific heat are energy per unit mass multiplied by the temperature (in Kelvin). From these units it can be seen that the specific heat is a measure of how much thermal energy a substance can store per unit mass. For this group of simulations, the specific heat was varied among 800, 1105, and 1840 J/ kg-° K (this range represented specific heat values for sand, stone, and soil, respectively).

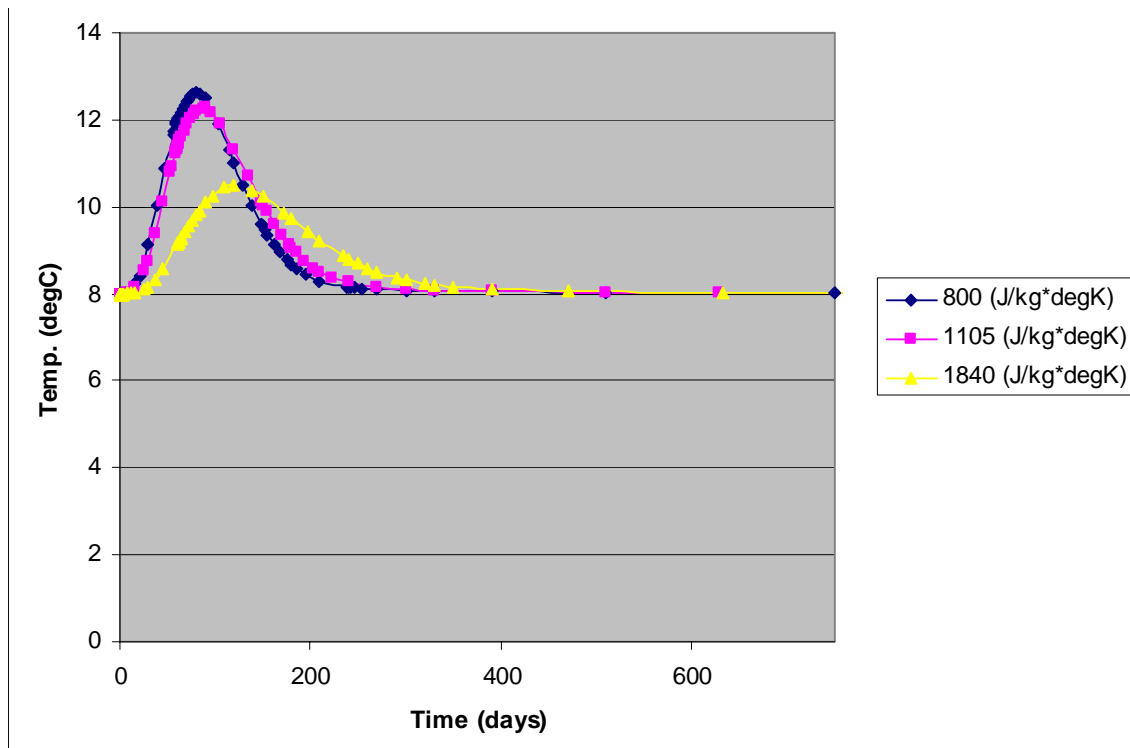


Figure 41. Temperature versus time plot for the specific heat injection simulations.

From Figure 41 it can be seen that lower values of specific heat cause the peak temperature of the river to be higher and time it takes for the peak value to reach the river to be longer. For the specific heat values of 800 and 1105 J/ kg \times $^{\circ}$ K (these values correspond to sand and stone, respectively), the differences are slight; however, for the 1840 J/ kg \times $^{\circ}$ K (that corresponds to a specific heat for soil), the differences were more pronounced.

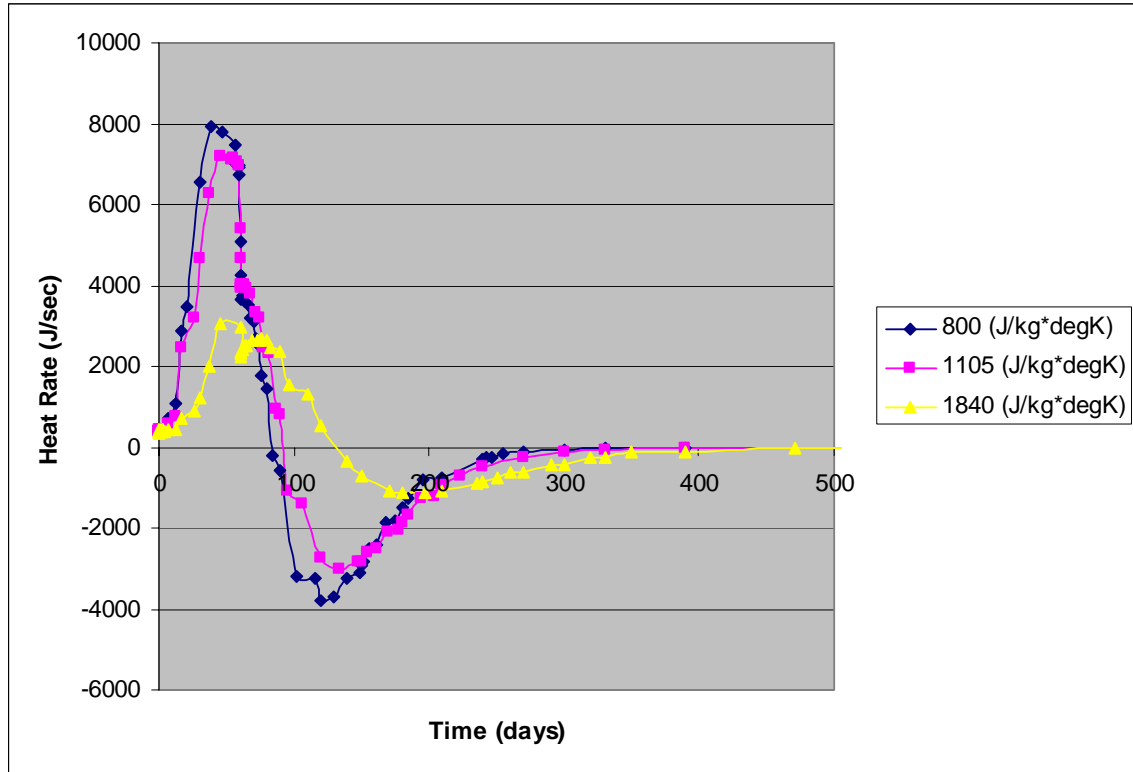


Figure 42. Heat rate (ΔH) versus time plot for the density varying SED simulations.

The heat fluxes (Figure 42) are similar to the temperature results (Figure 41).

Table 26. Percentage of injected heat entering river with varying specific heat.

Specific Heat J/ kg \times $^{\circ}$ K	Percentage of Heat Entering the River	Positive Integration
800	2.75%	13.61%
1105	2.90%	12.73%
1840	1.63%	7.15%

The total percentage of heat entering the river is largest for the middle value of 1105 J/ kg \times $^{\circ}$ K (stone), which is anomalous relative to the temperature results, but the integrals of only positive heat fluxes are consistent with those temperature results (Table 26).

Table 27. Peak river temperatures and scaled maximum changes in temperature with varying specific heat.

Specific Heat J/kg-°K	Maximum Temperature (°C)	Peak Time (sec)	Scaling Factor	Scaled Delta Temperature (°C)
800	12.6397	6887400	1618539	2.8666E-06
1105	12.2742	7.78E+06	1827360	2.339E-06
1840	10.511	10370000	2436950	1.03039E-06

The highest peak temperature for this group of simulations was for the specific heat of 800 J/°K-kg, though the 1105 J/°K-kg simulation was similar. The peak temperature for a specific heat of 1840 J/°K-kg was markedly lower than the other two simulations, which points to specific heat being an important design parameter in cooling of waste water in the hyporheic zone.

SED: Thermal conductivity

A material’s thermal conductivity is its ability to transmit heat. For this group of simulations, the thermal conductivity was varied in the range of 0.52 – 2.6 W/m-°K. These values are representative values for different subsurface substances (soil, sand, and stone).

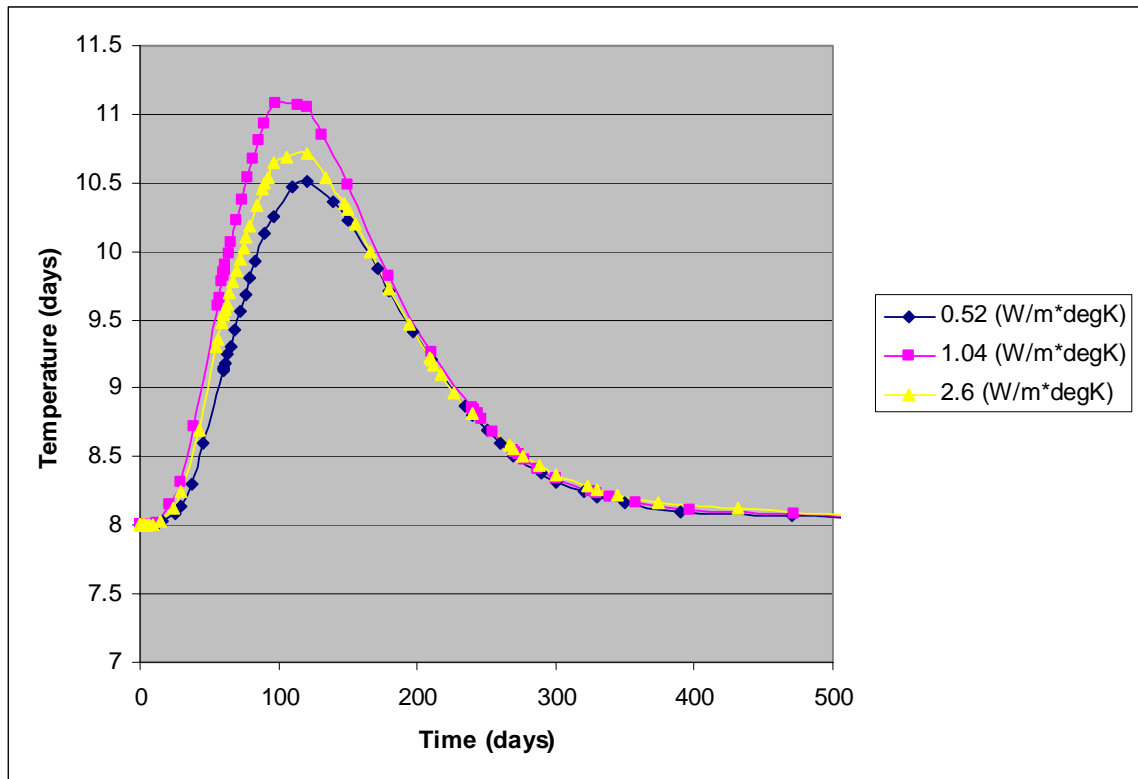


Figure 43. Temperature versus time plot for the thermal conductivity varying simulations.

Of interest in the temperature results is that the middle value of thermal conductivity (1.04 Watts/m×°K) has the highest peak temperature value (Figure 43). The lowest value of thermal conductivity, 0.52 W/m×°K, has the lowest peak temperature value (which makes intuitive sense); also of note is that the peak temperatures for each of the simulations occurred roughly at the same time. Changing thermal conductivity did not change the time it took for the heat to reach the river.

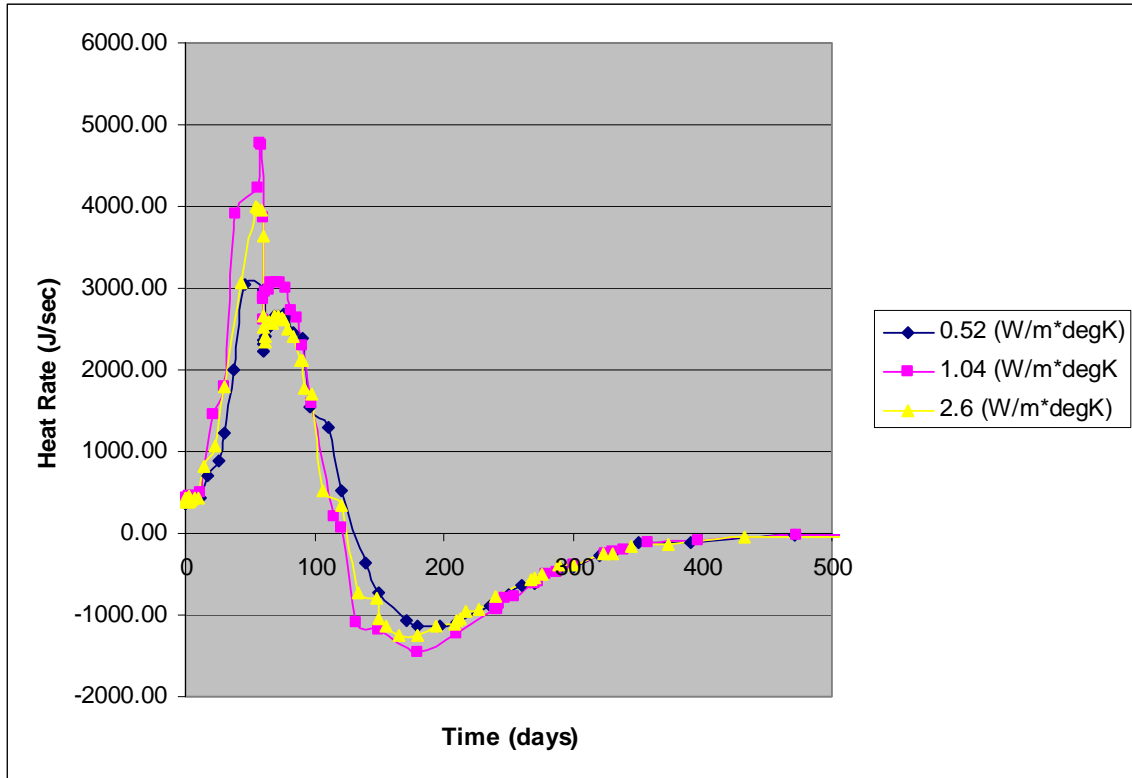


Figure 44. Heat rate (ΔH) versus time plot for the thermal conductivity varying simulations.

The heat fluxes (Figure 44) mirror the temperature results. The 1.04 W/m-°K simulation has the highest peak values for the heat rate, though all three simulations are similar in both magnitude and shape. Both the heat rate curves for 0.52 and 2.6 W/m-°K exhibit the “pressure wave” effect discussed in previous sections.

Table 28. Percentage of injected heat entering river with varying thermal conductivity.

Thermal Conductivity (W/m-°K)	Percentage of Heat Entering the River	Positive Integration
0.52	1.63%	7.15%
1.04	2.80%	9.49%
2.6	2.43%	8.34%

The percentages of heat entering the river (Table 28) were consistent with the scaled temperature results (Table 29): The middle value of 1.04 W/m²°K had the highest amount of heat entering the river. The percentage values were similar to the previous injection simulations.

Table 29. Peak river temperatures and scaled maximum changes in temperature with varying thermal conductivity.

Thermal Conductivity W/m-°K	Maximum Temperature (°C)	Peak Time	Scaling Factor	Scaled Delta Temperature (°C)
800	10.511	1.04E+07	2436950	1.03E-06
1105	11.0786	8.48E+06	1991625	1.55E-06
1840	10.7085	1.04E+07	2436950	1.11E-06

SED: Variable Precipitation

Another parameter that was varied for both the SED and the FPR case was the precipitation rate that fed the water table (and increased the groundwater velocity into the river). For this set of simulations, the precipitation/groundwater recharge ranged from 10⁻⁷ to 10⁻⁵ kg/sec.

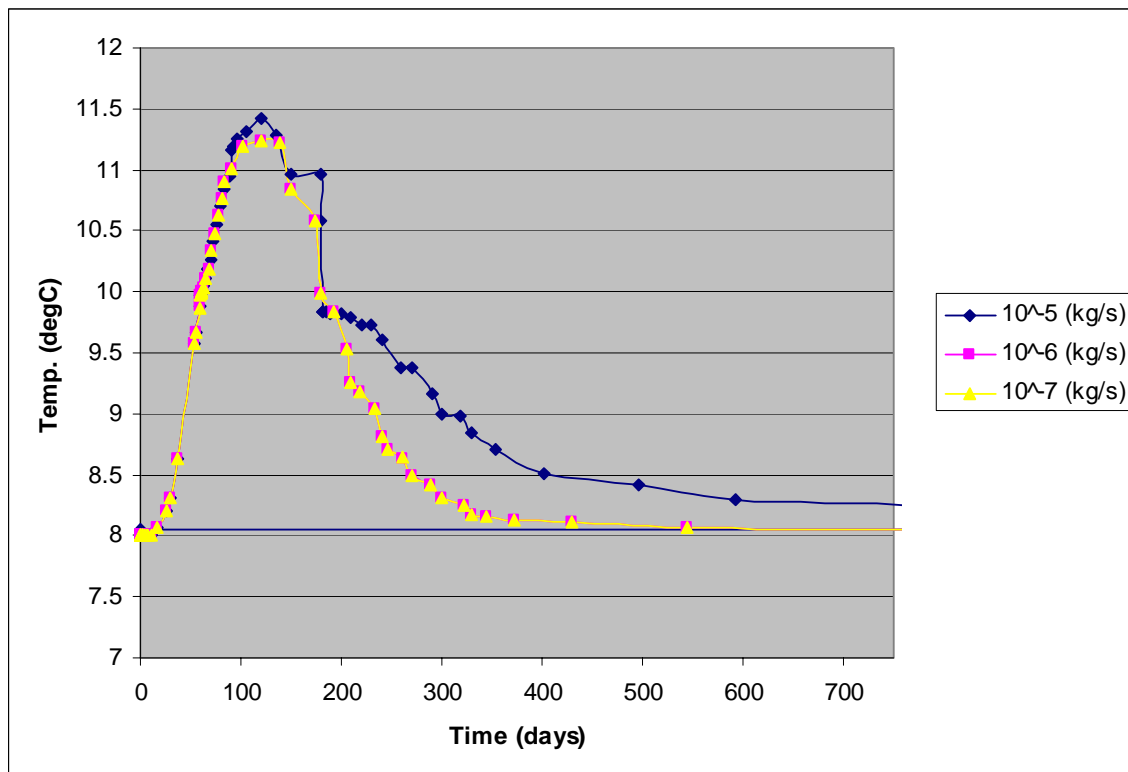


Figure 45. Temperature versus time plot for the precipitation varying SED simulations:

The precipitation recharge does not play a significant role the arrival time or magnitude of peak temperatures in the river but does appear to affect the rate at which temperatures subsequently decline: While the temperature results for precipitation rates of 10^{-6} and 10^{-7} kg/sec were nearly identical, the peak temperature for the greatest rate of 10^{-5} kg/s was slightly greater, and higher temperatures were sustained for longer than at the lower precipitation rates (Figure 45). The source of this difference is not obvious from the heat flux results, which are similar for all values of precipitation rate (Figure 46).

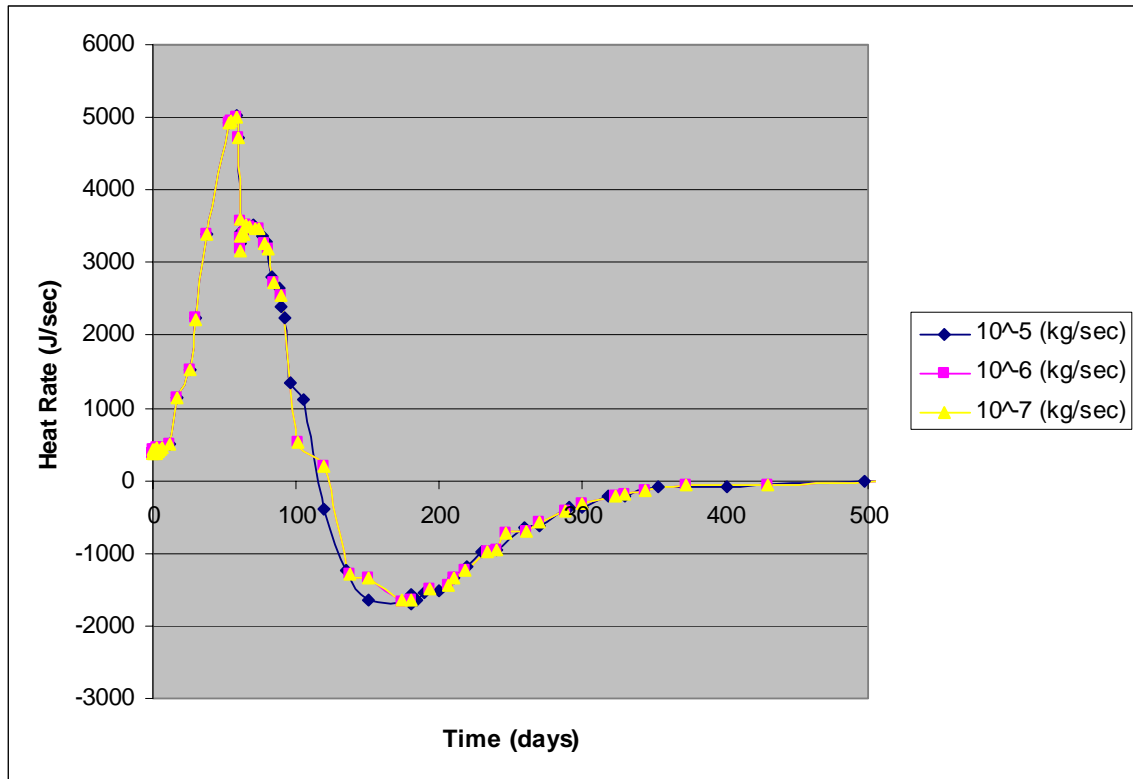


Figure 46. Heat rate (ΔH) versus time plot for the precipitation varying simulations.

Table 30. Percentage of injected heat entering river with varying precipitation rate.

Precipitation rate (kg/s)	Percentage of Heat Entering the River	Positive Integration
10^{-5}	2.42%	10.12%
10^{-6}	2.17%	9.66%
10^{-7}	2.16%	9.66%

The heat flux integrals (Table 30) and scaled temperature changes (Table 31) are consistent: Precipitation rate has only a small effect, and that effect is only apparent at higher rates.

Table 31. Peak river temperatures and scaled maximum changes in temperature with varying precipitation rate.

Precipitation Rate (kg/s)	Maximum Temperature (degC)	Peak Time (sec)	Scaling Factor	Scaled Delta Temperature (degC)
10 ⁻⁵	11.4176	1.04E+07	2436950	1.40E-06
10 ⁻⁶	11.24061	1.04E+07	2436950	1.33E-06
10 ⁻⁷	11.24059	1.04E+07	2444000	1.33E-06

Maximum Injection Simulations

The final scenario that the model produced was a “real life”, best case for injection of waste water at a mass flow rate of 1950 kg/s into the subsurface (this mass flow rate is typical for a city with a population of approximately 250,000). The mass flow rate of the model was increased to 10 kg/s/m², and the hydraulic conductivity was increased to 10⁻² m/s. The latter value was the highest hydraulic conductivity successfully resolved by the model, and the former value is the highest injection rate possible at that hydraulic conductivity. An actual wastewater diffuser’s area would have to be scaled to accommodate the limitation imposed by these values of injection rate and hydraulic conductivity. Equation (29) shows the maximum volumetric flow rate that can be injected into the subsurface:

$$(29) \quad Q_{\max} = A \times K$$

where Q_{\max} is the maximum injection rate in m³/s; A is the area over which the injection occurs in m²; and K is the hydraulic conductivity in m/s. Solving equation (29) for the area (A) and using a hydraulic conductivity of 10⁻² m/s (corresponding to loose gravel) and an injection rate of 1.94 m³/s (corresponding to a mass injection rate of 1950 kg/s), the required area is 194 m². If a width of 2 meters (6.56 feet) is assumed for the width of the injection area, the length of that same injection area would be 97 m, or 318 feet. This is roughly the length of one American football field.

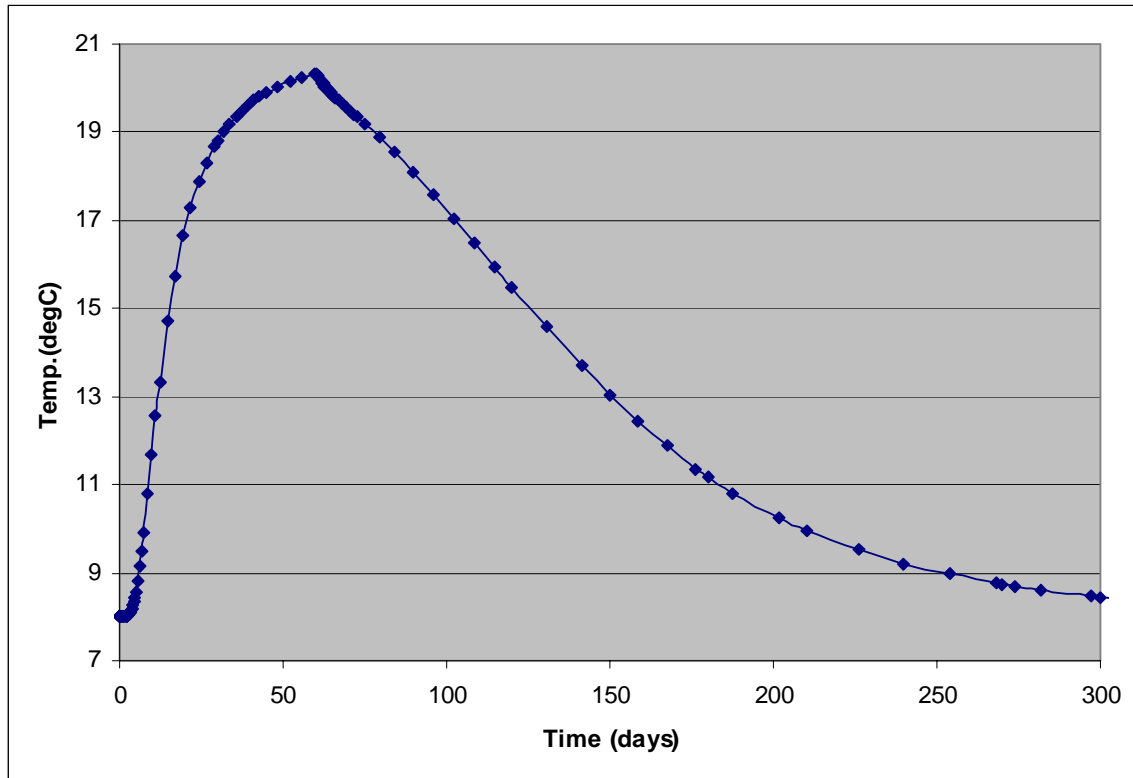


Figure 47. Temperature vs. time plot for the “best case” scenario.

The peak temperature occurs in the river after approximately 60 days (Figure 47), when the positive flow of heat due to injection ends (Figure 48). As in other simulations, the temperature signal is more dispersed than that of the heat flux because of conduction of heat to the subsurface and diffusion of groundwater ahead of the main body of the warm water pulse.

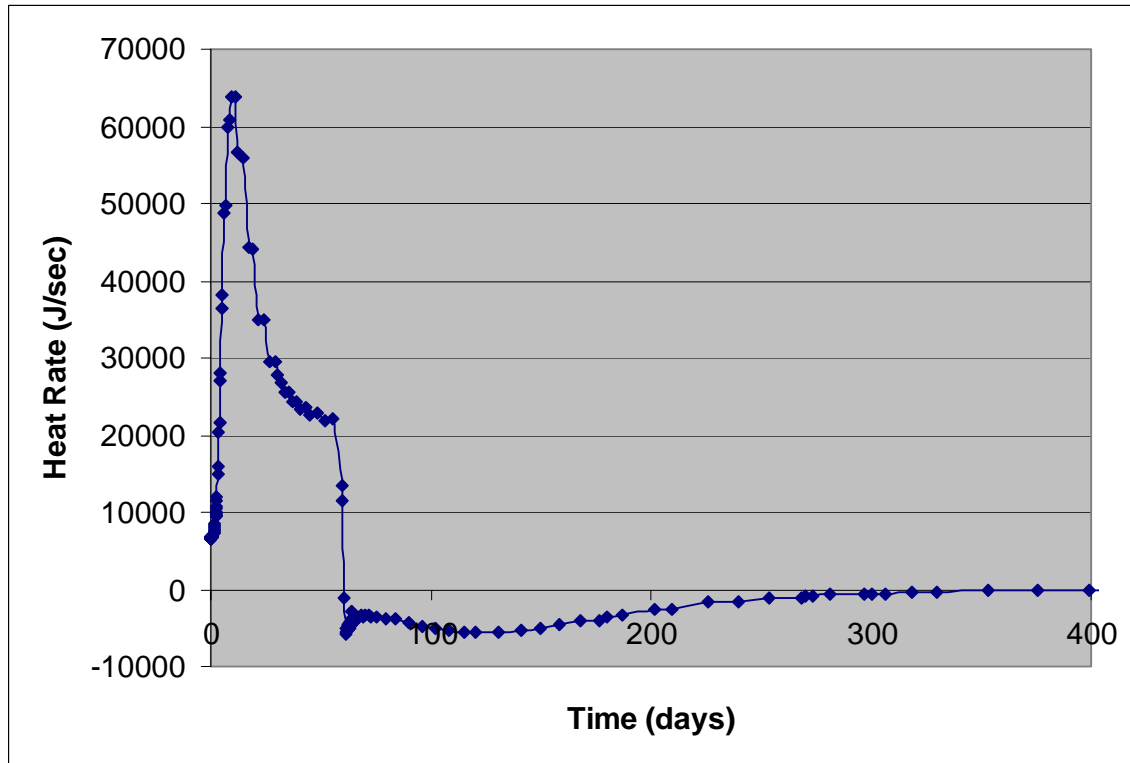


Figure 48. Heat rate (ΔH) vs. time plot for the “best case” scenario.

In Figure 48, a high initial positive heat rate is a function of the “pressure wave” effect and of the warm wastewater entering the river. This combined effect quickly subsides, and declines to 22,000 J/s beginning at 25 days. At 60 days, when injection ended, there was an immediate drop in the heat rate as heat conducted from the warm water of the river back into the subsurface. This conduction, which becomes apparent shortly after 60 days, takes much longer than the initial input of heat into the river via injection.

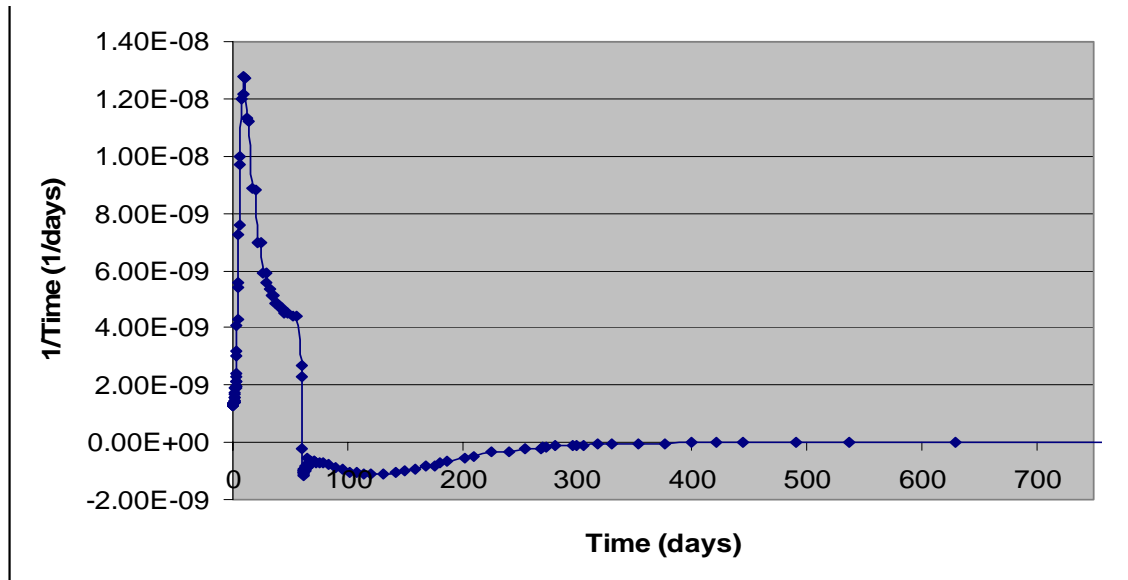


Figure 49. Normalized heat rate (ΔH_N) vs. time plot for the “best case” scenario.

The normalized heat flux, ΔH_N , for the maximum injection/hydraulic conductivity simulation is the same as the unnormalized heat offset, ΔH , except that all values of ΔH_N have been divided by 5.002×10^{12} Joules (the total amount of thermal energy injected into the model for this simulation). This plot is integrated to find the percentage of heat that has entered the river body over the time of model’s simulation. For the total integration, 1.71% of the total thermal energy enters the river. If re-conduction back into the subsurface is discounted (i.e., only positive heat fluxes are integrated), the integration is 3.07%. The maximum temperature during the simulation is 20.33 °C. The time to peak temperature is 5.05×10^6 s such that the scaling factor is 1.12×10^6 and the scaled temperature change is 1.81×10^{-5} °C.

Direct Mixing Analysis

Of interest for the SED case is how the river body temperature due to injection to the subsurface differs with direct injection (the current standard practice Willamette Valley municipalities). To compare, two assumptions about the river’s behavior had to be made. The first assumption was that at the point of injection, the river acts as a Continuously Stirred Tank Reactor (Figure 50); the second assumption was that the river and wastewater temperatures and flow rates remained fixed for the months of August – October.

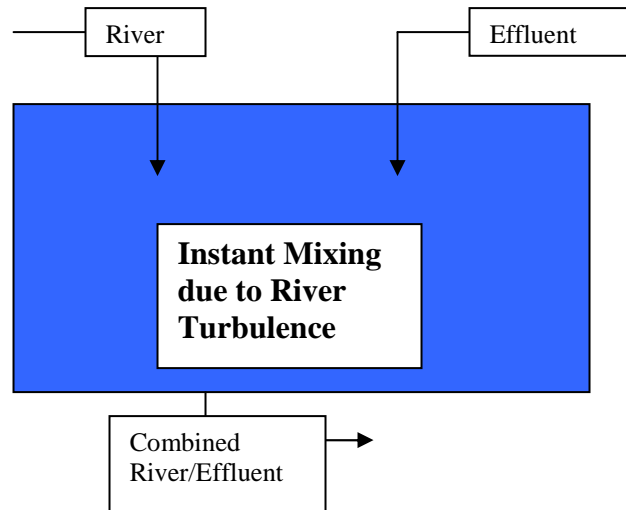


Figure 50. Idealized river-effluent interface as continuously stirred tank reactor (CSTR).

This means at the point that the warm wastewater effluent and the river meet, the two flows instantaneously mix, and reach thermal equilibrium. When this happens, the temperature of the combined flow becomes the volumetric flow-weighted average of the two streams (Figure 50).

$$(30) \quad T_{Combined} = \frac{Q_{effluent} T_{effluent} + Q_{River} T_{River}}{Q_{River} + Q_{effluent}}$$

Here $Q_{effluent}$ is the volumetric flow rate of the waste water directly injected into the river (m^3/s), $T_{effluent}$ is the temperature of the effluent ($^{\circ}C$), Q_{River} is the volumetric flow rate of the river, and T_{River} is the temperature of the river ($^{\circ}C$). $T_{Combined}$ is the temperature of the resulting flow assuming complete, instantaneous mixing. Using Table 32's values in equation (30), $T_{Combined}$ was found (Table 32).

Table 32. Parameters for and result of mixing analysis for combined temperature of river and effluent.

River Parameters	Units
$Q_{effluent}$	1.94(m^3/sec)
Q_{river}	195 (m^3/sec)
$T_{effluent}$	22.7 ($^{\circ}C$)
T_{river}	8 ($^{\circ}C$)
$T_{combined}$	8.1 ($^{\circ}C$)

Thus, assuming complete mixing, the river/effluent combined flow is raised 0.1 °C for the late summer/early fall months of August – October. Compared with the scaled peak temperatures for the various injection simulations, (0.1 °C versus 10⁻⁴ to 10⁻⁵ °C), injection to the subsurface becomes an attractive option.

To see if this was the case, a weighted average calculation similar to equation (30) for the SED case was used. The same assumptions of complete thermal mixing were made and calculations were performed using the model’s side channel and river volume, as well as the temperatures from each of those bodies of water. The result was

$$(31) \quad T_{Combined} = \frac{V_{River} T_{River} + V_{S.Channel} T_{S.Channel}}{V_{River} + V_{S.Chanel}}$$

Here V_{River} is the volume of the river in the model (m³), T_{River} is the temperature of the effluent (°C), $V_{S.Channel}$ is the volumetric flow rate of the river, and $T_{S.Channel}$ is the temperature of the side channel (°C). $T_{Combined}$ is the temperature of the resulting flow assuming complete, instantaneous mixing. Using Table 33’s values in equation (31), $T_{Combined}$ was found (Table 33).

Table 33. Parameters for and result of mixing analysis for combined temperature of river and side channel.

River Parameters	Units
V_{River}	6000 m ³
$V_{S.Channel}$	600 m ³
T_{River}	20.0 °C
$T_{S.Channel}$	8 °C
$T_{Combined}$	18.9 °C

Given this crude direct mixing calculation from equation (31) and the parameters in Table 33, direct injection/mixing of cool water would become an attractive option over the hyporheic “cold banking” effect seen in the modeling. Unfortunately, the economic/infrastructural realities of refrigeration and/or storage of large amounts of water would probably make this option infeasible to municipalities.

Discussion

Of primary interest is the result that, depending on the integration method, only 1 – 10% of heat injected in the SED scenario eventually arrives in the river. For all modeling scenarios, the amount of heat entering the river was small. The bulk of the heat passed out of the model under the river cells. This fact implies that the large simulated attenuation of the effluent’s heat signal is due in part to the particular boundary

conditions imposed in these simulations and invites the question: What attenuation is expected in the case where all injected heat enters the river?

While the boundary conditions used here may well be representative of the Willamette Valley, special care must be taken when applying these results, especially where boundary conditions are expected to be significantly different, such as with an alluvial aquifer thickness approaching the bankfull channel depth, in which case most of the subsurface flow would be forced into the channel rather than allowed to pass beneath it.

Also, heat “lost” to deeper flow paths in these simulations would, in reality, probably find its way back into the river at some point further downstream. Though the heat would not actually be lost, heat following longer flow paths would experience greater delay and dispersion before entering the stream than heat following shorter paths and would, therefore, still lessen the impact on stream temperatures during the critical months.

More importantly, given the scaled maximum temperatures reached during typical simulations, and even in the maximum injection case, heat attenuation would be significant even in the case that all injected heat entered the river directly rather than passing beneath it. In the maximum injection case, the maximum scaled temperature change is 1.81×10^{-5} °C, and the total integrated heat flux is 1.71% of that injected. In a case where this integrated amount is 100%, we multiply the temperature change by $(0.0171)^{-1}$ to get an estimated maximum temperature change of 1.06×10^{-3} °C, two orders of magnitude less than the temperature effect estimated from the direct mixing analysis. This estimate is conservative in the sense that the estimate of the percentage of heat entering the river used the total integral.

Another important result of the maximum injection simulation is that the peak temperature increase in the river did not occur until the end of the injection period of 60 days. This result indicates that, even neglecting attenuation of the injection’s temperature effect, much of that effect would likely be delayed until more favorable conditions regarding stream temperature.

The sensitivity analyses indicate that, while material characteristics such as density, thermal conductivity, and specific heat do affect the transfer of thermal energy to a river body, ultimately injection rate and hydraulic conductivity drive groundwater movement and are expected to be the major factors in determining the timing and magnitude of temperature change due to subsurface effluent discharge (SED).

This modeling project identified the major subsurface parameters for both SED and FPR scenarios that contributed to heat transfer in the subsurface. For both thermal energy mitigation strategies, the hydraulic conductivity is the major driver of heat transfer via groundwater. Given that subsurface water movement in TOUGH2 is governed by a three dimensional, multi-phase form of Darcy’s Law, this is not surprising. What is interesting is that river temperature did not significantly change during the sensitivity analysis for porosity. Porosity is present within the same afore-mentioned equation and was expected to affect groundwater velocity and, thus, heat transfer via groundwater to a greater degree.

Also, significant (and not expected) were the large effects of specific heat and, to a lesser extent, the density of the subsurface material on river temperature. These effects are due to the dependence of energy accumulation (equation (5)) on specific heat and density—their product being the heat capacity of a material.

For the SED case this meant that the denser materials would be more desirable because there would more mass per volume to absorb heat. For the FPR case, less dense materials would be better because they would allow more of the cooling energy to move with the groundwater. The other material parameter directly connected to the heat transfer capability of the subsurface is the thermal conductivity. For both the FPR and the SED scenarios, results were not particularly sensitive to this parameter.

Precipitation variation for both the SED and FPR case had little effect on river temperature, and for the FPR case, increasing the volume of the channel increased the cooling capacity; however, the overall change in temperature of the fluvial body was small, and thus the scaled peak temperature changes were very small.

Because the amount of cooling gained by the river from the side channel is small, any significant cooling benefit would require construction of large restoration projects (on the order of miles). Given development along the river, at least in the southern Willamette Valley, the inherent difficulties of restoration on such a scale would likely make this option prohibitively difficult and/or expensive. Though communities/municipalities might initially be squeamish about the subsurface injection of wastewater, the SED option, based upon the results of the TOUGH2 simulations, seems to be the most feasible option that was examined.

The modeling for this project produced a combination of intuitive and interesting results. The intuitive results included the magnitude of effect that variations in the hydraulic conductivity have on temperature variations within a water body for both the SED and FPR options. Interesting within the injection/hydraulic conductivity varying models was the lower temperatures for the two largest values of hydraulic conductivity.

This effect can be explained, at least in part, by the greater groundwater discharge associated with larger hydraulic conductivity and the same head gradient (Figure 51). This greater discharge leads to greater dilution of the warm injected water with cool groundwater and, hence, results in lower peak river temperatures than in the cases with lower hydraulic conductivity.

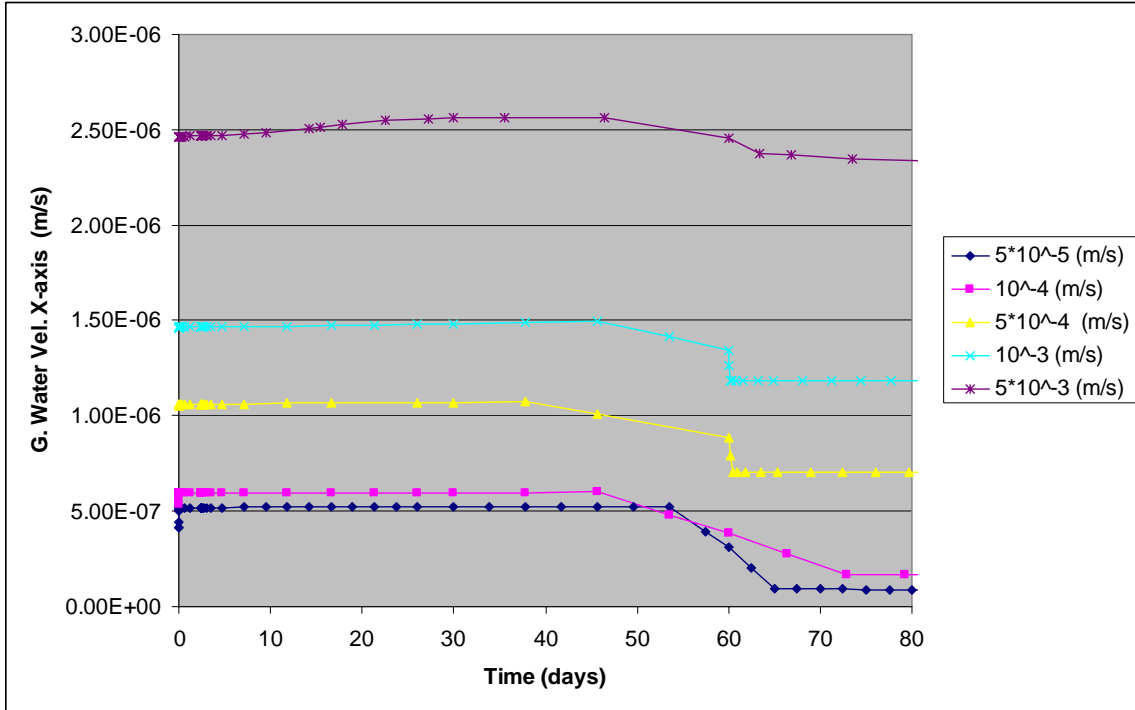


Figure 51. Groundwater velocity in the x-direction leaving the model. Greater velocity corresponds to greater discharge. At 60 days (2 months), subsurface injection ceased; for each of these simulations the drop off of groundwater velocity can be seen shortly thereafter.

Worthy of mention also is that this model represented an ideal case for hyporheic zone groundwater movement. The groundwater in the model moved perpendicular in the hyporheic zone to the river. In a real fluvial system, groundwater would move down the elevation gradient parallel to the river, as well as moving toward the river (Figure 52).

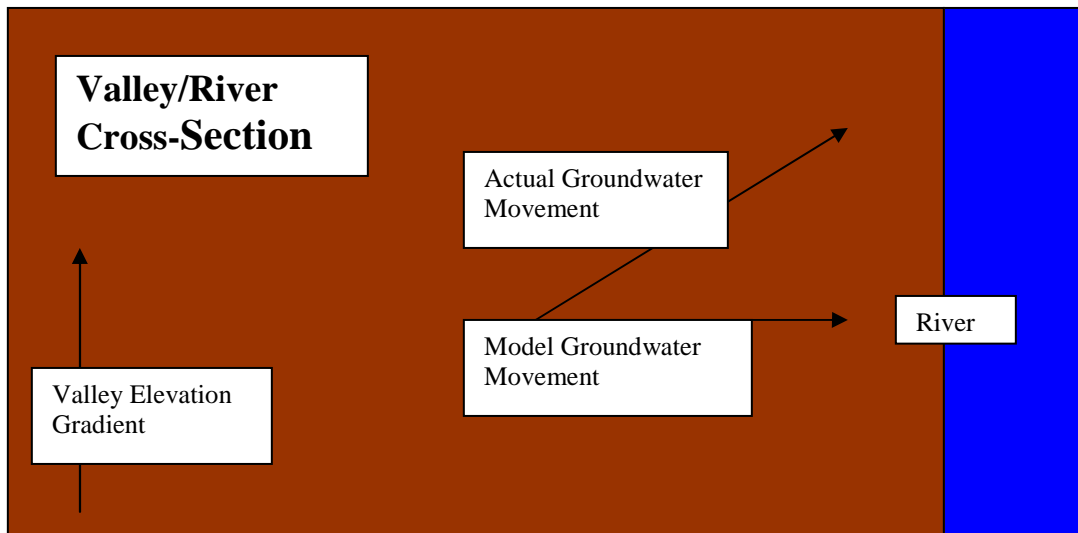


Figure 52. A plan (x-y plane) view of an idealized portion of the Willamette Valley that has the model's groundwater movement and hypothetical realistic movement of groundwater in the valley.

The logical next step would be to find a representative section of the southern Willamette River, quantify the subsurface parameters of interest (e.g., hydraulic conductivity, porosity, density), and study the interaction of hyporheic zone groundwater flow and the river.

Other ways in which the modeling scenarios differed from reality could have subtle but significant effects on outcomes. Perhaps most obvious is the fact that the surface water body in the models was nearly still rather than a flowing river. The major effect of this difference is in the dilution ratio, e.g., the ratio of the volume of warm effluent to the volume of river water into which that effluent flows. The scaling analysis performed herein is an attempt to account for that difference, but that analysis includes simplifications, e.g., the use of a single characteristic time, that may lead to some inaccuracies. This analysis should, therefore, be seen as an approximation rather than a precise calculation.

In order to keep the water body's temperature from changing in the absence of warm-water injection or cool-water seepage, temperatures of groundwater, surface water, porous medium, and precipitation were unrealistically homogeneous. In reality, the regional groundwater would be cooler, the surface water and the precipitation would be warmer, and the porous medium would have a temperature distribution ranging between the cool groundwater and warm surface water. While conduction of heat from warm surface water to the cooler subsurface has been measured in the field (Brown, 1969; Evans et al., 1998), in the SED scenario, conduction of heat from warmed surface water into the bed and banks was enhanced by this thermal homogeneity of the model, especially in cases with less dispersion (e.g., because of high hydraulic conductivity). In the model, the subsurface effluent discharge disproportionately warms the river because the latter is still and therefore dilutes the warm water less, as noted above. In contrast, once the warm water has entered the river, the bed and banks subsequently become disproportionately cold as the warm water is replaced by cool groundwater in the subsurface. This situation leads to an artificially large temperature gradient and, thus, enhanced conduction between the warmed river and its bed. We have attempted to account for this artificiality to some degree by reporting integrated heat inputs with and without inclusion of the negative heat fluxes from this enhanced conduction in the integrations.

The results presented herein, as well as the points addressed above, illustrate the complex role of hyporheic flow in determining stream temperature. Even in the simplified modeling scenarios, heat flow by advection, conduction, and convection involving both water and the porous medium produces some counter-intuitive results. Stream temperature in real rivers involves additional heat fluxes, most importantly solar radiation, as well as more complicated geometries and material heterogeneities. Still, the results presented here also indicate that the problem is potentially tractable given a rigorous, quantitative, process-based approach.

FPR Scenario Feasibility

The results of the FPR scenario point to the lack of feasibility for this scenario, at least for promoting cooling via hyporheic flow. While in the SED case small scaled peak changes in fluvial temperature were desirable; for the FPR case, large changes would have been favorable to see; however, this has not been the case. The scaled temperature changes for FPR case has been at most 10^{-3} °C. Because FPR assumes a once or twice a year flood event, this one-time temperature drop will not serve to cool a river body.

The reason probably stems from the small difference in thermal energy entering the river. The total heat offset from the default injection case was 2.54×10^{11} J. The “negative” cooling energy from the side channel was 7.52×10^9 J. Thus, the amount of cooling energy in the side channel was two orders of magnitude (in absolute value) less than the positive energy from injection.

A natural question to ask concerning “cold banking” becomes: What amount of floodplain restoration would make the FPR option feasible? Feasible could be defined many ways; however, for the purpose of this report, it will be defined as enjoying the same amount of input energy (albeit negative cooling energy) to the system as the default injection case. The ratio of input energies was used as a scaling ratio to find the length of the side channel needed to get the same input amount of energy:

$$(32) \quad SR = \frac{E_{SED}}{E_{FPR}}$$

Here the E_{FPR} is the energy input for FPR case (7.52×10^9 J) and E_{SED} is the energy input for the SED case (2.54×10^{11} J). Given equation (32) and the input energy for each case, the scaling ratio is 33.8. The dimensions of the side channel for the model are 5 m \times 60 m \times 2 m (x -, y -, and z -axes, respectively). Assuming that the dimensions in the x - and z -axes do not change, and multiplying 60 m by the scaling ratio, the length that the side channel would have to be along the y -axis is 2028 m.

This length, 2028 m, in the y -axis gives the same absolute value of energy input to the subsurface as the default injection total energy input. 2028 m (6654 ft) corresponds to more than a mile of flood plain restoration. It should be noted that the scaled changes in temperature for the injection cases were not large, and thus even with a larger restoration zone, river cooling from hyporheic flow via floodplain restoration would be difficult. For these reasons, the FPR option, as presented here, seems basically infeasible for reasons of promoting cooling via hyporheic flow.

That is not to say that floodplain restoration is not important and would not serve to cool Oregon’s rivers. If solar radiation is a significant portion of the heat input to a river during the summer, flood plain restoration (i.e. returning the river to its natural state), and the accompanying return of riparian zones would serve to cool the river. Even if the hyporheic cooling benefits of floodplain restoration are negligible, Oregon (and Oregonians) can still reap benefits from riparian shading and (presumably) wildlife habitat restoration near the river due to floodplain restoration.

For cooling via hyporheic flow, however, inundation approximately once a year, as was assumed here, is not enough to effect significant change. One obvious reason for the great disparity between the effects of the SED and FPR scenarios is the 60-day injection in the former vs. one-shot instantaneous filling and subsequent seepage in the latter. Promising restoration scenarios, then, will likely involve facilitating larger and more frequent hyporheic flows, e.g., between parts of the channel inundated during low flows when temperature problems are severe. The question remains whether significant warm or cold “banking” occurs at low flow, but a previous pilot study (A.G. Fernald and others, personal communication, 2005) indicates some promise in encouraging flow between the main channel and low-flow alcoves (i.e., water bodies connected to the main channel at only their downstream ends). The heat budget of hyporheic flow in such a situation is the subject of an upcoming study by the Principal Investigators of the present study. Should this and future studies support the initially promising results of Fernald and others, subsequent studies will seek to elucidate methods and scenarios by which hyporheic “cooling” at low stages (and warm months) might be encouraged (e.g., removal of bank-hardening structures in key locations to promote bank erosion and, thus, deposition of new gravel bars) and therefore figure into pollution credit trading schemes.

SED Scenario Feasibility

Of most interest for the injection modeling was the fact the majority of the heat from injection did not enter the river over the ten year simulation time. The majority of the heat escaped under the river, or out through the bottom of the model. This finding is significant because it raises the question: Is this the way heat will be transferred in an actual river /subsurface interaction? Because a river is the top of the water table for a given hydrologic sub-basin, in a river body, groundwater would not flow under a river to the other side of the catchment.

Assuming that these temperature and heat flow results are 100% accurate for the SED, the largest scaled temperature increase was no larger than 10^{-5} °C or, if it is assumed that 100% of the heat would enter the river, no larger than 10^{-3} °C. This result points to the SED option as a viable means of temperature reduction for Oregon’s water ways. Hydraulic conductivity is the primary subsurface parameter that determines the movement of groundwater, and the region of interest for subsurface discharge would have to be “calibrated” with respect to the time when the warm water would enter the river. Smaller hydraulic conductivities will more greatly disperse the heat and lower the peak temperature reached in the river, while larger hydraulic conductivities will allow greater injection rates. Other parameters of interest would be the specific heat and the material density. Increasing both density and specific heat will assist to mitigate the thermal effects.

The fact that groundwater may move underneath a river alone merits further study concerning heat transfer via hyporheic groundwater flow (Bedient and Huber, 2002). It is not unreasonable to believe that groundwater would run under the river, only to emerge somewhere down-gradient where an elevation change would cause an upwelling of groundwater into the river. Also, this movement of groundwater under a river in the hyporheic zone could only serve to further cool the waste water and disperse heat.

Finally, the scaled changes in peak temperature for the SED scenario point to the possibility of significant temperature reductions over the current direct injection practice. If all Willamette Valley municipalities were to use this strategy between the months of August and October, the effect on stream temperatures in the Willamette River could be significant. Analysis of the entire Willamette Valley's municipal waste water infrastructure is outside the realm of this project; however, as a future source of study, it is an important consideration.

It should be noted that subsurface injection has some pitfalls that were outside the scope of this project. One drawback of this option is the significant amount of surface area/undeveloped land required to utilize this option. Another issue is mixing with groundwater. Care will have to be taken to select sites that have minimal mixing with the greater groundwater system of the area. Whether this is a reasonable task is debatable, so a study of the implications of subsurface injection should be examined from both a biological and aquatic chemistry point of view.

Further Study

The next step for this project would be to select some representative section of the southern Willamette Valley and actually inject warm water (with a conservative tracer), and measure temperatures, groundwater directions/velocities, and times of tracer arrival in the river. Along with these measurements, the applicable subsurface parameters should be quantified, and analytical solutions should be used to check the empirical results of the study. Such an experiment would validate the model and, more importantly, provide a better understanding of the thermal energy budget in the hyporheic zone. An upcoming study by the PIs will use modeling, wells, and tracers to construct a preliminary heat budget for the hyporheic zone at low flows but will not actually inject warm water.

Another further study topic would be combining fluid flow and heat transfer parameters for the hyporheic zone in such a way that would create a dimensional number that would compare conductive versus convective heat transfer in the subsurface. The generation of a dimensionless number that would compare these heat transfer conveyances would be useful as a rough estimate for municipal wastewater facility operators and designers to understand if a site is suitable for subsurface injection. A great deal of study would have to go into the both the generation and empirical testing of this number; however, an accepted analytical tool that could quickly assess the thermal energy mitigation effect for a given site would be useful for future wastewater plant design and maintenance.

Conclusions

This modeling study indicates the potential feasibility of mitigating the effects of warm effluent on stream temperatures by subsurface injection of that effluent during summer months, when streams such as the Willamette River are typically temperature-limited. Mitigating effects include:

1. dispersion of the warm effluent pulse before reaching the river such that the temperature signal is spread out and peak temperature effect is reduced;

2. delay of the temperature effect due to subsurface travel time;
3. bypassing of the river as warm water passes beneath it;
4. conduction of heat from the river back into the bed and banks.

The first two effects are likely present in most or all potential injection sites, and the latter two are dependent on the particular boundary and initial conditions used in the modeling. Even neglecting the latter two effects, however, **likely mitigation would be at least a 100-fold decrease in peak river temperature impacts of effluent discharge** and a substantial delay of those impacts, potentially until the end of the temperature-limited months of late summer and early fall.

Sensitivity analyses reveal that the greatest sensitivities for this scenario are to (a) hydraulic conductivity of the porous medium, (b) distance between the injection site and the river, and (c) injection rate. Hydraulic conductivity is a highly variable property in nature and directly affects the subsurface flow rate. Thus, this property affects the amount of pulse dispersion, the delay, and the rate at which effluent can be injected into the subsurface. Distance affects dispersion and delay—dispersion and delay are both greater over greater travel distances. Injection rate, of course, is equivalent to the amount of heat added to the system and so directly affects the temperature effect on the river.

Floodplain restoration, in the form of providing additional side channels accessible to flows at flood stages, was also tested as a mitigation strategy. Modeling results indicate that this strategy is unlikely to significantly affect river temperatures by increasing the amount of cool water in the hyporheic zone. First, the dispersion that provides beneficial effects for effluent injection also dampens the effect of cold flood water on river temperature. Second, rare inundation during floods is unlikely to provide enough benefit to justify the cost.

It is important to note the limitations of the analysis regarding floodplain restoration. First, only the effects of increased cold water in the hyporheic zone were considered. Other benefits would likely include greater shading due to riparian canopy and greater diversity of aquatic and terrestrial habitats. Second, only the effects of rare inundation (i.e., at high stages) were considered. Restoration measures that would increase hyporheic flow during the low flows of the warm summer months appear promising and are the subject of upcoming studies by the authors but were not considered here. Such measures might include selective removal of bank-hardening structures (revetments) to allow bank erosion, channel widening, and thus deposition of new gravel bars. Such new gravel would likely have high hydraulic conductivity and thereby promote greater hyporheic flows than presently occur in many older gravel bars.

Table of Variables

Variables	Units	Description
A	m ²	Area
B	Unitless	Phase of a substance in TOUGH2
C	J/kg×°K	Specific heat

D	m^2/s	Diffusion coefficient vector
E_T	J	Thermal energy contained in the river
F	$kg/m^2 \times s$	Mass or energy flux (vector)
f_S	Unitless	Scaling factor for conversion of model temperatures to "real" river temperatures
g	m/s^2	gravitational acceleration vector
$H_{Injection}$	J/s	Heat rate of injected waste water
H_{out}	J/s	Thermal energy leaving the river/out of the model
H_0	J/s	The amount of heat per unit time entering the river from groundwater recharge
H_R	J/s	The combined amount of heat per unit time entering the river due to the SED/FPR and groundwater recharge
h		specific enthalpy
K	m/s	Hydraulic conductivity
k	m^2	permeability
M^K	$(kg \text{ or } J)/m^3$	Mass or energy per unit volume for a substance K
n	Unitless	Normal vector
n	Unitless	Porosity
P	N/m^2	Pressure
Q	m^3/sec	flow rate
q^K	$(kg \text{ or } J)/s$	Source/Sink for a given substance/thermal energy K in TOUGH2
S_B	Unitless	Fraction of phase B in the pores of the subsurface
T	$^{\circ}C$	Temperature
t	sec	time
u	J/kg	specific energy of a substance
X_B^K	Unitless	Mass fraction of substance K in phase B
V	m^3	Volume
V_x	m/s	Groundwater velocity leaving the model in the x-direction
Γ	m^2	Surface area that TOUGH2 integrates over to find the advective flux through cells
ΔH	J/s	The amount of heat per unit time entering the river only due to the SED/FPR
ΔH_N	1/sec	normalized heat rate into the river
λ	$W/m \times ^{\circ}K$	thermal conductivity
μ	$(N \times s)/m^2$	fluid viscosity
ρ	kg/m^3	Material Density

References

Bedient P.B., Huber W.C. (2002) Hydrology and Floodplain Analysis 3rd Edition pgs 86 – 89.

- A.J. Boulton, S Findlay, P. Marmonier, E.H. Stanley, and H.M. Valett (1998) The Functional Significance of the Hyporheic Zone in Steams and Rivers, Annual Review of Ecological Systems, Vol 29 pgs 59 – 81.
- Bowman, A.J., *Ancillary Habitat Restoration Through Water Quality Trading: Expanding the Functional Hyporheic Zone of the Willamette River to Reduce Elevated Water Temperatures*. Private Lands Conservation Counsel, Defenders of Wildlife, West Linn, OR, November 4, 2003.
- Brown, G. W. (1969). “Predicting temperatures of small streams.” *Water Resources Research* **5**(1): 68-75.
- Das M. B., (1998) Principles of Geotechnical Engineering 4th Edition pg 164 – 166.
- Evans, E. C., G. R. McGregor, et al. (1998). “River energy budgets with special reference to river bed processes.” *Hydrological Processes* **12**: 575-595.
- A.G. Fernald, P.J. Wigington Jr., and Dixon H. Landers (2001) Transient Storage and Hyporheic Flow Along the Willamette River: Field Measurements and Model Estimates, *Water Science Research*, Vol. 37, No. 6, June 2001.
- B.G. Fraser and D. D. Williams Seasonal Boundary (1997) Dynamics of a Groundwater/Surface-Water Ecotone, *Ecology*: Vol. 79, No. 6, pp. 2019–2031.
- D. R. Geist, T. P. Hanrahan, E. V. Arntzen, G. A. McMichael, C. J. Murray, and Y.J. Chien (2002), Physicochemical Characteristics of the Hyporheic Zone Affect Redd Site Selection by Chum Salmon and Fall Chinook Salmon in the Columbia River, *North American Journal of Fisheries Management*, Vol. 22, pgs 1077 – 1085.
- Hiscock K(2005), *Hydrogeology: Principles and Practice* pgs 18 – 21.
- Incropera F.P., DeWitt D.P. (1996) *Fundamentals of Thermodynamics* 4th Edition, Appendix A: pg 837, 16 – 20.
- McClave J.T., Dietrich F.H., (1994) *Statistics* 6th Edition pg 220.
- ODEQ, Draft Willamette Basin Total Maximum Daily Load (TMDL) and Water Quality Management Plan, Oregon Department of Environmental Quality, Salem, Oregon, October, 2004. Available at <http://www.deq.state.or.us/WQ/TMDLs/WillametteBasin.htm>. Last accessed 12/22/2005.
- ODEQ, Willamette Basin: Proposed Temperature TMDL, Oregon Department of Environmental Quality, Salem Oregon, 10-10-04, Available at : http://www.deq.state.or.us/wq/wqfact/WR_tempFS.pdf. Last accessed 12/26/05.
- ODEQ, Southern Willamette Valley Groundwater Assessment 2000 – 2001G. Aitken, J. Arendt, A Auldridge, Oregon Department of Environmental Quality, Salem Oregon, 10-10-04, Available at : http://www.deq.state.or.us/wq/groundwa/SWVGWAssessmentNitrateStudyTOC_Report.pdf.

- G.C. Poole, and C.H. Berman, Pathways of Human Influence on Water Temperature Dynamics in Stream Channels, Environmental Management, Feb 2002.
- Pruess K, Oldenburg C, and G Moridis (1999) TOUGH2 Users Guide, Version 2 Earth Science Division/ Lawrence Berkley Laboratory.
- Sonntag R.E., Borgnakke C., and Van Wylen G.J., (1998) Fundamentals of Thermodynamics 5th Edition, Appendix B; pgs 664 -671.
- S.A. Thomas, H.M. Valett, P.J. Mulholland C.S. Fellows, J.R. Webster, C.N. Dahm, and C.G. Peterson (2001) Nitrogen Retention in Headwater Streams: The Influence of Groundwater-Surface Water Exchange, Proceedings on the 2nd Annual International Nitrogen Conference on Science and Policy.
- Thunderhead Engineering Consultants, Inc., *Examples Using the PetraSim Pre- and Post-Processor for TOUGH2*. Manhattan, KS, June, 2005, <http://www.thunderheadeng.com/petrasim/help/tough/examples/manuals/TOUGH2%20Examples%20-%202005-06-15.pdf>.
- H.M. Valett, J.A. Morrice, M. E. Campana, and C.N. Dahm (1996) Parent Lithology, Surface-Groundwater Exchange, and Nitrate Retention in Headwater Streams, American Society of Limnology and Oceanography, Vol 41, No. 2, (1996).
- White, DS. (1993) Perspectives on defining and delineating hyporheic zones. Journal of the North American Benthological Society, Vol. 12, no. 1, pp. 61-69. 1993.
- G.J. Wroblicky, M. E. Campana, C. N. Dahm, H.M. Valett, J.A. Morrice, K. S. Henry, and M. A. Baker (1994) Simulations of Stream-Groundwater Exchange and Near-Stream Flow Paths of Two First Order Mountain Streams Using MODFLOW, Second International Conference on Groundwater Ecology, March 1994.

Appendix A: Annotated Bibliography of Heat Transport in the Hyporheic Zone of Big Rivers

This annotated bibliography was put together over the summer of 2005 and attempts to find all studies of heat transport in the hyporheic zone, particularly as it applies to large rivers such as the Willamette. While a number of papers were not tracked down and perhaps 20 references were not pursued, this annotated bibliography represents the most important work on the subject to date.

1. Arscott, D. B., K. Tockner, et al. (2001). "Thermal heterogeneity along a braided floodplain river (Tagliamento River, northeastern Italy)." Canadian Journal of Fisheries and Aquatic Science **58**: 2359–2373.

Suggests that lower-elevation (larger river) floodplains are more heterogeneous wrt temperature due to standing water bodies. Paper suggests that hyporheic exchange reduces maximum temperatures and increases minimum temperatures.

2. Bartholow, J. M. (1989). Stream temperature investigations: Field and analytical methods. Ft. Collins, Colorado, USFW, Biological Report 89(17), : 139 p.

Methods description, somewhat dated, for measuring stream temperature and heat budgets. May not be relevant for hyporheic exchange but looks like a good methods overview.

3. Bogan, T., O. Mohseni, et al. (2003). "Stream temperature-equilibrium temperature relationship." Water Resources Research **39**(9): 1245, doi:10.1029/2003WR002034.

Shows that stream temperature averages over 7 day periods are most strongly determined by atmospheric conditions (radiation and air temperature). Uses 596 USGS stream records to find a regression based on "equilibrium temperature". By definition, equilibrium temperature ignores things like hyporheic exchange, which is not mentioned in the paper.

4. Bogan, T., H. G. Stefan, et al. (2004). "Imprints of secondary heat sources on the stream temperature/equilibrium relationship." Water Resources Research **40**: W12510, doi:10.1029/2003WR002733.

Examines "secondary heat sources", i.e., everything but the atmosphere and some things that aren't really heat sources but are sinks. Looks at shading, groundwater inputs, wind sheltering and does an analysis of 596 streams from USGS records to try to determine their effects. No mention of hyporheic zone in paper.

5. Brown, G. W. (1969). "Predicting temperatures of small streams." Water Resources Research **5**(1): 68-75.

Evans et al. 1998 references this as suggesting stream bed processes may be a significant component of stream heat budgets.

6. Brown, L. E., D. M. Hannah, et al. (2005). "Spatial and temporal water column and streambed temperature dynamics within an alpine catchment: implications for benthic communities." Hydrological Processes **19**: 1585–1610.

Looks at thermal heterogeneity in a group of small streams (all less than 1 m³/s, most less than 100 L/s) in the Pyrenees. Quite a lot of data, including water column, stream bed (hyporheic zone), plus air temp and solar radiation. Data look to be quite different from that in Evan and Petts 1997, in that hyporheic temps appear to be much more similar to the stream (but lagged).

7. Bundschuh, J. (1993). "Modeling Annual Variations of Spring and Groundwater Temperatures Associated with Shallow Aquifer Systems." Journal of Hydrology **142**(1/4): 427-444.

Modeling paper. Abstract says 4 different cases of heat flow in aquifers were modeled and compared to temperature measurements made in the field. Paper suggests a method using amplitude and phase differences between surface (source) and depth to determine influence of groundwater mixing.

8. Caissie, D., M. G. Satish, et al. (2005). "Predicting river water temperatures using the equilibrium temperature concept with application on Miramichi River catchments (New Brunswick, Canada)." HYDROLOGICAL PROCESSES **19**: 2137–2159.

Paper neglects hyporheic zone because it is using the equilibrium approach for long time periods (days?)

9. Clark, E., B. W. Webb, et al. (1999). "Microthermal gradients and ecological implications in Dorset rivers." Hydrological Processes **13**: 423-438.

Paper reports on the heterogeneity of temperature in streams and the hyporheic zone (referred to as the stream bed). Unfortunately the paper is hard to read - for example, it never says whether "Dorset rivers" are big, small or in between. The paper seems to struggle with having a central theme other than that temperature varies spatially (primarily with depth) in both the water and substrate. From our perspective, possibly its most important contribution is that it highlights the fact that temperature can vary by many degrees over short distances in rivers. It also raises the issue (also in Evans and Petts 1997) that hyporheic temperature is a mixture of stream and regional(?) groundwater temperature.

10. Comer, L. E. and W. J. Grenney (1977). "Heat transfer processes in the bed of a small stream." Water Research **2**(8): 743-744.

Technical note?

11. Constantz, J. (1998). "Interaction between stream temperature, streamflow, and groundwater exchanges in alpine streams." Water Resources Research **34**(7): 1609-1615.

Study showing quantitatively that streamflow influences stream temperature (i.e., idea that stream temperature is proportional to heat load/discharge), with Figure 10 being fairly conclusive on this point. Paper also introduces the point that stream temperature

influences the hydraulic conductivity of the stream bed via the viscosity of water, so that in a losing reach there can be a positive feedback between discharge and stream temperature (i.e., lower discharge leads to increased temperature resulting in higher K and greater losses, yet lower discharge).

12. Constantz, J., M. H. Cox, et al. (2003). "Comparison of heat and bromide as ground water tracers near streams." Ground Water **41**(5): 647-56.

Compared heat and bromide as tracers by calibrating model to temperature and then using it to simulate bromide transport. Instrumented 17 km reach at 5 sites each with 6 piezometers. Injected NaBr in stream and measured breakthrough at most of the piezometers. Used VS2DH (Healy & Ronan 1996) and VS2DT (Healy 1990) to do modeling. As far as I can tell the data were collected in the saturated zone, so the vadose zone capability of the model is superfluous in this study.

13. Constantz, J., A. E. Stewart, et al. (2002). "Analysis of temperature profiles for investigating stream losses beneath ephemeral channels." Water Resources Research **38**(12): 1316, doi:10.1029/2001WR001221.

Uses stream bed temperature to estimate recharge in ephemeral streams. Has a brief discussion of alternative models on 3rd page of article. They used VS2DH but mention TOUGH2. May be a good place to learn a bit about modeling of hyporheic temperature.

14. Constantz, J., D. Stonestrom, et al. (2001). "Analysis of streambed temperatures in ephemeral channels to determine streamflow frequency and duration." Water Resources Research **37**(2): 317-328.

Modeled streambed temperature using VS2DH. Niswonger involved (our contact for TOUGH2 at USGS). Modeling details not presented in paper.

15. Constantz, J. and C. L. Thomas (1996). "The use of streambed temperature profiles to estimate the depth, duration, and rate of percolation beneath arroyos." Water Resources Research **32**(12): 3597-3602.

First of the papers on heat as a tracer. Data and no modeling.

16. Constantz, J. and C. L. Thomas (1997). "Stream bed temperature profiles as indicators of percolation characteristics beneath arroyos in the Middle Rio Grande Basin, USA." Hydrological Processes **11**: 1621-1634.

Early paper that Constantz used to show that periodic recharge events in a dry climate (Albuquerque, NM) can be recorded by measuring temperature. Lots of data in this paper, but the modeling is in other papers.

17. Evans, E. C., G. R. McGregor, et al. (1998). "River energy budgets with special reference to river bed processes." Hydrological Processes **12**: 575-595.

Conducts a detailed, quantitative heat balance on a stream, looking at hyporheic zone (stream bed) in particular. They conclude that stream bed processes are responsible for about 16% of the heat output of the stream (i.e., cooling), but most of this is due to conduction. If I read their discussion and conclusions section correctly, they state that

about 20% of the 16% may be due to advection, so perhaps 3-4% of the heat loss in the stream is due to hyporheic exchange.

18. Evans, E. C. and G. E. Petts (1997). "Hyporheic temperature patterns within riffles." Hydrological Sciences **42**(2): 199-213.

Examines hyporheic temperature in 2 riffles in a moderate-sized river (catchment area of 110 km²) in the UK. Logged data at 12 min intervals in 20 piezometers for a 5-day period. While it appears they have not done much quantitative work with the data, they have a large quantity of data and it may be relevant for some of our questions. **In particular, their Figure 3 shows that the hyporheic zone temperatures of their river are some kind of lagged average of stream and groundwater temperatures.** This seems to go against the idea that the hyporheic zone is only a storage zone for heat and not a mixer of heat, and it is in support of the general ideas proposed by Fernald et al.

19. Fernald, A., D. Landers, et al. (2000). Water quality effects of hyporheic processing in a large river. Riparian Ecology and Management in Multi-Land Use Watersheds, Portland, Oregon, American Water Resources Association.

Forerunner for submitted paper. Contains some temperature data for hyporheic zone in the Willamette.

20. Fernald, A. G., D. H. Landers, et al. (2005). "Water quality changes along hyporheic flow paths between a large gravel bed river channel and alcove habitats." submitted to Water Resources Research (do not cite).

Only paper that explicitly deals with the temperature effect of the hyporheic zone on a large river? Motivational for our NSF study in that it shows that the hyporheic zone may have a significant effect on stream temperature of a big river. Study on Willamette River between Corvallis and Albany, largely south of Harrisburg.

21. Geist, D. R., T. P. Hanrahan, et al. (2002). "Physicochemical characteristics of the hyporheic zone affect redd site selection by chum salmon and fall chinook salmon in the Columbia River." North American Journal of Fisheries Management **22**: 1077-1085.

Found that hyporheic zone temperature in Columbia River affected fall chinook redds spawn at hyporheic downwelling sites but chum spawn at hyporheic upwelling sites, which they hypothesize explain the difference in spawning locations. One of only a few papers that deal with both the hyporheic zone and temperature in a large river.

22. Hannah, D. M., I. A. Malcolm, et al. (2004). "Heat exchanges and temperatures within a salmon spawning stream in the Cairngorms, Scotland: Seasonal and sub-seasonal dynamics." RIVER RESEARCH AND APPLICATIONS **20**: 635-652.

Did quantitative study of temperature in stream and hyporheic zone of 500 L/s stream. Very interestingly found that friction of water on the stream bed is an important heat source. Found hyporheic zone is a significant factor in stream temp.

23. Hondzo, M. and H. G. Stefan (1994). "Riverbed heat conduction prediction." Water Resources Research **30**(5): 1503–1514.

Calculates that heat conduction (not advection) into a river bed could be important, resulting in up to 40 W/m² heat exchange and 0.8 °C per meter depth of water temperature change in stream. Ignores flowing water.

24. Jackman, A. P. (1977). Thermal loading of natural streams, USGS, U.S. Geological Survey Professional Paper 991, : 39 p.

Covers basics of heat transport and heat loading in streams, providing overview of physics and 1-D equations, and provides examples. Uses framework of excess temperature.

25. Johnson, S. L. (2003). "Stream temperature: scaling of observations and issues for modelling." Hydrological Processes **17**: 497-499.

26. Johnson, S. L. (2004). "Factors influencing stream temperatures in small streams: substrate effects and a shading experiment." Canadian Journal of Fisheries and Aquatic Sciences **61**(doi: 10.1139/F04-040): 913-923.

Very important paper dealing with the effect of shading and the hyporheic zone on stream temperature. Excellent set of data and clearly thought out analysis in WS03 in the HJ Andrews. Shows that shading (incident radiation) has a large impact on the stream and that in the absence of incident radiation (both long and shortwave, I think) that the stream actually **cools** due primarily to evaporative and convective heat losses. Also shows the very important moderating effect of hyporheic exchange. Shows a nice conceptual and quantitative heat balance for WS03.

27. Lewis, S. L., G. E. Grant, et al. (2005). Literature review of possible effects of gravel augmentation on stream temperature. Corvallis, Oregon, Oregon State University, : 11 p.

Literature review of hyporheic stream temperature as it relates to relicensing project on Clackamas for PGE.

28. Malard, F., A. Mangin, et al. (2001). "Thermal heterogeneity in the hyporheic zone of a glacial floodplain." Canadian Journal of Fisheries and Aquatic Sciences **58**: 1319–1335.

Study of temperature in surface and hyporheic zone of glacial streams in Roseg River (Switzerland). Used SiO₂ concentrations to help determine residence time of hyporheic water (i.e., to distinguish HZ water w short res time and therefore likely to have short lag time on temperatures from HZ water w long res time). Used cross-correlation between stream and HZ temperatures to examine lag times. Their results show average daily temperatures in the hyporheic zone equal to average daily temperatures in some parts of the stream (short HZ res time) but that in other places the average daily temp of the HZ is different than the stream. New terminology (to us) for streams: kryal (glacial-fed), rhithral (snowmelt-fed), and krenal (groundwater-fed).

29. Malcolm, I. A., C. Soulsby, et al. (2002). "Thermal regime in the hyporheic zone of two contrasting salmonid spawning streams: Ecological and hydrological implications." Fisheries Management and Ecology **9**: 1-10.

Examines the effect of the hyporheic temperature on salmon spawning in 2 small streams in the UK (Scotland). A moderate amount of temperature data, no modeling.

30. Mellina, E., R. D. Moore, et al. (2002). "Stream temperature responses to clearcut logging in British Columbia: the moderating influences of groundwater and headwater lakes." Canadian Journal of Fisheries and Aquatic Sciences **59**: 1886-1900.

Studied temperatures in small streams (headwater and lake-fed) before and after clear-cutting. Found cooling downstream of lake and warming downstream of headwater reach both before and after clear-cutting. Cooling explained as due to groundwater. Hyporheic exchange not studied in paper, though hypothesized to play a role.

31. Poole, G. C. and C. H. Berman (2001). "An Ecological Perspective on In-Stream Temperature: Natural Heat Dynamics and Mechanisms of Human-Caused Thermal Degradation." Environmental Management **27**(6): 787-802.

Good overview of effects on stream temperature, including the hyporheic zone - this would be a good paper to introduce stream temperature with. Has one of the few discussions in the literature of the effects of the hyporheic zone on a large river (scale of Willamette), but it is speculative, with no data.

32. Poole, G. C., J. A. Stanford, et al. (2000). A Linked GIS/Modeling Approach to Assessing the Influence of Flood-plain Structure on Surface- and Ground-water Routing in Rivers, 4th International Conference on Integrating GIS and Environmental Modeling (GIS/EM4): Problems, Prospects and Research Needs. Banff, Alberta, Canada, September 2 - 8, 2000.

Paper modeling surface-water groundwater interactions on a floodplain. Web paper at <http://www.eco-metrics.com/BasePages/Publications/Pooleetal2000/>

33. Power, G., R. S. Brown, et al. (1999). "Groundwater and fish - insights from northern North America." Hydrological Processes **13**: 401-422.

34. Rivers-Moore, N. A. and G. P. W. Jewitt (2004). "Intra-annual thermal patterns in the main rivers of the Sabie Catchment, Mpumalanga, South Africa." Water SA **30**(4): 445-452.

Study of stream temperature in Kruger National Park, South Africa. References potential importance of hyporheic exchange on stream temperature, but did not collect data on it.

35. Ronan, A. D., D. E. Prudic, et al. (1998). "Field study and simulation of diurnal temperature effects on infiltration and variably saturated flow beneath an ephemeral stream." Water Resources Research **34**(9): 2137-2135.

Uses vadose zone temperature to estimate recharge below an ephemeral stream. Probably not too relevant for unless transient temperature in the vadose zone is deemed important. Model used was VS2DH (Healy & Ronan, 1996).

36. Sinokrot, B. A. and H. G. Stefan (1993). "Stream temperature dynamics: Measurements and modeling." Water Resources Research **29**(7): 2299-2312.

Important paper that overviews the basic equations and physics of stream temperature. Key paper for modeling stream temperature.

37. Sinokrot, B. A. and H. G. Stefan (1994). "Stream Water-Temperature Sensitivity to Weather and Bed Parameters." Journal of Hydraulic Engineering **120**(6): 722-736.

Models stream bed conduction (ignores advection) and concludes that this is not very important to the AVERAGE daily temperature.

38. Stallman, R. W. (1965). "Steady one-dimensional fluid flow in a semi-infinite porous medium with sinusoidal surface temperature." Journal of Geophysical Research **70**(12): 2821-2827.

Develops a closed-form solution to the 1-D heat transport equation with a varying boundary condition.

39. Stonestrom, D. A. and K. W. Blasch (2003). Determining temperature and thermal properties for heat-based studies of surface-water ground-water interactions. Heat as a Tool for Studying the Movement of Ground Water Near Streams, Circular 1260. D. A. Stonestrom and J. Constantz. Reston, Virginia, US Geological Survey: 73-80.

40. Stonestrom, D. A. and J. Constantz, Eds. (2003). Heat as a Tool for Studying the Movement of Ground Water Near Streams, Circular 1260. Reston, Virginia, US Geological Survey.

41. Story, A., R. D. Moore, et al. (2003). "Stream temperatures in two shaded reaches below cutblocks and logging roads: downstream cooling linked to subsurface hydrology." Canadian Journal of Forest Research **33**: 1383-1396.

Study in BC showing that in a small stream (maximum effect below 5 L/s) hyporheic exchange and bed conduction accounted for about 60% of observed cooling of 3 °C on the maximum daily temperature.

42. Uehlinger, U., F. Malardi, et al. (2003). "Thermal patterns in the surface waters of a glacial river corridor (Val Roseg, Switzerland)." Freshwater Biology **48**: 284-300.

43. Webb, B. W., P. D. Clack, et al. (2003). "Water-air temperature relationships in a Devon river system and the role of flow." Hydrological Processes **17**: 3069-3084.

44. White, D. S., C. H. Elzinga, et al. (1987). "Temperature Patterns Within the Hyporheic Zone of a Northern Michigan River." Journal of the North American Benthological Society **6**(2): 85-91.

45. Younus, M., M. Hondzo, et al. (2000). "Stream temperature dynamics in upland agricultural watersheds." Journal of Environmental Engineering **126**(6): 518-523.

Appendix B: Spatial Datalayers for Willamette Temperature Study

For this portion of the project, we selected two different types of spatial data layers, containers and base data. The containers, or clips, were used to subset the base datasets and the data outcomes of this process were examined. Spatial data consisted of three clips or containers, and up to ten base data layers. Using a “cookie analogy”, the containers can be thought of as cookie cutters, and the base layers as cookie dough. The containers and base data layers are listed and briefly described below.

Spatial Containers

All spatial containers (a.k.a. “clips”, “cookie cutters”) run from Albany upriver to Eugene.

1. Maximum lateral extent of historical flooding (at minimum at USACE 100 year floodplain; in many areas extends beyond). It should be noted that this is a lateral extent. It does not provide any flood depths, and it does not include any areas that may not have been flooded (e.g. small hills within the floodplain).
2. Maximum lateral extent of 1996 flood. The same caveats concerning depth and non-flooded islands apply to this container as well.
3. Equidistant “bands” extending laterally from Willamette River 2000 primary active channel.

Band widths are:

120 m
240 m
360 m
480 m
600 m

Note that these 5 bands are combined into a single clip file to reduce the proliferation of files. Determination of band distances was based on a combination of current land use laws for riparian buffers, requests from ODEQ, and base data layers with minimum pixel size of 30 m.

4. The spatial containers listed above were also subdivided by 1-km wide floodplain slices to provide additional information on a longitudinal axis. Unlike features such as river mile, the floodplain slices are comparatively constant over time.

Base Datalayers

The spatial clips described above were each applied to the following spatial datalayers.

1. 30 meter Digital Elevation Model (DEM). All coordinates (x,y,z) are in meters.

2. 10 meter DEM. The x and y coordinates are in meters, to correspond to all of the other datalayers. However, we let the z-axis units stay in feet to provide additional vertical detail. Note this decision makes for very large files. Also, the 10-meter DEM is less than satisfactory for this portion of the Willamette Valley. It is based on interpolation of USGS topo maps.
3. Public land ownership. 30-meter pixel size. Includes federal, state, county, city parcels ranging from ODOT right-of-way to national wildlife refuges and city parks.
4. Soil type from the SSURGO database provided by NRCS. We are focusing only on the “hydrogroup” soil classification for purposes of this project. However, all available fields are included in this data layer, including depth to water table, soil erodibility, and soil capability, etc.
5. Land use-land cover for 2000. This is based on TM satellite imagery analysis (30 m pixel grain). There are approximately 65 class types in the raw data. We have combined these into two levels of coarser scale lumping in a lookup table:
 - a. Type 1: Natural Vegetation, Agriculture, Built, Water, Miscellaneous
 - b. Type 2: Forest, Shrubland, Grassland, Savanna, Wetland (all Natural Vegetation), Grass, Intensive, Woody (all Agriculture), urban, rural, transportation (all Built), Water, Miscellaneous.
6. Pre-settlement vegetation from General Land Office surveys circa 1850. This data layer provides a snapshot of land cover change over the past 150 years, and provides some clues for what type of plant community would most suitable for restoration at a given locale (e.g., prairie or forest).

In addition to these 18 data layers (6 base layers X 3 spatial containers), we also have data for the current and historic Willamette River. The historic data provide locations of “lost” features such as secondary channels, alcoves or floodplain lakes. These areas are important in determining potential sites for river and floodplain restoration.

1. Length of river by channel type (main channel, secondary channel, alcove) for the river in 1850, 1895, 1932 and 2000.
2. Area of river features by channel type (as above, plus islands and off-channel wet features such as remnant floodplain lakes and gravel pits) for 1850, 1895, 1932 and 2000.

Results and Products

We are providing ODEQ with the following products for each of the data layers we generated using the clipping approach outlined above. Information for each product is listed in a spreadsheet within the data directory.

1. The compressed spatial data layer as either an ARC export file (coverage.e00) or a grid (grid.zip).
2. Lookup tables as needed for some of the data layers (land use/land cover for 2000, public land ownership, vegetation ca. 1851).
3. The database table from each data layer as a .dbf file.
4. The database table imported into an Excel spreadsheet (.xls) for all data except that generated from the 10 meter DEM (too many records for Excel to handle). Within each spreadsheet, we have performed some preliminary database sorting and summarizing using Excel pivot tables.
5. For a subset of these data, we have made a number of graphic outputs. These include line and stacked bar graphs (from SigmaPlot) as well as map imagery (from Arc/GIS). All images are available as TIFF's, and can be easily pulled into other formats (such as PowerPoint). All of the graphs are in "EKG" format to highlight the variation of each parameter along the floodplain axis between Albany and Eugene.

There are a total of 27 data layers provided, each with a data base and spreadsheet file (some exceptions, see below). There are also over 30 graphs and maps to use for reports or presentations.

The data layers and spreadsheets are largely self-explanatory. However, listed below are some additional results.

1. Given the greater vertical spatial resolution of the 10-meter DEM, we have decided not to include results from the 30-meter DEM. However, the grids and coverages pertaining to it are available if desired. Note that due to large file size, the database file for the 10-meter DEM sorted by floodplain kilometer has not been imported into spreadsheet format.
2. We have also provided a shaded relief map of the study area using the 10-meter DEM.
3. During our conference call of 6 December 2005, elevation transects were also requested. We have generated two of these products, one through Kiger Island and another through Green Island. The graphic outputs of these transects for historic floodplain, 1996 flood extent, and the Willamette River ca. 2000 are provided both as maps and line graphs.

4. Also requested in the same conference call were data on the areas of the different spatial containers. This information, both as absolute area (in hectares) and relative area (percentages of the historical and 1996 flood extents), are provided as line graphs.
5. We provided the graphic outputs to give some idea of the types of data available and how they can be analyzed and used. We would like to point out that these products barely scratch the surface of future analyses. For example, interactions among locations of remnant river channels, soil hydrogroup type and current land use could be used to facilitate location of sites for both river and floodplain restoration. We hope we have provided some of the tools to continue this process.